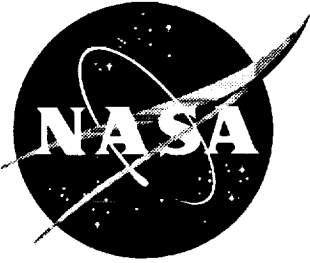NASA/TM-2001-211030
ARL-TR-2540

Influence of Specimen Preparation and Specimen Size on Composite Transverse Tensile Strength and Scatter

T. Kevin O'Brien
U. S. Army Research Laboratory
Vehicle Technology Directorate
Langley Research Center, Hampton, Virginia

Arun D. Chawan
Syracuse University, Syracuse, New York

Kevin DeMarco
Virginia Polytechnic Institute & State University, Blacksburg, Virginia

Isabelle Paris
Langley Research Center, Hampton, Virginia

July 2001

The NASA STI Program Office ... in Profile

Since its founding, NASA has been dedicated to the advancement of aeronautics and space science. The NASA Scientific and Technical Information (STI) Program Office plays a key part in helping NASA maintain this important role.

The NASA STI Program Office is operated by Langley Research Center, the lead center for NASA's scientific and technical information. The NASA STI Program Office provides access to the NASA STI Database, the largest collection of aeronautical and space science STI in the world. The Program Office is also NASA's institutional mechanism for disseminating the results of its research and development activities. These results are published by NASA in the NASA STI Report Series, which includes the following report types:
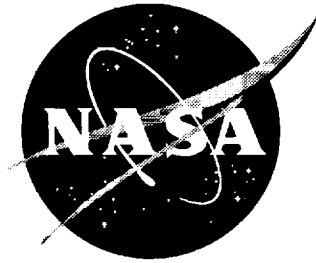
- TECHNICAL PUBLICATION. Reports of completed research or a major significant phase of research that present the results of NASA programs and include extensive data or theoretical analysis. Includes compilations of significant scientific and technical data and information deemed to be of continuing reference value. NASA counterpart of peer-reviewed formal professional papers, but having less stringent limitations on manuscript length and extent of graphic presentations.

- TECHNICAL MEMORANDUM. Scientific and technical findings that are preliminary or of specialized interest, e.g., quick release reports, working papers, and bibliographies that contain minimal annotation. Does not contain extensive analysis.

- CONTRACTOR REPORT. Scientific and technical findings by NASA-sponsored contractors and grantees.

- CONFERENCE PUBLICATION. Collected papers from scientific and technical conferences, symposia, seminars, or other meetings sponsored or co-sponsored by NASA.

- SPECIAL PUBLICATION. Scientific, technical, or historical information from NASA programs, projects, and missions, often concerned with subjects having substantial public interest.

- TECHNICAL TRANSLATION. English-language translations of foreign scientific and technical material pertinent to NASA's mission.

Specialized services that complement the STI Program Office's diverse offerings include creating custom thesauri, building customized databases, organizing and publishing research results ... even providing videos.

For more information about the NASA STI Program Office, see the following:

- Access the NASA STI Program Home Page at *http://www.sti.nasa.gov*

- E-mail your question via the Internet to help@sti.nasa.gov

- Fax your question to the NASA STI Help Desk at (301) 621-0134

- Phone the NASA STI Help Desk at (301) 621-0390

- Write to:
  NASA STI Help Desk
  NASA Center for AeroSpace Information
  7121 Standard Drive
  Hanover, MD 21076-1320

NASA/TM-2001-211030
ARL-TR-2540

Influence of Specimen Preparation and Specimen Size on Composite Transverse Tensile Strength and Scatter

T. Kevin O'Brien
U. S. Army Research Laboratory
Vehicle Technology Directorate
Langley Research Center, Hampton, Virginia

Arun D. Chawan
Syracuse University, Syracuse, New York

Kevin DeMarco
Virginia Polytechnic Institute & State University, Blacksburg, Virginia

Isabelle Paris
Langley Research Center, Hampton, Virginia

July 2001

INFLUENCE OF SPECIMEN PREPARATION AND SPECIMEN SIZE ON COMPOSITE TRANSVERSE TENSILE STRENGTH AND SCATTER

T. Kevin O'Brien
U.S. Army Research Laboratory
Vehicle Technology Directorate
NASA Langley Research Center
Hampton, Virginia

Arun D. Chawan
Syracuse University
Syracuse, New York

Kevin DeMarco
Virginia Polytechnic Institute & State University
Blacksburg, Virginia

Isabelle Paris
National Research Council
NASA Langley Research Center
Hampton, Virginia

ABSTRACT

The influence of specimen polishing, configuration, and size on the transverse tension strength of two glass-epoxy materials, and one carbon-epoxy material, loaded in three and four point bending was evaluated. Polishing machined edges, and/or tension side failure surfaces, was detrimental to specimen strength characterization instead of yielding a higher, more accurate, strength as a result of removing inherent manufacture and handling flaws. Transverse tension strength was typically lower for longer span lengths due to the classical weakest link effect. However, strength was less sensitive to volume changes achieved by increasing specimen width. The Weibull scaling law typically over-predicted changes in transverse tension strengths in three point bend tests and under-predicted changes in transverse tension strengths in four point bend tests. Furthermore, the Weibull slope varied with specimen configuration, volume, and sample size. Hence, this scaling law was not adequate for predicting transverse tension strength of heterogeneous, fiber-reinforced, polymer matrix composites.

INTRODUCTION

Matrix ply cracking is a common initial damage mechanism in fiber reinforced composites. Because matrix ply cracking is seldom catastrophic for laminates subjected to membrane loading, few researchers have tried to identify and overcome the difficulties involved in characterizing transverse tensile strength, one of the fundamental material properties associated with matrix ply crack formation. However, for composite structures that undergo bending, or other out-of-plane loading, the formation of matrix cracks may lead to immediate delamination formation and unstable growth [1,2]. Hence, accurate characterization of the transverse tensile strength of composite materials may be required to accurately predict matrix ply cracking in these structures.

The influence of material volume, in the form of a ply thickness dependence on matrix crack formation, is well established. Hence, for a strength-based characterization to be truly generic, volume scaling must be achieved through a Weibull Scaling Law [3]. Early attempts to achieve this characterization were performed using 90-degree laminate tension tests [4]. However, a large percentage of the failures occurred at the grips. An alternate technique would be to create transverse tension failures in 90-degree laminates subjected to bending loads. This type of loading has the added benefits of requiring simple fixtures and relatively small specimen sizes. Hence, a greater number of specimens may be tested for a given specimen size for the same amount of material required to perform uni-axial tension tests. These larger sample sizes facilitate the generation of the large number of replicates required for statistical characterization and generation of the parameters required for the Weibull scaling law.

In this study, 90-degree unidirectional glass-epoxy and carbon-epoxy laminates were tested in three and four point bending to characterize the composite transverse tensile strength. The influence of edge flaws due to machining, and surface flaws due to manufacture and handling, were assessed by testing specimens in both the natural (as-manufactured and machined) condition as well as testing specimens with polished edges, polished bottom failure surfaces, or both. Furthermore, the dependence of transverse tensile strength on volume was assessed by testing specimens with different widths and spans. A large number of specimens were tested for each unique combination of specimen preparation, geometry, and loading.

MATERIALS

Three different fiber reinforced polymer matrix composites were tested. These included two glass-epoxy materials (S2/F584 and S2/8552) and a carbon-epoxy material (IM7/8552) with two different laminate thicknesses (24-ply and 36-ply).

S2/F584 glass-epoxy

Two sets of panels were supplied by the Boeing Company, Mesa, Arizona. The original prepreg material used to manufacture the first set was flagged by the material supplier, Hexcel Corporation, as having contaminates in the form of small spots of aluminum silicate (i.e. grease, etc.). This material was replaced by new prepreg material to manufacture the second set. However, because no significant flaws were detected in ultrasonic inspection, both sets of panels were tested in this study. The S2 glass fiber density for both panels was 2.48 g/cm^3. The fiber aerial weight was 218 g/m^2 for the original prepreg material and 223 g/m^2 for the new prepreg material.

All panels from both materials were cured in an autoclave using the manufacturer's recommended curing cycle. This consisted of a temperature rise of 3.5 K (7°F) per minute up to 451 K (350°F) at a pressure of 689 KPa (100 psi). This was followed a 120 minute hold, then cooling down at the same rate while maintaining pressure until the temperature was less than 334 K (140°F). The panels were made with 24 plies of prepreg and were 406 mm (16 in) long in the fiber direction and 305 mm (12 in) wide in the direction transverse to the fibers. The nominal panel thickness was 4.45 mm (0.175 in), corresponding to a nominal ply thickness of 0.185 mm (0.0073 in). Nominal fiber volume fraction was 47.3% and 48.4% for the original and new panels, respectively, as estimated from the following equation

$$\% V_f = \frac{N(FAW)}{t(FD)} \times 100 \qquad (1)$$

where N is the number of plies, t is the panel thickness, FAW is the fiber aerial weight and FD is the fiber density. This fiber volume fraction compares well with the average volume fraction measured using ASTM standard D3171 for fiber volume fraction by digestion of the polymer matrix. This technique was used on the thinnest and thickest specimen from each test configuration. Fourteen samples from two panels of the original prepreg material, and 24 samples from three panels of the new prepreg

material, were digested using concentrated sulfuric acid and 30% hydrogen peroxide until no resin remained. The average fiber volume fraction determined this way was 48.0% for the original prepreg material and 48.1% for the new prepreg material. The volume fraction measurement coefficient of variation was 4.8% and 4.5%, respectively, for the original and new prepreg material.

S2/8552 glass-epoxy

A single panel was manufactured from unidirectional prepreg tape by Bell Helicopter Company, Fort Worth, Texas. The S2 glass fiber density was 2.48 g/cm^3. The Fiber aerial weight was 295 g/m^2. The uncured resin content was 34% by weight.

The panel was cured in an autoclave using the manufacturer's recommended curing cycle. This consisted of 120 minutes at 454 K (355°F) and 621 KPa (90 psi) pressure. The panel consisted of 24 plies of unidirectional prepreg tape and measured 762 mm (30 in) square. The nominal panel thickness was 5.56 mm (0.219 in), corresponding to a nominal ply thickness of 0.231 mm (0.0091 in). No significant flaws were detected in ultrasonic inspection of this panel.

Nominal fiber volume fraction was 51.3 %, as estimated from equation (1). This fiber volume fraction compares well with the average volume fraction measured using the ASTM standard D3171 for fiber volume fraction by digestion of the polymer matrix. This technique was used on the thinnest and thickest specimen from each test configuration. Eighteen samples were digested using concentrated sulfuric acid and 30% hydrogen peroxide until no resin remained. The average fiber volume fraction determined this way was 49.8%. The volume fraction measurement coefficient of variation was 2.5%.

IM7/8552 carbon-epoxy

Three panels were manufactured from IM7/8552 unidirectional prepreg by the Boeing Company, Philadelphia, Pennsylvania. The IM7 carbon fiber density was 1.75 g/cm^3. The Fiber aerial weight was 148 g/m^2. The uncured resin content was 34% by weight.

The panels were cured in an autoclave using the manufacturer's recommended curing cycle. This consisted of a 2 hours hold at 454 K (355°F) under 621 KPa (90 psi) pressure. Two of the panels consisted of 24 plies of unidirectional prepreg tape and the third panel consisted of 36 plies

of unidirectional prepreg tape. All three panels measured 610 mm (24 in) by 305 mm (12 in). For the 24-ply panels, the nominal panel thickness was 3.32 mm (0.1305 in), corresponding to a nominal ply thickness of 0.137 mm (0.0054 in). For the 36-ply panel, the nominal panel thickness was 4.93 mm (0.194 in), corresponding to a nominal ply thickness of 0.137 mm (0.0054 in). No significant flaws were detected in ultrasonic inspection of these panels.

Nominal fiber volume fraction, as estimated from equation (1), was 62.1 % for both the 24-ply and 36-ply laminates. This fiber volume fraction compares well with the average volume fraction measured using the ASTM standard D3171 for fiber volume fraction by digestion of the polymer matrix. This technique was used on the thinnest and thickest specimen from each test configuration. For both the 24-ply and 36-ply laminates, fourteen samples were digested using concentrated sulfuric acid and 30% hydrogen peroxide until no resin remained. The average fiber volume fraction determined this way was 63.0% for the 24-ply laminates and 62.6% for the 36-ply laminates. The volume fraction measurement coefficient of variation was 6.2% and 6.4%, respectively, for the 24-ply and 36-ply laminates.

SPECIMEN PREPARATION

Specimen cutting

Test specimens with fibers oriented at ninety degrees to the longitudinal axis were cut from the panels fabricated for all three materials. All specimens were cut from panels using a diamond saw. A 6.35 mm (0.25 in) plexi-glass sheet was placed beneath each panel during the machining to minimize any fiber spalling on the back side of the saw cut.

S2/F584 glass-epoxy test specimens

Specimens were cut from two panels (TO3 and TO5) made from the original prepreg material and three panels (TN2, TN3, and TN6) from the new prepreg material (table 1). Panels TO3, TO5, and TN2 were cut into 5 columns, 57.2 mm (2.25 in) wide. Hence, test specimens cut from these columns were 57.2 mm (2.25 in) long (B configurations, table 1). All test specimens cut from panel TO3 columns were 6.35 mm (0.25 in) wide (Configurations B-2, B-3, and B-4 in table 1). For the columns from panels TO5 and TN2, specimens were cut in a repeated pattern consisting of repeated sets of two specimens 6.35 mm (0.25 in) wide (configurations B-A

and B-B), one specimen 12.7 mm (0.5 in) wide (configuration B-C), and one specimen 19.1 mm (0.75 in) wide (configuration B-D). This cutting pattern was chosen to minimize any strength dependence on specimen panel position. Selected specimen configurations from panels TO3, TO5, and TN2 were polished on the edges, bottom surface, or both, prior to testing (table 1). Panel TN3 was cut into four columns with four different widths. Specimens cut from these columns had lengths of 31.8 mm (1.25 in) for configuration A, 57.2 mm (2.25 in) for configuration B, 82.6 mm (3.25 in) for configuration C, and 108 mm (4.25 in) for configuration B3. Panel TN6 was cut into four columns, two with widths of 57.2 mm (2.25 in) and two with widths of 82.6 mm (3.25 in). Specimens cut from these columns had lengths of 57.2 mm (2.25 in) for configurations B and A1 and 82.6 mm (3.25 in) for configurations A2 and B2. All test specimens cut from panels TN3 and TN6 were 6.35 mm (0.25 in) wide (table 1). All specimens cut from panels TN3 and TN6 were polished on the edges only.

S2/8552 glass-epoxy test specimens

The large 762 mm (30 in) square panel was first cut into four 381 mm (15 in) square panels to facilitate further cutting into test specimens. These four smaller panels were then cut into columns with different widths. These columns were cut into test specimens with lengths of 31.8 mm (1.25 in) for configuration A, 57.2 mm (2.25 in) for all B configurations and configuration A1, 82.6 mm (3.25 in) for configurations C, A2, and B2, and 108 mm (4.25 in) for configuration B3 (table 2). One of the 57.2 mm (2.25 in) columns from each of the four quadrants (I-IV) of the original large panel were cut into specimens using a repeated pattern. This pattern consisted of repeated sets of two specimens 6.35 mm (0.25 in) wide (configurations B-A and B-B), one specimen 12.7 mm (0.5 in) wide (configuration B-C), and one specimen 19.1 mm (0.75 in) wide (configuration B-D). This cutting pattern was chosen to minimize any strength dependence on specimen panel position. One set of the 6.35 mm (0.25 in) wide specimens (configuration B-B) was polished on the edges and bottom surface (table 2). In addition, a set of 57.2 mm (2.25 in) long by 6.35 mm (0.25 in) wide specimens (configuration B-2) from a column in a single quadrant of the original panel was also polished on the edges only. All remaining specimens were tested in their as-cut, unpolished, condition.

6

IM7/8552 carbon-epoxy test specimens

24-Ply Panels

The two 610 mm (24 in) by 305 mm (12 in) panels were each cut into two 305 mm (12 in) square panels to facilitate further cutting into test specimens. The first panel (24-1) was cut into five 57.2 mm (2.25 in) wide columns yielding 57.2 mm (2.25 in) long specimens. Test specimens of three different widths were cut from these columns (table 3). Columns were cut in a pattern consisting of repeated sets of four specimens 6.35 mm (0.25 in) wide (configurations B-A to B-D), one specimen 12.7 mm (0.50 in) wide (configuration B-E), and one specimen 19.1 mm (0.75 in) wide (configuration B-F). This cutting pattern was chosen to minimize any strength dependence on specimen panel position. Selected configurations were polished on the edges, bottom surface, or both, prior to testing (table 3). The second panel (24-2) was cut into columns with four different widths. These columns were cut into 6.35 mm (0.25 in) wide test specimens with lengths of 31.8 mm (1.25 in) for configuration A, 57.15 mm (2.25 in) for configurations B and A1 and 82.55 mm (3.25 in) for configurations C, A2 and B2 (table 3).. All specimens from the second panel were tested in their as-cut, unpolished, condition.

36-Ply Panel

One 610 mm (24 in) by 305 mm (12 in) panel was first cut into two 305 mm (12 in) square panels to facilitate further cutting into test specimens. These two smaller panels were then cut into columns with four different widths. These columns were cut into 6.35 mm (0.25 in) wide test specimens with lengths of 31.8 mm (1.25 in) for configuration A; 57.2 mm (2.25 in) for configurations B and A1; 82.6 mm (3.25 in) for configurations C, A2 and B2; and 108 mm (4.25 in) for configuration B3 (table 3). All specimens from this panel were tested in their as-cut, unpolished, condition.

Polishing procedure

Specimen edges and bottom surfaces were polished for selected specimens using the following procedure. Specimens were first sanded on a Buhler Ecomet III Polisher/Grinder using 600 grit Buhler carbiMet paper discs. Next, specimens were polished on this same machine using 1200 grit Lapmaster international Silicon Carbide paper discs. Finally, specimens were polished using a very fine nap cloth (Chem-met) and Buehlers

Masterprep (.05 micron Alumina suspension solution) with a lubricant of soapy water (pH 7). Polished surfaces had a mirror image finish upon completion of this polishing process. In some cases, this process was also performed on specimens that had been tested without previous polishing to facilitate post-mortem microscopic observation of the failure orientation.

Thickness and width measurement

The thickness and width of each specimen was measured at three points along the specimen length using flat nose digital calipers. The average of these three measurements, as well as the percentage variation in thickness and width along the specimen length, were calculated and tabulated along with the individual measurements. For specimens that were polished, thickness and width measurements were performed after polishing and before testing. For each test configuration on each material, the average thickness and coefficient of variation are shown in tables 1-3.

EXPERIMENTAL PROCEDURE

Test apparatus

Three and four point bending tests were performed on an MTS model 858 table-top hydraulic load frame with an MTS model 458 controller (figure 1). This load frame was equipped with a 22.2 kN (5000 lb) load cell. An additional 2.22 kN (500 lb) load cell was placed in series with this standard load cell to more accurately measure the small loads anticipated. This smaller load cell was typically run at the 50% range corresponding to a 1.1 kN (250 lb) load at full scale. Both load cells, and the internal LVDT that controlled the stroke of the ram, were calibrated according to NIST traceable ISO 9001 specifications just before the test series was begun.

The load frame was equipped with three and four point bending fixtures that were designed and built at NASA Langley (figure 2). The fixtures consisted of individual upper and lower pieces that included the load point supports. These supports were machined to a radius of 3.18 mm (0.125 in), and were bolted to the cross member so that the span length could be adjusted between 25.4 mm (1 in) and 102 mm (4 in). An angle bracket and a set of metal strips, clamped to the bracket, were used to center the specimen width on the load point supports.

Bending test configurations

Three-point bending tests were performed in three configurations, A, B, and C, shown in figure 3a with span lengths of 25.4 mm (1.0 in), 50.8 mm (2.0 in), and 76.2 mm (3.0 in). Four point bending tests were performed using four configurations (A1, A2, B2, B3) also shown in figure 3a. These configurations had combinations of inner spans ,s-ℓ, of 25.4 mm (1.0 in) or 50.8 mm (2.0 in) and outer spans, s, of 50.8 mm (2.0 in) to 102 mm (4.0 in).

Test Procedure

Tests were performed in stroke control using a programmed loading ramp. Stroke rates were determined by estimating the maximum center point displacement at failure using beam theory and programming a stroke rate so that specimen failure would occur in approximately one minute. Hence, different specimen configurations were tested at different stroke rates so that the time to failure would be similar for all specimens tested. Tables 1-3 show the stroke rates used for each test configuration and material. For each unique configuration for a given material, all tests were completed on the same day, by the same operator, under the same ambient laboratory environmental conditions.

Failure loads were recorded using peak detectors in the MTS 458 controller. In addition, for each test a continuous plot of load versus load-point displacement was recorded using an analog X-Y recorder. Specimens were removed from the load frame as it was unloaded. Immediately thereafter, the distance from the failure location along the length to the center load point in the three point tests, and to the center of the specimen span in the four point tests, was measured and recorded. For each configuration tested, the maximum mid-span deflection, δ_{max}, normalized by the average specimen thickness, t_{avg}, were recorded (tables 4-6). For most of the configurations tested, δ_{max}, was less than t_{avg}, and hence, $\delta_{max} / t_{avg} < 1$.

Data Reduction

For the three point bending tests shown in figure 3b, with span length, s and width, b, specimen strengths were determined from the beam theory expression for the maximum tension stress, σ_{max}, under the center load nose using the maximum load at failure, P_c, and the average specimen thickness, t_{avg},

$$\sigma_{max} = \frac{3P_c s}{2bt_{avg}^2} \tag{2}$$

For the four point bending tests shown in figure 3b, with outer span, s, inner span, s-ℓ, and width, b, specimen strengths were determined from the beam theory expression for the maximum uniform tension stress, σ_{max}, between the inner load points using the maximum load at failure, P_c, and the average specimen thickness, t_{avg},

$$\sigma_{max} = \frac{3P_c \ell}{2bt_{avg}^2} \tag{3}$$

Figure 4 shows a failed S2/8552 glass-epoxy specimen that was tested in 3-point bending configuration A. This is the shortest span and thickest specimen tested, and hence, would be the most prone to fail in transverse shear as opposed to transverse tension. Figure 4 shows the crack that formed at 90 degrees to the bottom of the beam, illustrating that the failure was due to transverse tension. This same failure pattern was observed for all three materials for all of the 3-point and 4-point bend configurations.

TRANSVERSE STRENGTH CHARACTERIZATION

The strength of a material is typically characterized assuming either a symmetric (normal) distribution or a skewed (Weibull) distribution. For the normal distribution, the mean strength and coefficient of variation, CV, (standard deviation divided by the mean strength) are calculated. The mean strength characterizes the central tendency of the strength distribution, whereas the CV quantifies the scatter in the strength distribution. However, since most strength data is not normally distributed, a Weibull distribution is often assumed as an alternative.

Weibull assumed an extreme value, or "weakest link", distribution for material strength by developing a two parameter function for the probability of failure at a given stress level, P(σ), of the form

$$P(\sigma) = 1 - e^{-\left(\sigma / \sigma_c\right)^m} \tag{4}$$

Where σ_c is the location parameter known as the characteristic strength, and m is the shape parameter known as the Weibull slope [3]. The location parameter, σ_c, provides a measure of the central tendency of the distribution, similar to the mean for a normal distribution. The Weibull slope, m, provides a measure of the scatter in the distribution, with a small value of m corresponding to a large amount of scatter in the data. Therefore, the amount of scatter is inversely proportional to m. Hence, as the magnitude of m increases, the scatter decreases. Equation 4 may also be recast into an equation of the form

$$y = m \ln \sigma + b \tag{5}$$

Where

$$y = \ln\left[\ln\left(\frac{1}{1 - P(\sigma)}\right)\right] \tag{6}$$

And

$$b = -m \ln \sigma_c \tag{7}$$

Then by assuming a probability of failure corresponding to a median ranking of the data

$$P(\sigma) = \frac{(i-1) + 0.7}{n + 0.4} \tag{8}$$

Where n is the total number of data points in the sample and i is the number of the data points in ascending order from 1 to n; a least squares regression fit of the logarithmic equation 5 may be performed to determine m and σ_c.

For each least squares regression analysis, the goodness of the fit was quantified using Pearson's "r" value given by

$$r = \frac{\sum_{i}^{N}\left(x_i - \bar{x}\right)\left(y_i - \bar{y}\right)}{\sqrt{\sum_{i}^{N}\left(x_i - \bar{x}\right)^2}\sqrt{\sum_{i}^{N}\left(y_i - \bar{y}\right)^2}} \tag{9}$$

An "r" value close to 1.0 indicates a good fit to the data.

In addition to characterizing the strength distribution for a given material, Weibull postulated that the characteristic strengths for two different volumes, V_1 and V_2, of the same material will obey the following scale law [3]

$$\frac{(\sigma_c)_1}{(\sigma_c)_2} = \left(\frac{V_2}{V_1}\right)^{1/m} \tag{10}$$

This scaling law was used previously to characterize transverse tension strength via tension testing of 90 degree unidirectional carbon fiber epoxy laminate [4].

For all three materials tested, characterization of the transverse tension strength for each configuration was performed assuming both a normal distribution and a Weibull distribution. Because of the inverse relationship between the Weibull slope and the degree of scatter in the data, the inverse of the Weibull slope, $1/m$, was tabulated and plotted to allow a more intuitive feeling for the trends observed. In addition, it is the inverse Weibull slope that appears as the exponent in the Weibull volume scale law in equation 10. Furthermore, the decimal value of CV and the inverse Weibull slope, $1/m$, have similar magnitudes. Hence, these quantities were tabulated and plotted together.

The scaling law in equation 10 assumes that the two volumes being compared are subjected to a uniform tensile stress throughout the volume. However, the stress distributions in the three and four point bend tests are not uniform (fig.3b). Hence, the scaling law was modified in reference 5 for 3-point bending as

$$\frac{\sigma_f^{3pt}}{\sigma_t} = \left[2(m+1)^2 \frac{V_t}{V_f^{3pt}}\right]^{1/m} \tag{11}$$

Where the subscript "f" corresponds to the stress and volume in the flexure test and the subscript "t" corresponds to the stress and volume under uniform tension. A similar expression was derived in reference 5 for 4-point bending as

$$\frac{\sigma_f^{4pt}}{\sigma_t} = \left[\frac{4(m+1)^2}{(m+2)} \frac{V_t}{V_f^{4pt}}\right]^{1/m}$$

(12)

Equation (12) is applicable for quadrant point loading only. Hence, this would apply for configurations A1 and B3 only. Similar expressions were derived in the appendix for configurations A2 and B2.

The relationship between the 4-point quadrant point loading and 3-point bending cases may be expressed by combining equations 11 and 12 to yield

$$\frac{\sigma_f^{4pt}}{\sigma_f^{3pt}} = \left[\left(\frac{2}{m+2}\right) \frac{V_f^{3pt}}{V_f^{4pt}}\right]^{1/m}$$

(13)

Equation (13) is applicable for quadrant point loading only. Hence, this would apply for configurations A1 and B3 only. Similar expressions were derived in the appendix for configurations A2 and B2.

EXPERIMENTAL RESULTS

Results for the strength and scatter, as characterized using both a normal and Weibull distribution, are given in tables 4-6 for the three materials tested. Strengths and scatter parameters were also recalculated for smaller sample sizes than the total n tested to determine the influence of sample size on the results. All populations were evaluated starting from the first specimen tested up to the desired number in the order of testing as determined by random number generation. Results for each of the three materials tested are described in detail in the following sections. The figures will show results in SI units only. Results are also tabulated in English units in tables 4-6.

S2/F584 Glass-epoxy

Influence of Specimen Preparation

Figure 5a shows the mean and characteristic strengths for configuration B specimens from panel TO3 and TO5 that had different specimen preparation. There was less than 2% difference in the strengths of the unpolished specimens, B-2, and specimens with polished edges, B-3.

13

Therefore, any flaws created due to cutting the plate do not appear to significantly affect the specimen strength. However, specimens with polished bottom (tension side) surfaces, either with (B-B) or without (B-4) polished edges, had 5.7% and 10.6% lower strengths, respectively. Hence, instead of increasing the measured strength as a result of removing inherent flaws in the material due to manufacture and handling, polishing appears to be detrimental to specimen strength. In addition, for 2 of the 3 polished configurations (B-3 and B-B), polishing the edges resulted in greater scatter than was obtained in tests with unpolished edges, as indicated when comparing the values of CV and 1/m in figure 5b.

In order to eliminate the influence of sample size on these comparisons, strengths and scatter for each of these configurations were recalculated with a common sample size of n=35. This number was chosen because it is the smallest common sample size for the configurations being compared. In all cases, the first 35 specimens tested were used in the calculation. As shown in figure 6a, the smaller sample size resulted in some numerical differences, but the same relative comparisons noted previously were still observed. The only exception was for configuration B-B where the CV for this polished configuration was 2.5% lower than the CV for the unpolished configuration B-2 (fig. 6b).

Figure 7a shows the mean and characteristic strengths for configuration B specimens from panel TN2 made with the new prepreg material. Both configurations had polished edges, but just as was observed with specimens made from the original prepreg material, edge polished specimens with polished bottom surfaces (configuration B-B) had lower strengths than the edge polished specimens with unpolished bottom surface specimens (configuration B-A). Furthermore, the specimens with polished bottom surfaces had greater scatter, as shown in figure 7b.

Influence of Specimen Width

Figure 8a shows the mean and characteristic strengths for original prepreg configuration B specimens from panels TO3 and TO5 with three different widths: 6.35 mm (configuration B-2), 12.7 mm (configuration B-C), and 19.7 mm (configuration B-D). Results are presented for a common sample size of n=35. No trend is apparent, as the strength appears to decrease by 6.2% between the 6.35 mm (0.25 in) and 12.7 mm (0.50 in) wide specimens, then increases by 2.3% between the 12.7 mm (0.50 in) and 19.7 mm (0.75 in) wide specimens. Similarly, there is no apparent trend in the scatter with specimen width, as shown in figure 8b.

Figure 9a shows the mean and characteristic strengths for new prepreg configuration B specimens from panel TN2 with three different widths: 6.35 mm (configuration B-A), 12.7 mm (configuration B-C), and 19.7 mm (configuration B-D). Results are presented for a common sample size of n=35. As was the case with the original prepreg material specimens, no significant trend is apparent, with only a 2.2% increase in strength with increasing specimen width. Hence, the anticipated trend of decreasing strength with increasing width, and hence increasing volume, that would be anticipated from the Weibull scaling law was not observed for specimens from either the original, or new prepreg materials. As shown in figure 9b, for the new material (panel TN2) specimens, the scatter increases with increasing specimen width, with the CV for the widest configuration (B-D) being 1.7% greater than the CV for the narrowest configuration (B-A),.

Influence of panel-to-panel variability

Figure 10a shows the mean and characteristic strengths for identical configuration B specimens with polished edges from different panels (TO3, TN2, TN3, TN6) calculated for a common sample size of n=35. There is clearly some variability in strength from panel to panel. This variability is fairly small (4.2%) compared to the absolute strength, but it is greater than the 2.2% variability found with increasing specimen width for panel TN2 (fig.9a). There is a greater variability in scatter between panels, as shown in figure 10b, with the panel from the original prepreg material (TO3) showing the greatest scatter. This could possibly be due to the contamination found in the prepreg.

Influence of Span Length

Figure 11a shows the mean and characteristic strengths for three point bending configurations with three different span lengths of 25.4 mm (1.0 in), 50.8 mm (2.0 in), and 76.2 mm (3.0 in) calculated for a common sample size of n=47. Specimens tested in each of these configurations were from a single panel (TN2) and had polished edges. There is a slight decrease (1.8%) in strength with increasing span length, and hence increasing volume, as anticipated based on the Weibull scaling law. In addition, there is a noticeable trend of decreasing scatter with increasing span length as shown in figure 11b. Similar trends in strength and scatter dependence with span length were obtained for a smaller common sample size of n=35.

Figure 12a shows the mean and characteristic strengths calculated for a common sample size of n=47, for four-point bending configurations with different span length combinations. Specimens tested in each of these configurations had polished edges. There is an 11% decrease in strength with increasing outer span length, s, from configuration A1 to A2 and an 8.3% decrease in strength with increasing inner span, s-ℓ, from configuration A2 to B2. Specimens for all three of these configurations were cut from the same panel (TN6). However, strength increased by almost 10% with increasing outer span length, s, from configuration B2 (panel TN6) to configuration B3 (panel TN3). Hence, the anticipated trend of decreasing strength with increasing volume may be masked by significant panel-to-panel variability. In addition, unlike the three point bending case, there is a noticeable trend of increasing scatter with increasing span length for the three configurations from the same panel (TN6), as shown in figure 12b. However, the scatter for specimens from panel TN3 did not follow this trend. Similar strength and scatter dependence with span length were obtained for a smaller common sample size of n=35.

S2/8552 Glass-epoxy

Influence of Specimen Preparation

Figure 13a shows the mean and characteristic strengths for configuration B specimens that had different specimen preparation.
For the configurations that were tested with specimens from all four quadrants of the original large panel (B-A, B-B), strengths for polished specimens were slightly lower (1.5%) than strengths for unpolished specimens. Similarly, for the configurations that were tested with specimens from a single quadrant of the original large panel (B-1, B-2), strengths for polished specimens were also slightly lower (0.8%) than strengths for unpolished specimens. Hence, instead of increasing the measured strength as a result of removing inherent flaws in the material due to manufacture and handling, polishing appears to be detrimental to specimen strength. For the specimens from all four quadrants of the original large panel (B-A, B-B) polishing resulted in 1.15% greater CV than obtained in tests with unpolished edges, as shown in figure 13b. However, the opposite was true for specimens cut from a single quadrant of the original large panel, with polished specimens (B-2) having 0.88% lower CV than unpolished specimens (B-1).

Influence of Specimen Width

Figure 14a shows the mean and characteristic strengths for configuration B specimens with three different widths: 6.35 mm (0.25 in), 12.7 mm (0.50 in), and 19.1 mm (0.75 in). Results are presented for a common sample size of n=25. No trend is apparent, as the strength decreases by 3.2% between configurations B-A and B-C, then increases by 0.9% between configurations B-C and B-D. Hence, the anticipated trend of decreasing strength with increasing width, and hence increasing volume, that would be anticipated from the Weibull scaling law was not observed. However, the scatter increased with increasing specimen width, as shown in figure 14b.

Influence of Span Length

Figure 15a shows the mean and characteristic strengths for three point bending configurations with three different span lengths of 25.4 mm (1.0 in), 50.8 mm (2.0 in), and 76.2 mm (3.0 in). All specimens tested in each of these configurations were unpolished. There is no decrease in strength between span lengths of 25.4 mm (1.0 in) and 50.8 mm (2.0 in), however, there is a 6.0% decrease in strength between span lengths of 50.8 mm (2.0 in) and 76.2 mm (3.0 in), as anticipated based on the Weibull scaling law. In addition, there is a noticeable trend of decreasing scatter with increasing span length as shown in figure 15b. Similar trends in strength and scatter dependence with span length were obtained for a smaller common sample size of n=35.

Figure 16a shows the mean and characteristic strengths for four-point bending configurations with different span length combinations. All specimens tested in each of these configurations were unpolished. There is a noticeable decrease in strength with increasing inner (s-ℓ) or outer (s) span length for these configurations. In addition, strength decreases as the inner span length is increased relative to a constant outer span length (i.e., from configuration A2 to B2), thereby increasing the volume of material subjected to the maximum bending stress. These observations are consistent with the anticipated trend of decreasing strength with increasing volume based on the Weibull scaling law. However, the scatter appeared to increase with span length for all but the longest span configuration B3, as shown in figure 16b.

IM7/8552 Carbon-epoxy

Influence of Specimen Preparation

Figure 17a shows the mean and characteristic strengths for 24-ply, configuration B specimens that had different specimen preparation. Strengths for specimens polished on the edges or bottom only were slightly lower (1-2%) than strengths for unpolished specimens. Strengths for specimens polished on both the edges and bottom surface were nearly identical (within 0.5%) to the strengths for unpolished specimens. Hence, polishing does not appear to significantly increase the measured strength as a result of removing inherent flaws in the material due to manufacture and handling. As shown in figure 17b, with the exception of configuration B-C, polished specimens (B-A and B-B) had greater scatter than obtained in tests with unpolished edges (B-D).

Influence of Specimen Width

Figure 18a shows the mean and characteristic strengths for 24-ply, configuration B specimens with three different widths: B-D, 6.35 mm (0.25 in), B-E, 12.7 mm (0.50 in), and B-F, 19.7 mm (0.75 in). Strengths decreased with increasing width, with a maximum difference of 5.4% between configurations B-F and B-D. This is consistent with the anticipated trend of decreasing strength with increasing width, and hence increasing volume, that would be anticipated from the Weibull scaling law. However, the scatter increased with increasing specimen width, as shown in figure 18b, with a maximum rise in CV of 2.36% from configurations B-D to B-F. Similar trends in strength and scatter dependence with span length were obtained for a smaller common sample size of n=35.

Influence of panel-to-panel variability

Figure 19a shows the mean and characteristic strengths for unpolished 24 ply, configuration B specimens from different panels. There is clearly some variability in strength (4.7%) between the two panels. The variability in scatter between panels was small, as shown in Figure 19b, with a difference of 0.8% in CV.

Influence of Span Length

24-ply panel

Figure 20a shows the mean and characteristic strengths for three point bending configurations with three different span lengths of 25.4 mm (1.0 in), 50.8 mm (2.0 in), and 76.2 mm (3.0 in). All specimens tested in each of these configurations were unpolished. Strength decreased by almost 10% between span lengths of 25.4 mm (1.0 in) and 50.8 mm (2.0 in). However, strength increased by 7.3% between span lengths of 50.8 mm (2.0 in) and 76.2 mm (3.0 in). In addition, there is a noticeable trend of decreasing scatter with increasing span length as shown in figure 20b. Similar trends in strength and scatter dependence with span length were obtained for a smaller common sample size of n=35.

Figure 21a shows the mean and characteristic strengths for four-point bending configurations with different span length combinations. All specimens tested in each of these configurations were unpolished. There is a noticeable decrease in strength (4.2%) with increasing outer span length, s, from configurations A1 to A2. However, strength increased by 2.5% from configuration A2 to B2 as the inner span length, s-ℓ, was increased relative to a constant outer span length, s, thereby increasing the volume of material subjected to the maximum bending stress. Similar trends were observed for strengths calculated for a smaller common sample size of n=35. Furthermore, as shown in figure 22b, the scatter exhibited trends similar to those observed for strength.

36-ply panel

Figure 22a shows the mean and characteristic strengths for three point bending configurations with three different span lengths of 25.4 mm (1.0 in), 50.8 mm (2.0 in), and 76.2 mm (3.0 in). Specimens tested in each of these configurations were unpolished. There is a significant decrease (4.8-9.3%) in strength with increasing span length, and hence increasing volume, as anticipated based on the Weibull scaling law. In addition, there is a noticeable trend of decreasing scatter with increasing span length as shown in figure 22b. Similar trends in strength and scatter dependence with span length were obtained for a smaller common sample size of n=35.

Figure 23a shows the mean and characteristic strengths for four-point bending configurations with different span length combinations. All specimens tested in each of these configurations were unpolished. There is a

3.4% increase in strength with increasing outer span length, s, between configurations A1 and A2. However, strength decreases by 14.1% with increasing outer span length, s, between configurations B2 and B3. In addition, strength increased by 3.4% as the inner span length, s-ℓ, was increased relative to a constant outer span length, s, from configuration A2 to B2. Similar trends were observed for strengths calculated for a smaller common sample size of n=35. Scatter appeared to increase with both inner and outer span length for all but the shortest span configuration (A1) as shown in figure 23b.

Influence of Specimen Thickness

Figures 24a and 24b compare mean strengths for identical configurations of 24-ply and 36-ply IM7/8552 specimens tested in 3-point and 4-point bending, respectively. For specimens subjected to uniform tension, the weakest link theory would predict a lower strength for the thicker specimen. However, for the specimens tested in flexure in this study, the thicker specimen was weaker for only one of the three 3-point bend configurations (C) and for only one of the three 4-point bend configurations (A1). Failure initiates on the bottom surface in these flexure tests. Hence, the differences in strength observed for specimens with different thicknesses may be attributed more to variability between panels than to the classical weakest link effect, which assumes a greater probability of a defect causing failure in a thick laminate with a large volume.

Discussion of Experimental Results

In order to summarize the comparisons made in the previous section, results were plotted for all four material and thickness combinations for each effect studied (width, span, etc.).

The trend of decreasing strength with increasing specimen width, and hence increasing volume, that would be anticipated from the Weibull scaling law was not clearly apparent (fig.25). In contrast, a small decrease in strength with increasing 3-point span was observed for all three materials (fig.26). In addition, for the 4-point bending tests, a decrease in strength with increasing inner and outer span length was typically observed for the two glass-epoxy materials (fig.27). However, this expected scaling was occasionally masked by more significant panel-to-panel variability (S2/F584 configuration B3). The variation in strength with span length was not as consistent for the carbon-epoxy materials (fig.27).

For all three materials tested in 3-point bending, scatter typically increased with increasing specimen width (fig.25). However, scatter typically decreased with increasing 3-point span for all three materials (fig.26). For all three materials, scatter in the 4-point bending tests typically increased with increasing span length (fig.27). However, this trend was not consistent for all four configurations tested.

HISTOGRAMS OF FAILURE LOCATIONS

3-point bending

Histograms showing the frequency of occurrence of failure locations, relative to the center load nose, for the 3-point bend configurations are shown for (1) S2/F584 (panel TN3) glass-epoxy in figures 28 a-c, (2) for the S2/8552 glass-epoxy in figures 29 a-c, (3) for the 24-ply IM7/8552 carbon-epoxy in figures 30 a-c, and (4) for the 36-ply IM7/8552 carbon-epoxy in figures 31 a-c. Failure occurs near, but not always directly under, the center load nose where the beam theory indicates the tension stress is a maximum (fig.3b), thus illustrating the sensitive to flaws in the microstructure.

4-point bending

Histograms showing the frequency of occurrence of failure locations, relative to the inner load noses, for the 4-point bend configurations are shown for (1) S2/F584 (panel TN3) glass-epoxy in figures 32 a-d, (2) for the S2/8552 glass-epoxy in figures 33 a-d, (3) for the 24-ply IM7/8552 carbon-epoxy in figures 34 a-c, and (4) for the 36-ply IM7/8552 carbon-epoxy in figures 35 a-d. Failures occurred primarily between the inner load noses. However, some failures also occurred under these load points, and between the inner and outer load noses, reflecting the sensitive to flaws in the microstructure. For the S2/8552 glass-epoxy, failures were concentrated more toward one load nose for the longest span (configuration B3). For the 24-ply IM7/8552 carbon-epoxy, failures were concentrated more toward one load nose for the smallest span configurations A1 and A2. No tests were performed on configuration B3 for this thin material because of the large deflections that would occur. For the 36-ply IM7/8552 carbon-epoxy, more failures where concentrated near one load nose than the other for three of the four configurations tested.

POST MORTEM EXAMINATION

After failure had occurred, selected specimens were potted in epoxy, polished on the edges and examined in a light microscope to identify the details of the failure location. Figure 36 shows the photomicrographs taken at the failure location for two of the S2/8552 3-point bend specimens. The left and right sides of the specimen are shown at the failure location for each specimen.

For the specimen that had a low strength, there is a pocket of resin on the bottom surface at the failure location. This resin pocket was not present at the failure location for the other specimen that had a high strength. Hence, transverse tension strength may be influenced by the presence of a resin pocket. However, a larger sampling of photomicrographs is needed to determine if this is a real trend or simply coincidence.

EVALUATION OF WEIBULL SCALING LAW

Goodness of fit

Before applying the Weibull scaling law, it is prudent to first establish if the strength data fits an extreme value Weibull distribution. Figures 37 a-d show the Pearson's "r" value from equation (9) for the S2/F584, S2/8552, and IM7/8552 materials three and four point bend configurations used to evaluate span effects on transverse tension strength. These data fit the Weibull distribution well. Only two configurations had an "r" value less than 0.95. Most configurations had "r" values greater than 0.96. As noted earlier, an "r" value close to 1.0 indicates a good fit to the data.

In order to verify that the Weibull Scaling law is applicable for fiber reinforced composites, measured data from one volume should be used with this scaling law to accurately predict the strength of any other volume of the same material with the same failure mode. The following section documents attempts to do this for transverse tension strength measurement using the 3-point and 4-point bending tests utilized in this study.

Three Point Bend Tests

For S2/F584, S2/8552, and IM7/8552 configuration B specimens tested in three point bending, strengths of the wider specimens were predicted (fig.38 a-c) using the characteristic strength, σ_c, and $1/m$ for the 6.35 mm (0.25 in) wide specimens and the relative volumes of the

specimens in tension. This volume consisted of the product of the test span, specimen width, and one half of the specimen thickness. In addition, as shown in figure 39 a-d, configuration B specimens were used to predict the strengths of specimens with identical widths of 6.35 mm (0.25 in) but with shorter and longer spans (configurations A & C). Because all the configurations were tested in three point bending, and hence have similar tensile stress distributions (fig.3b), predictions were made using equation 10. For these cases, the predicted strength decrease with increasing width or span was between 1.6% and 6.5%.

At first glance, the predictions in figures 38 and 39 appear reasonably close to the measured strengths. However, as noted earlier, the anticipated trends in the measured data do not always follow the trends anticipated by the Weibull theory. In most cases, the Weibull scaling law over predicted changes in transverse tension strengths in three point bend tests. For the S2/F584 and S2/8552 glass-epoxy materials, the predicted strength variation was typically greater than the measured variation in strength with width or span length. The maximum variation in measured strength with specimen width was only 1.4%. The maximum variation in measured strength with span length for the S2/F584 material was only 1.9%. However, the maximum variation in measured strength with span length for the S2/8552 material was 6.7%. For the IM7/8552 carbon-epoxy, the predicted strength variation was also greater than the measured variation in strength with width, but less than the measured variation in strength with span length. The maximum variation in measured strength with specimen width was only 0.5%, whereas the maximum variation in measured strength with span length was 10.4%.

Four Point Bend Tests

The strength of S2/F584, S2/8552, and IM7/8552 four point bend configurations A2, B2, and B3 were predicted using, σ_c, and $1/m$ for configuration A1 and the relative volumes of the specimens in tension (fig.40 a-d). This volume consisted of the product of the test span, s, width, and one half of the specimen thickness. Scaling coefficients were derived in the appendix for predicting the strengths of configurations A2 and B2 using the measured strength of quadrant point loading configuration A1. Equation 10 was used to predict the strength of quadrant point loading configuration B3.

Unlike the 3-point bend cases, the strength predictions for 4-point bending, shown in figure 40, do not always appear close to the measured strengths. Also, as noted earlier, the anticipated trends in the measured data

do not always follow the trends anticipated by the Weibull theory. Furthermore, Unlike the three point bending tests, predicted strength variations between the 4-point bending configurations were often significantly smaller than the measured variation in strengths.

For the S2/F584 glass-epoxy materials, predicted strengths for the four configurations differed by 4 percent or less, whereas measured strengths for the four configurations differed by 10-17 percent. For the S2/8552 glass-epoxy materials, predicted strengths for the four configurations differed by 4 percent or less, whereas measured strengths for the four configurations differed by 4-22 percent. For the 24-ply IM7/8552 carbon-epoxy material, predicted strengths for the four configurations differed by 4 percent or less, whereas measured strengths for the four configurations differed by 1-5 percent. For the 36-ply IM7/8552 carbon-epoxy material, predicted strengths for the four configurations differed by 5 percent or less, whereas measured strengths for the four configurations differed by 2-7 percent. However, for the 36-ply IM7/8552 material, measured strengths for two configurations (A2 and B2) exceeded the reference strength for configuration A1.

In addition, 24-ply data were used in equation 10 to predict the strengths of the 36-ply data for each of the IM7/8552 carbon-epoxy 4-point bend configurations A1, A2, and B2 (fig. 41). Predicted strengths were greater than measured strengths for all three configurations.

Comparison of three and four point bend test results

The strengths of S2/F584, S2/8552 and IM7/8552 four point bend configurations A1, A2, B2, and B3 were predicted using, σ_c, and $1/m$ from the three point bend configuration B. As before, the volume consisted of the product of the test span, s, width, and one half of the specimen thickness for each configuration. Equation 13 was used to predict the strength of quadrant point loading configurations A1 and B3 using the measured strength of 3-point bending configuration B. Scaling coefficients were derived in the appendix for predicting the strengths of configurations A2 and B2 using the measured strength of 3-point bending configuration B.

Results for the S2/F584 and S2/8552 glass-epoxy materials are shown in figures 42 a-b. For both materials, predicted strengths decreased with increasing span lengths. This trend was also observed for the measured strengths of the S2/8552 material (figure 42b). However, the change in strength with span length predicted by the Weibull scaling law was significantly less than the measured changes in strength with increasing

span. For the S2/8552 glass-epoxy materials, predicted strengths for the four configurations differed from the reference 3-point bend configuration B strength by 12-15 percent, whereas measured strengths for the four configurations differed from the reference 3-point bend configuration B strength by 9-30 percent. For the S2/F584 material, measured strengths also decreased with increasing span length except for the longest span configuration B3 (fig.42a). However, configuration B3 specimens were cut from a different panel (TN3) than the other three configurations tested (TN6). Hence, this difference may simply reflect the panel-to-panel variability. However, for the three shortest span configurations that exhibited the expected trend, the change in strength with span length predicted by the Weibull scaling law was also significantly less than the measured changes in strength with increasing span. For the S2/F584 glass-epoxy materials, predicted strengths for the three configurations from the same panel differed from the reference 3-point bend configuration B strength by 10-13 percent, whereas measured strengths for the four configurations differed from the reference 3-point bend configuration B strength by 2-19 percent.

Results for the 24-ply and 36-ply IM7/8552 carbon-epoxy materials are shown in figures 42 c-d. For both the 24-ply and 36-ply specimens, predicted strengths decreased with increasing span lengths. However, no trend was apparent for the measured strengths of either thickness.

Discussion of Weibull Scaling law

As noted earlier, because failure initiates on the bottom surface in these flexure tests, the differences in strength observed for specimens with different thicknesses may be attributed more to variability between panels than to the classical weakest link effect, which assumes a greater probability of a defect causing failure in a thicker laminate with a larger volume. Furthermore, equations 10-13 assume that the inverse Weibull slope parameter (1/m) is a material constant, independent of volume. However, the three and four point bend test data indicate that the parameter (1/m), and hence the scatter in the data, varies with specimen size (tables 4-6). For the three point bend tests, 1/m increased with increasing specimen width (fig.25) for configuration B specimens; but for the 6.35 mm wide specimens, the parameter (1/m) decreased with increasing span length (fig.26). In contrast, for the four point bend specimens, 1/m typically increased with increasing span length (fig.27). In addition, the parameter (1/m), also varied to some degree with sample size (see figure 43, for example). Hence, this scaling law was not adequate for predicting transverse

tension strength of heterogeneous, fiber-reinforced, polymer matrix composites.

CONCLUSIONS

The influence of specimen polishing, specimen configuration, and specimen size on the transverse tension strength of two glass-epoxy materials, and one carbon-epoxy material, loaded in three and four point bending was evaluated. Polishing specimen edges had little, or no, effect on the transverse tension strength of 90-degree laminate tested in three and four point bending. However, polishing bottom (tension side) surfaces resulted in lower strengths. Furthermore, in most cases, specimens with polished edges and bottom surfaces had greater scatter than unpolished specimens. Hence, polishing appears to be detrimental to specimen strength characterization instead of yielding a higher, more accurate, strength as a result of removing inherent manufacture and handling flaws in the material.

The trend of decreasing strength with increasing specimen width, and hence increasing volume, that would be anticipated from the Weibull scaling law was not clearly apparent. In contrast, a decrease in strength with increasing span was observed for 3-point and 4-point bending for all three materials. However, this expected scaling was occasionally masked by more significant panel-to-panel variability. In addition, for the 4-point bending tests, a decrease in strength with increasing inner and outer span length was also observed for the two glass-epoxy materials. However, the variation in strength with span length was not as consistent for the carbon-epoxy materials. Because failure initiates on the bottom surface in these flexure tests, the differences in strength observed for specimens with different thicknesses may be attributed more to variability between panels than to the classical weakest link effect, which assumes a greater probability of a defect causing failure in a thicker laminate with a larger volume.

For all three materials, scatter increased with increasing width for specimens tested in 3-point bending. However, scatter decreased with increasing 3-point span for all three materials. For all three materials, scatter in the 4-point bending tests typically increased with increasing span length. However, this trend was not consistent for all four configurations tested.

Histograms were plotted showing the frequency of occurrence of the failure locations relative to the center load nose in 3-point bending and relative to the inner load noses where the tension stress is a maximum in 4-point bending. For 3-point bending, failure occurred near, but not always

directly under, the center load nose where the beam theory indicates the tension stress is a maximum, thus illustrating the sensitive to flaws in the microstructure. For 4-point bending, failures occurred primarily between the inner load noses, where the beam theory indicates the tension stress is a maximum. However, some failures also occurred under these load points, and between the inner and outer load noses, reflecting the sensitive to flaws in the microstructure. In addition, failures were concentrated more toward one load nose for the longest span of the S2/8552 glass-epoxy material and for most configurations of the IM7/8552 carbon-epoxy material.

In most cases, the Weibull scaling law over predicted changes in transverse tension strengths in three point bend tests and under predicted changes in transverse tension strengths in four point bend tests. Furthermore, the Weibull slope varied with specimen configuration, volume and sample size. Hence, this scaling law was not adequate for predicting transverse tension strength of heterogeneous, fiber-reinforced, polymer matrix composites.

REFERENCES

1) Minguet, P.J, and O'Brien, T.K., "Analysis of Test Methods for Characterizing Skin/Stringer Debonding Failures in Reinforced Composite Panels", *Composite Materials: Testing and Design, Twelfth Volume, ASTM STP 1274*, August, 1996, p.105-124.

2) O'Brien, T.K., and Sen, J.K., "Tension-Torsion Behavior of Glass-epoxy Flexbeam Laminatetes", *ASTM Journal of Composites Technology and Research, JCTRER*, Vol. 20, No.4, October, 1998, pp. 221-226.

3) Weibull, W., "A Statistical Theory of the Strength of Materials", *Ing. Vetenskaps Akad. Handl. (Royal Swedish Institute Engineering Research Proceedings)* NR151, 1939.

4) O'Brien, T. K. and Salpekar, S. A., "Scale Effects on the Transverse Tensile Strength of Carbon-epoxy Composites", *Composite Materials: Testing and Design, Eleventh Volume, ASTM STP 1206*, 1993, pp.23-52.

5) Bullock, R.E., "Strength Ratios of Composite Materials in Flexure and in Tension", *Journal of Composite Materials*, Vol.8, April. 1974, p.200.

ACKNOWLEDGEMENTS

APPENDIX

The Weibull theory was used to describe the probability of survival of a specimen containing a distribution of flaws throughout its volume and subjected to a stress distribution σ (x, y, z):

$$S = \exp\left\{-\int_V \left[\frac{\sigma(x,y,z)-\sigma_u}{\sigma_o}\right]^m dxdydz\right\} \qquad (A.1)$$

where
   m is the Weibull slope,
   σ_o is the characteristic strength,
   σ_u is the threshold stress below which the material will never fail,
   V is the volume of the specimen that is being stressed.

The probability of survival for a specimen subjected to a uniform tensile stress throughout the volume was derived as:

$$S_t = \exp\left\{-V_t\left(\frac{\sigma_t}{\sigma_o}\right)^m\right\} \qquad (A.2)$$

and that the probability of survival for a rectangular specimen under three-point bending was derived as:

$$S_{3pt} = \exp\left\{-V_f^{3pt}\left(\frac{\sigma_f^{3pt}}{\sigma_o}\right)^m\left[\frac{1}{2(m+1)^2}\right]\right\} \qquad (A.3)$$

where σ_f^{3pt} is the maximum tensile stress at the central point load and V_f^{3pt} is the volume of the specimen between the supports. Therefore, the ratio of the median failure stresses in three-point bending and tension was obtained by setting $S_{3pt}=S_t$ in equation A.2 and A.3, yielding:

$$\frac{\sigma_f^{3pt}}{\sigma_t} = \left[2(m+1)^2\frac{V_t}{V_f^{3pt}}\right]^{1/m} \qquad (A.4)$$

The probability of survival may also be calculated for a rectangular specimen under four-point loading. The dimensions are defined in Figure A.1
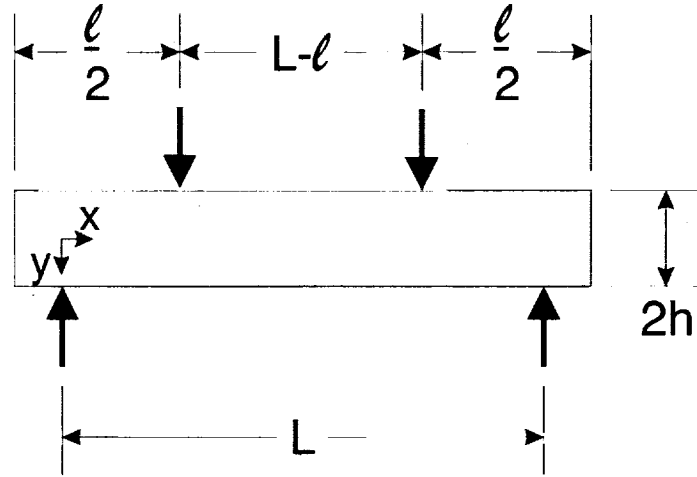
Figure A.1 Four-point bending specimen geometry

The stress distribution in the part of the specimen subjected to tension (bottom half of the specimen) is:

$$\sigma(x,y) = \begin{cases} \dfrac{2\sigma_f xy}{\ell h} & if\ 0 < x < \dfrac{\ell}{2} \\[2ex] \dfrac{\sigma_f y}{h} & if\ \dfrac{\ell}{2} < x < L - \dfrac{\ell}{2} \\[2ex] \dfrac{-2\sigma_f(x-L)y}{\ell h} & if\ L - \dfrac{\ell}{2} < x < L \end{cases} \tag{A.5}$$

Placing equation A.5 into equation A.1 and integrating over the volume of the specimen that is under tensile stress, yields:

$$S_{4pt} = \exp\left\{ -V_f^{4pt}\left(\frac{\sigma_f^{4pt}}{\sigma_o}\right)^m \frac{\left(m+1-\dfrac{\ell m}{L}\right)}{2(m+1)^2} \right\} \tag{A.6}$$

where V_f^{4pt} is the volume of the specimen between the support:

$$V_f^{4pt} = 2bhL \tag{A.7}$$

Therefore, the ratio of the median failure stress in four-point bending and tension is obtained by setting $S_{4pt}=S_t$ in equations A.2 and A.6, yielding:

$$\frac{\sigma_f^{4pt}}{\sigma_t} = \left[\frac{2(m+1)^2}{\left(m+1-\dfrac{\ell m}{L}\right)} \frac{V_t}{V_f^{4pt}} \right]^{1/m} \tag{A.8}$$

The ratio of the median failure stress in three-point and four-point bending is obtained by setting $S_{3pt}=S_{4pt}$ in equations A.3 and A.6, yielding:

$$\frac{\sigma_f^{4pt}}{\sigma_f^{3pt}} = \left[\left(\frac{1}{m+1-\dfrac{\ell m}{L}} \right) \frac{V_f^{3pt}}{V_f^{4pt}} \right]^{1/m} \tag{A.9}$$

In our study, configuration A1 and B3 are quadrant-point loading configurations, i.e. $\ell = L/2$. Therefore, equation A.8 and A.9 become:

$$\frac{\sigma_f^{4pt}}{\sigma_t} = \left[\frac{4(m+1)^2}{(m+2)} \frac{V_t}{V_f^{4pt}} \right]^{1/m} \tag{A.10}$$

and

$$\frac{\sigma_f^{4pt}}{\sigma_f^{3pt}} = \left[\left(\frac{2}{m+2} \right) \frac{V_f^{3pt}}{V_f^{4pt}} \right]^{1/m} \tag{A.11}$$

Equation A.10 and A.11 are shown as equation 12 and 13 in the text and agree with note 1 concerning quadrant-point loading in reference [5].

For configuration A2, $\dfrac{\ell}{L} = \dfrac{2}{3}$ and equation A.9 becomes:

$$\frac{\sigma_f^{4pt}}{\sigma_f^{3pt}} = \left[\left(\frac{3}{m+3} \right) \frac{V_f^{3pt}}{V_f^{4pt}} \right]^{1/m} \tag{A.12}$$

For configuration B2, $\dfrac{\ell}{L} = \dfrac{1}{3}$ and equation A.9 becomes:

$$\frac{\sigma_f^{4pt}}{\sigma_f^{3pt}} = \left[\left(\frac{3}{2m+3} \right) \frac{V_f^{3pt}}{V_f^{4pt}} \right]^{1/m} \tag{A.13}$$

Four-point bending configurations A2 and A1 may be compared by taking the ratio of equations A.11 and A.12:

$$\sigma_{A2}^{4pt} = \left[\frac{3}{2} \left(\frac{m+2}{m+3} \right) \right]^{1/m} \sigma_{A1}^{4pt} \tag{A.14}$$

Similarly, for A1 and B2:

$$\sigma_{B2}^{4pt} = \left[\frac{3}{2} \left(\frac{m+2}{2m+3} \right) \right]^{1/m} \sigma_{A1}^{4pt} \tag{A.15}$$

Table 1. S2/F584 glass epoxy test sets

Panel	(•)Config.& set number	Length mm (in)	Polished surfaces	Average t, mm (in)	thickness CV, %	Stroke rate, mm/min (in/min)
TO3	B-2	57.2 (2.25)	none	4.50 (0.177)	3.2	0.635 (0.025)
	B-3	57.2 (2.25)	edges	4.67 (0.184)	1.5	0.635 (0.025)
	B-4	57.2 (2.25)	bottom	4.57 (0.180)	1.8	0.635 (0.025)
TO5	B-B	57.2 (2.25)	edges+bottom	4.67 (0.184)	3.7	0.635 (0.025)
	*B-C	57.2 (2.25)	none	4.75 (0.187)	3.7	0.635 (0.025)
	**B-D	57.2 (2.25)	none	4.75 (0.187)	3.7	0.635 (0.025)
TN2	B-A	57.2 (2.25)	edges	4.37 (0.172)	2.7	0.635 (0.025)
	B-B	57.2 (2.25)	edges+bottom	4.39 (0.173)	3.1	0.635 (0.025)
	*B-C	57.2 (2.25)	edges	4.39 (0.173)	2.7	0.635 (0.025)
	**B-D	57.2 (2.25)	edges	4.39 (0.173)	2.4	0.635 (0.025)
TN3	A	31.8 (1.25)	edges	4.37 (0.172)	1.6	1.59 (0.0625)
	B	57.2 (2.25)	edges	4.11 (0.162)	1.5	0.635 (0.025)
	C	82.6 (3.25)	edges	4.32 (0.170)	1.5	1.27 (0.05)
	B3	108 (4.25)	edges	4.44 (0.175)	1.7	5.08 (0.20)
TN6	B	57.2 (2.25)	edges	4.19 (0.165)	3.0	0.635 (0.025)
	A1	57.2 (2.25)	edges	4.42 (0.174)	2.9	1.27 (0.05)
	A2	82.6 (3.25)	edges	4.39 (0.173)	3.1	3.05 (0.12)
	B2	82.6 (3.25)	edges	4.42 (0.174)	2.8	2.03 (0.08)

All specimens 6.35 mm (0.25 in) wide, except * 12.7 mm (0.5 in) wide and ** 19.1 mm (0.75 in) wide

(•) see figure 3

Table 2. S2/8552 glass epoxy test sets

Panel Quad	(•) Config.& set number	Length, mm (in)	Polished surfaces	Average t, mm (in)	thickness CV, %	Stroke rate, mm/min (in/min)
I-IV	B-A	57.2 (2.25)	none	5.59 (0.220)	2.5	1.02 (0.04)
I-IV	B-B	57.2 (2.25)	edges+bottom	5.54 (0.218)	2.4	1.02 (0.04)
I-IV	*B-C	57.2 (2.25)	none	5.59 (0.220)	2.5	1.02 (0.04)
I-IV	**B-D	57.2 (2.25)	none	5.59 (0.220)	2.4	1.27 (0.05)
I	B-1	57.2 (2.25)	none	5.54 (0.218)	1.1	1.02 (0.04)
II	B-2	57.2 (2.25)	edges	5.61 (0.221)	1.4	1.02 (0.04)
III	A	31.8 (1.25)	none	5.61 (0.221)	1.5	0.203 (0.008)
IV	B	57.2 (2.25)	none	5.28 (0.208)	1.8	1.02 (0.04)
I	C	82.6 (3.25)	none	5.56 (0.219)	1.3	1.91 (0.075)
II	A1	57.2 (2.25)	none	5.59 (0.220)	1.5	1.27 (0.05)
II	A2	82.6 (3.25)	none	5.64 (0.222)	1.6	5.08 (0.20)
III	B2	82.6 (3.25)	none	5.61 (0.221)	1.6	1.78 (0.07)
IV	B3	108 (4.25)	none	5.56 (0.219)	1.7	4.06 (0.16)

All specimens 6.35 mm (0.25 in) wide, except * 12.7 mm (0.5 in) wide and ** 19.1 mm (0.75 in) wide
(•) see figure 3

Table 3. IM7/8552 Carbon epoxy test sets

Panel	(•) Config.& set number	Length, mm (in)	Polished surfaces	Average t, mm (in)	thickness CV, %	Stroke rate, mm/min (in/min)
24-1	B-A	57.2 (2.25)	edges	3.30 (0.130)	4.3	2.29 (0.09)
	B-B	57.2 (2.25)	bottom	3.30 (0.130)	4.0	2.29 (0.09)
	B-C	57.2 (2.25)	edges+bottom	3.33 (0.131)	2.6	2.29 (0.09)
	B-D	57.2 (2.25)	none	3.35 (0.132)	2.9	2.29 (0.09)
	*B-E	57.2 (2.25)	none	3.35 (0.132)	3.8	2.29 (0.09)
	**B-F	57.2 (2.25)	none	3.33 (0.131)	3.4	2.03 (0.08)
24-2	A	31.8 (1.25)	none	3.35 (0.132)	2.3	0.508 (0.02)
	B	57.2 (2.25)	none	3.17 (0.125)	2.7	2.29 (0.09)
	C	82.6 (3.25)	none	3.25 (0.128)	2.3	4.57 (0.18)
	A1	57.2 (2.25)	none	3.17 (0.125)	4.4	2.03 (0.08)
	A2	82.6 (3.25)	none	3.43 (0.135)	2.0	4.57 (0.18)
	B2	82.6 (3.25)	none	3.43 (0.135)	2.0	3.30 (0.13)
36-1	A	31.8 (1.25)	none	4.44 (0.175)	1.9	3.30 (0.13)
	B	57.2 (2.25)	none	5.21 (0.205)	1.2	1.27 (0.05)
	C	82.6 (3.25)	none	4.75 (0.187)	2.3	2.54 (0.10)
	A1	57.2 (2.25)	none	5.13 (0.202)	1.4	1.02 (0.04)
	A2	82.6 (3.25)	none	4.93 (0.194)	2.8	2.79 (0.11)
	B2	82.6 (3.25)	none	4.98 (0.196)	2.3	2.03 (0.08)
	B3	108 (4.25)	none	5.08 (0.200)	2.1	4.83 (0.19)

All specimens 6.35 mm (0.25 in) wide, except * 12.7 mm (0.5 in) wide and ** 19.1 mm (0.75 in) wide
(•) see figure 3

Table 4. S2/F584 glass epoxy strength and scatter

Panel	Configuration & set number	Number tested, n	δ_{max} / t_{avg}	Mean Strength, MPa (Ksi)	CV, %	Characteristic Strength, MPa (Ksi)	1/m
TO3	B-2	35	0.19	102 (14.79)	6.50	104 (15.14)	0.0592
	B-3	38	0.19	100 (14.51)	9.30	104 (15.13)	0.0830
	B-4	38	0.18	91.1 (13.22)	6.40	93.8 (13.61)	0.0550
TO5	B-B	44	0.17	96.2 (13.95)	7.40	99.3 (14.40)	0.0610
	B-C	40	0.21	96.7 (14.02)	8.70	101 (14.59)	0.0776
	B-D	35	0.18	97.6 (14.15)	7.50	101 (14.62)	0.0641
TN2	B-A	42	0.21	103 (14.87)	5.70	105 (15.24)	0.0479
	B-B	43	0.20	96.9 (14.06)	7.60	101 (14.59)	0.0707
	B-C	40	0.21	102 (14.82)	5.50	105 (15.18)	0.0467
	B-D	35	0.20	102 (14.85)	6.30	105 (15.27)	0.0539
TN3	A	47	0.07	106 (15.35)	7.80	109 (15.88)	0.0667
	B	47	0.23	105 (15.26)	7.40	109 (15.77)	0.0634
	C	47	0.47	104 (15.08)	5.80	107 (15.48)	0.0491
	B3	48	1.13	89.0 (12.91)	6.20	91.6 (13.28)	0.0530
TN6	B	47	0.21	101 (14.65)	5.60	104 (15.02)	0.0476
	A1	47	0.32	98.7 (14.31)	6.60	102 (14.74)	0.0567
	A2	47	0.67	87.8 (12.74)	6.90	90.5 (13.13)	0.0582
	B2	48	0.62	80.5 (11.68)	10.1	84.3 (12.22)	0.0898

36

Table 5. S2/8552 glass epoxy strength and scatter

Panel Quad	Config.& set number	Number tested, n	δ_{max}/t_{avg}	Mean Strength, MPa (Ksi)	CV, %	Characteristic Strength, MPa (Ksi)	1/m
I-IV	B-A	35	0.21	140 (20.30)	5.85	144 (20.84)	0.0503
I-IV	B-B	33	0.21	138 (20.00)	7.00	142 (20.61)	0.0598
I-IV	B-C	34	0.21	141 (20.43)	8.46	146 (21.21)	0.0733
I-IV	B-D	27	0.21	139 (20.10)	8.27	144 (20.84)	0.0716
I	B-1	51	0.21	145 (21.10)	6.99	150 (21.78)	0.0603
II	B-2	51	0.21	144 (20.94)	6.11	148 (21.51)	0.0515
III	A	49	0.05	145 (21.03)	7.98	150 (21.78)	0.0682
IV	B	48	0.33	145 (21.05)	6.31	149 (21.65)	0.0533
I	C	50	0.45	136 (19.78)	6.25	140 (20.33)	0.0525
II	A1	52	0.26	131 (18.99)	6.54	135 (19.55)	0.0552
II	A2	51	0.52	125 (18.07)	7.39	129 (18.69)	0.0652
III	B2	43	0.55	115 (16.64)	12.17	121 (17.50)	0.1057
IV	B3	52	0.83	101 (14.67)	8.61	105 (15.22)	0.0724

Table 6. IM7/8552 Carbon epoxy strength and scatter

Panel	Config. & set number	Number tested, n	δ_{max}/t_{avg}	MeanStrength, MPa (Ksi)	CV, %	Characteristic Strength, MPa (Ksi)	1/m
24-1	B-A	51	0.49	121 (17.58)	6.76	125 (18.11)	0.0567
	B-B	46	0.51	120 (17.41)	8.44	125 (18.07)	0.0733
	B-C	42	0.51	123 (17.85)	5.23	126 (18.27)	0.0440
	B-D	41	0.54	122 (17.76)	5.57	126 (18.21)	0.0478
	B-E	44	0.51	117 (16.95)	6.91	120 (17.47)	0.0585
	B-F	44	0.49	116 (16.80)	7.93	120 (17.39)	0.0676
24-2	A	37	0.13	129 (18.71)	6.90	133 (19.29)	0.0586
	B	37	0.51	117 (16.92)	4.77	119 (17.28)	0.0406
	C	37	1.24	126 (18.26)	4.26	128 (18.61)	0.0363
	A1	37	0.72	115 (16.62)	6.17	118 (17.08)	0.0530
	A2	37	1.34	110 (15.93)	4.88	112 (16.28)	0.0412
	B2	37	1.44	113 (16.34)	7.80	117 (16.91)	0.0675
36-1	A	41	0.11	134 (19.43)	7.20	138 (20.05)	0.0611
	B	43	0.26	127 (18.49)	6.24	131 (19.01)	0.0531
	C	43	0.67	121 (17.62)	4.10	124 (17.98)	0.0380
	A1	43	0.30	107 (15.57)	8.61	111 (16.17)	0.0748
	A2	43	0.63	111 (16.11)	5.59	114 (16.52)	0.0475
	B2	43	0.70	115 (16.68)	7.16	119 (17.21)	0.0604
	B3	42	0.98	98.8 (14.33)	10.40	103 (14.99)	0.0905

500 lb Load cell
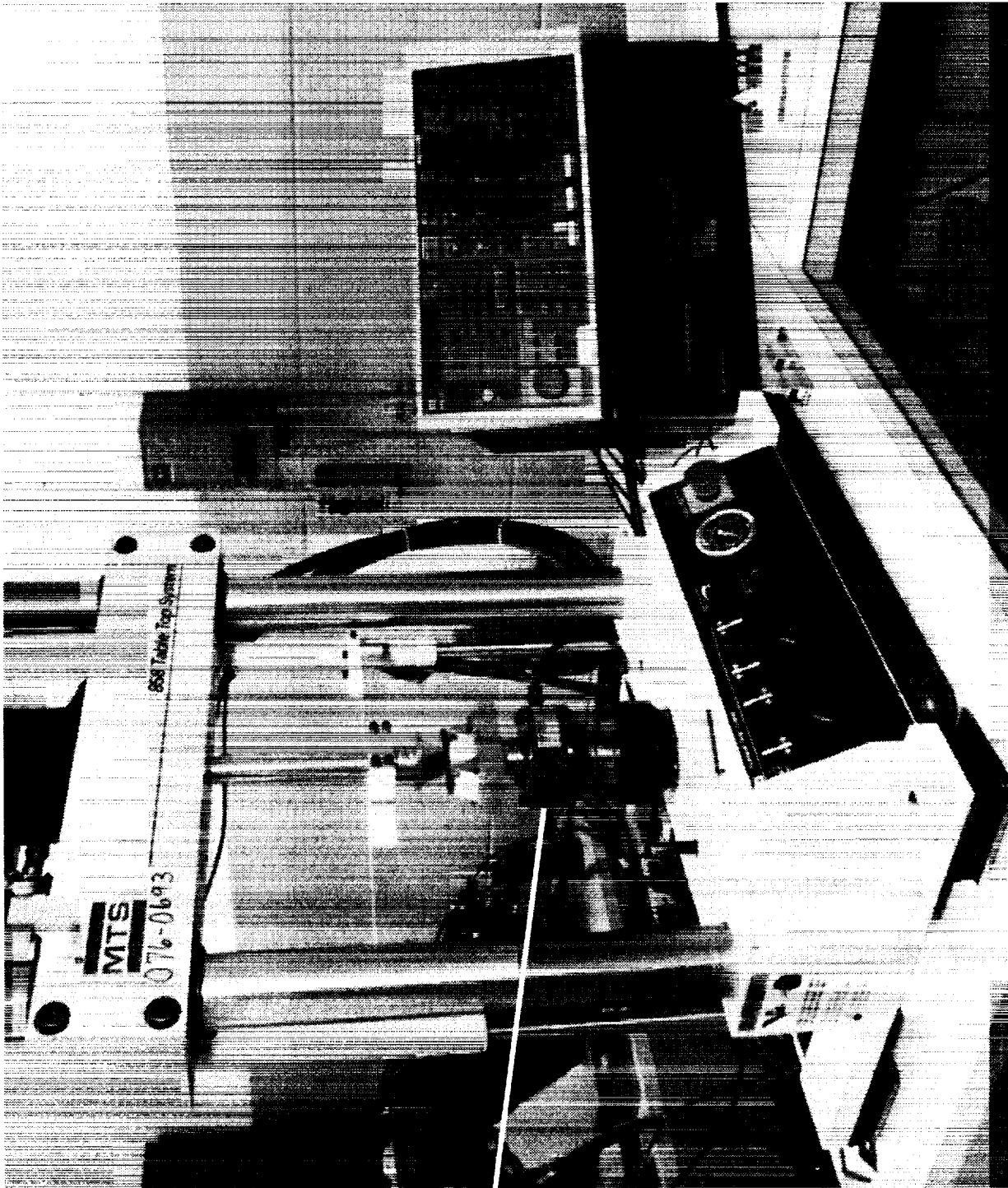
Fig.1 Hydraulic Load Frame
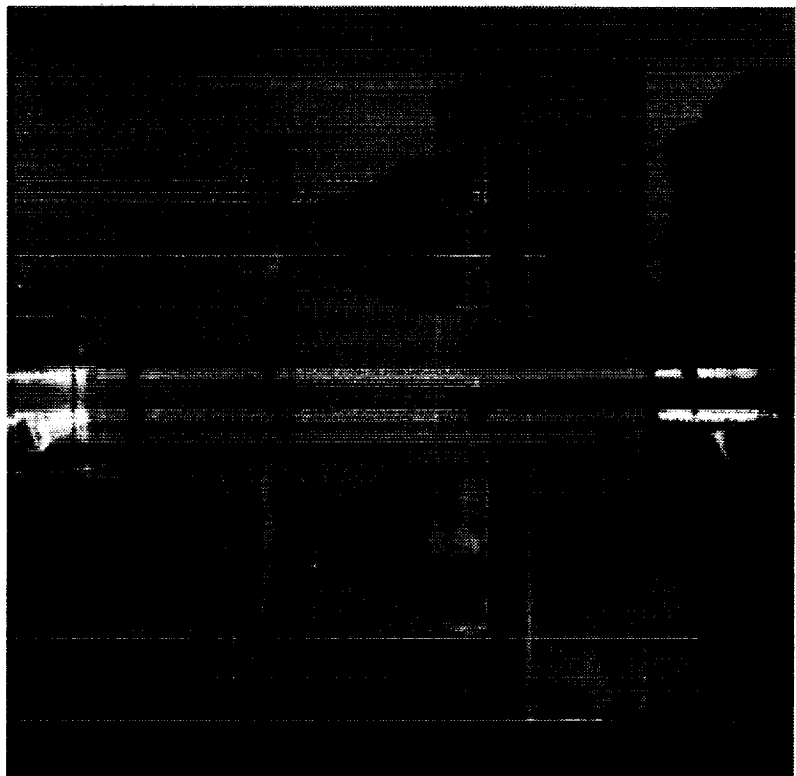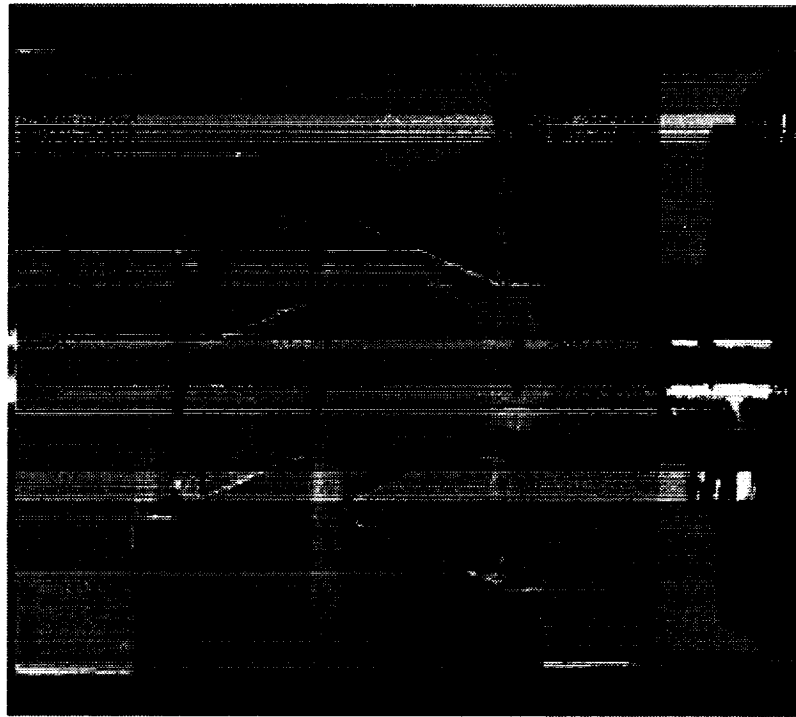
Fig.2. Test apparatus and specimens

Configuration	s, mm
A	25.4
B	50.8
C	76.2

Config.	s, mm	$\ell/2$, mm	$s\ell$, mm
A1	50.8	12.7	25.4
A2	76.2	25.4	25.4
B2	76.2	12.7	50.8
B3	102	25.4	50.8
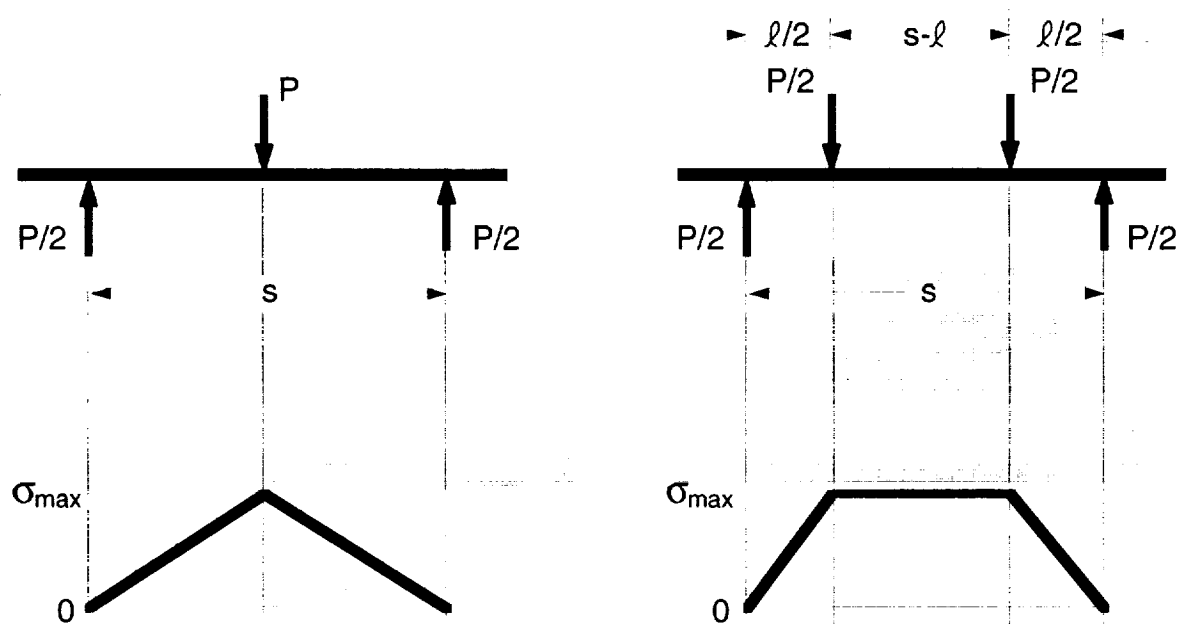
3-Point Bending

4-Point Bending

Figure 3 – (a) Bending Test Configurations and
(b)Beam Theory Stress Distributions
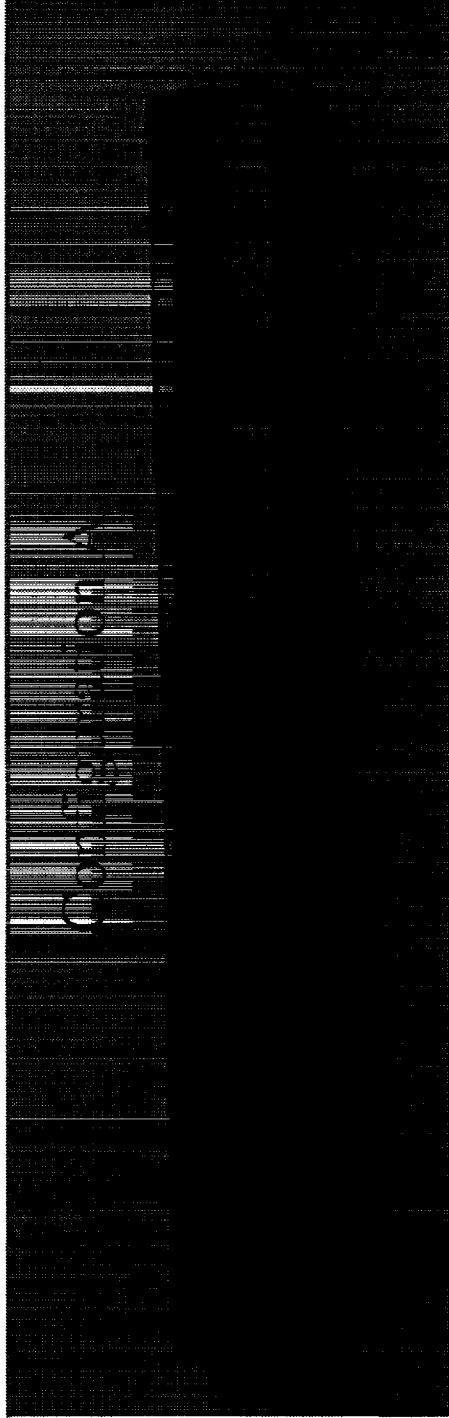
Transverse tension
failure oriented at
90 degrees to
maximum bending stress
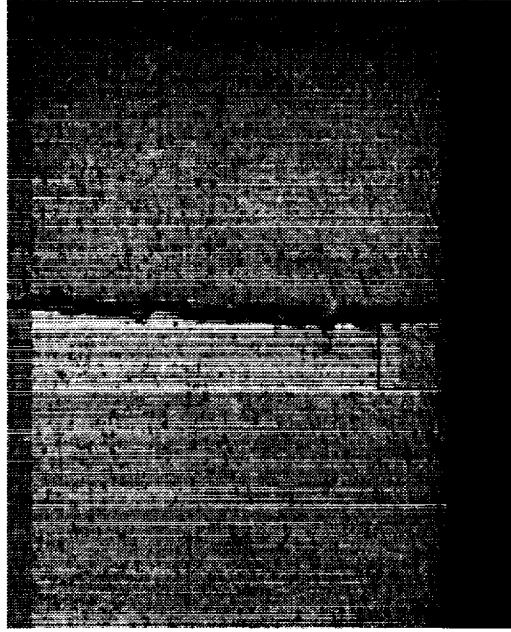
Fig. 4 - Failure Orientation for Three Point Bend Test Specimen
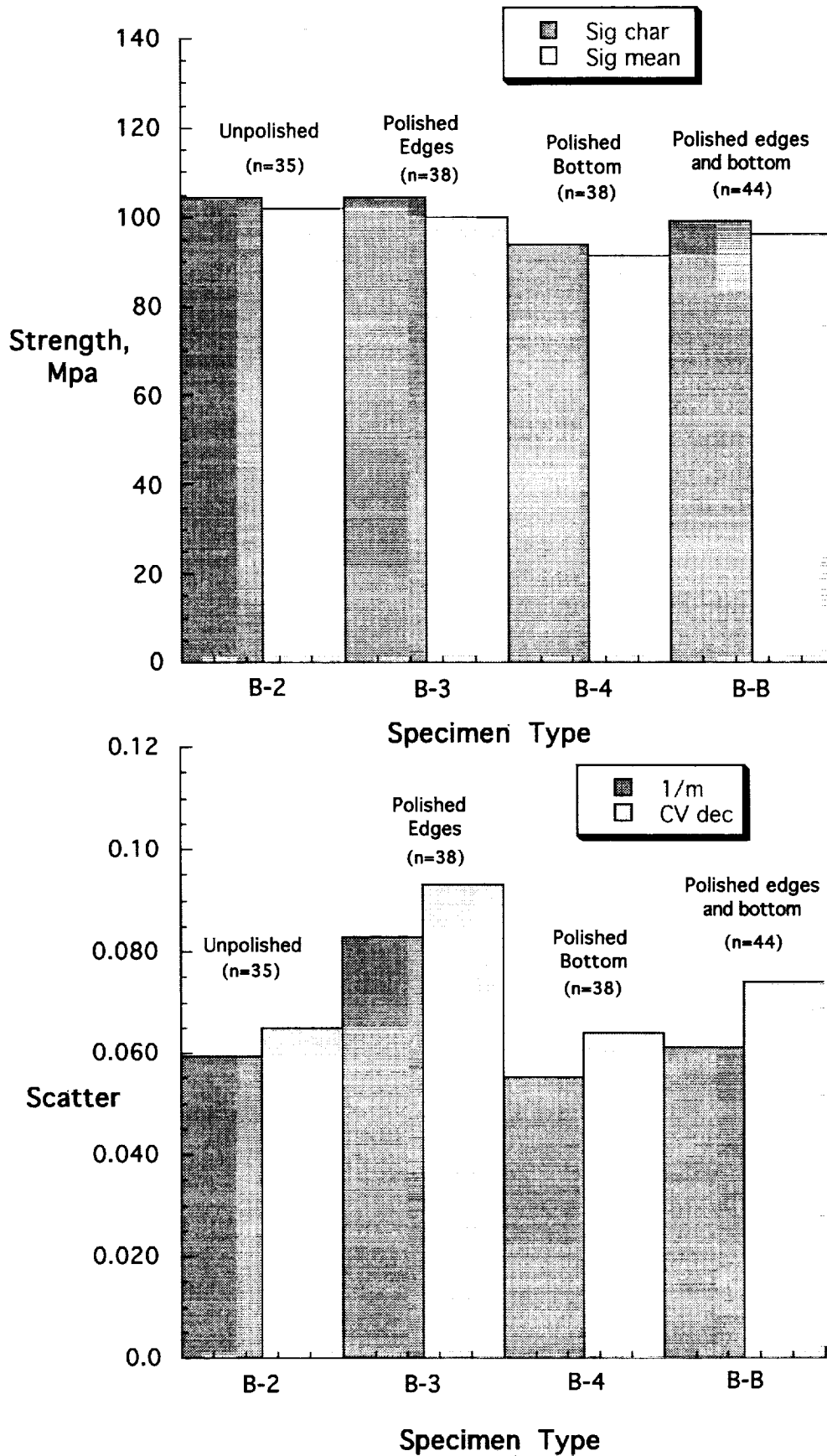
Fig. 5 – Effect of Polishing on (a) Transverse Tension Strength and (b) Scatter
S2/F584, 3-Point bending, Panels TO3 and TO5
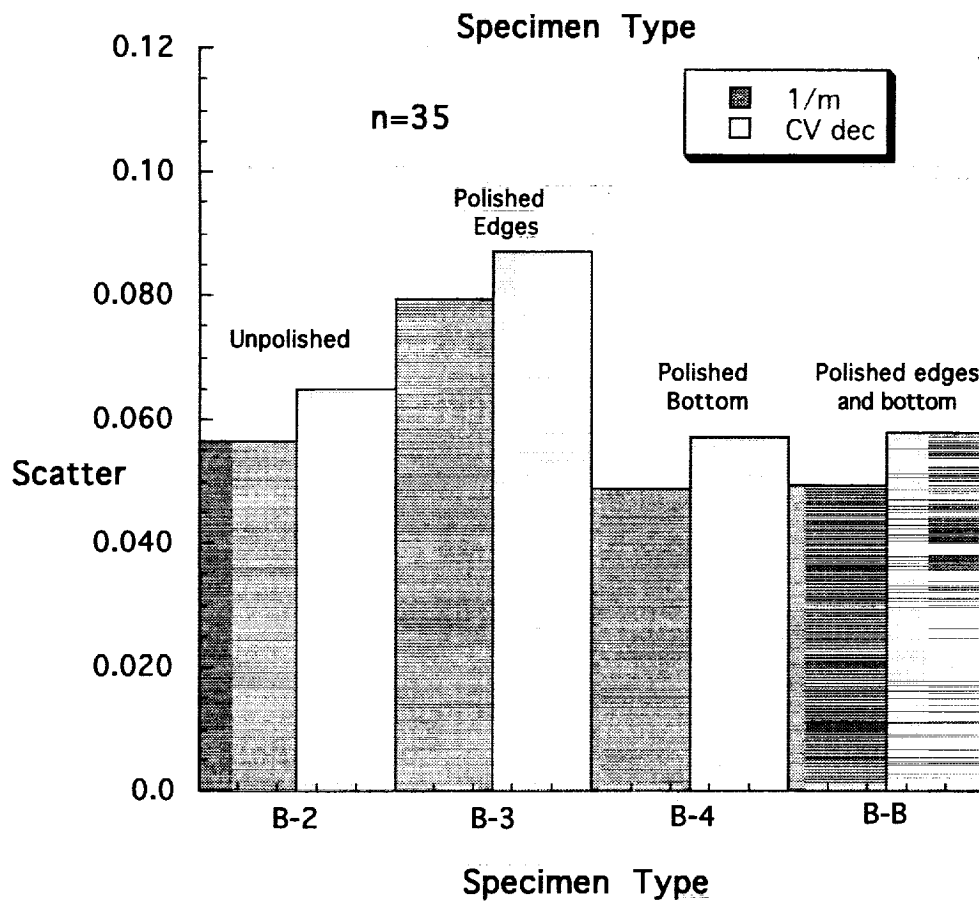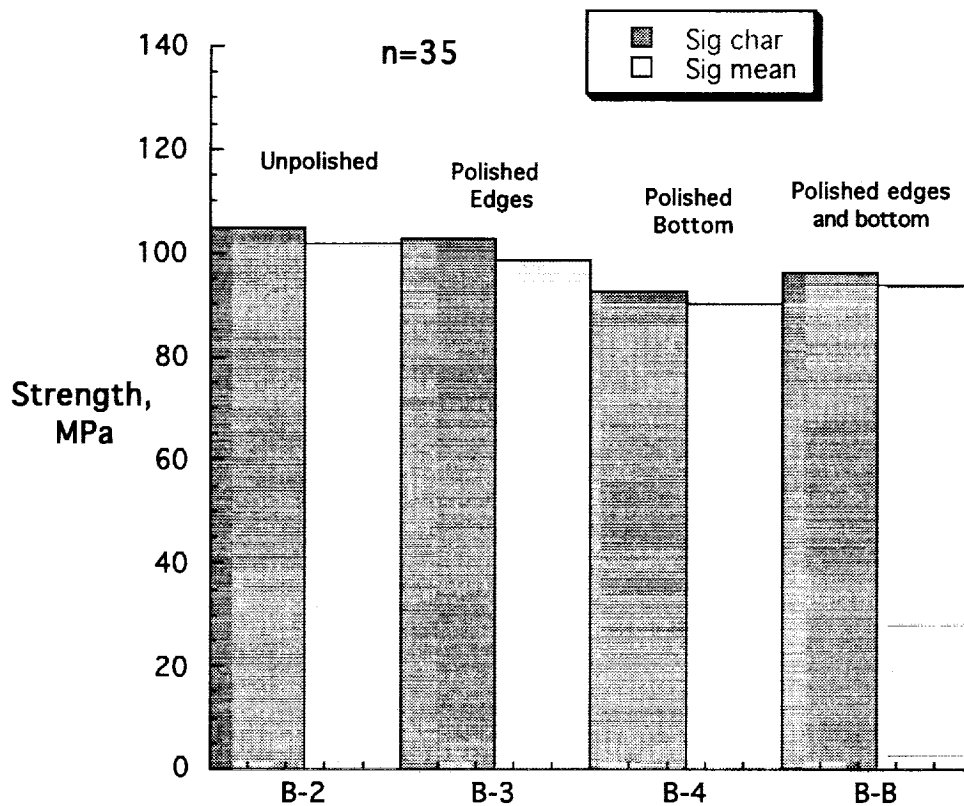
Fig. 6 – Effect of Polishing on (a) Transverse Tension Strength and (b) Scatter
S2/F584, 3-Point bending, Panels TO3 and TO5, n=35
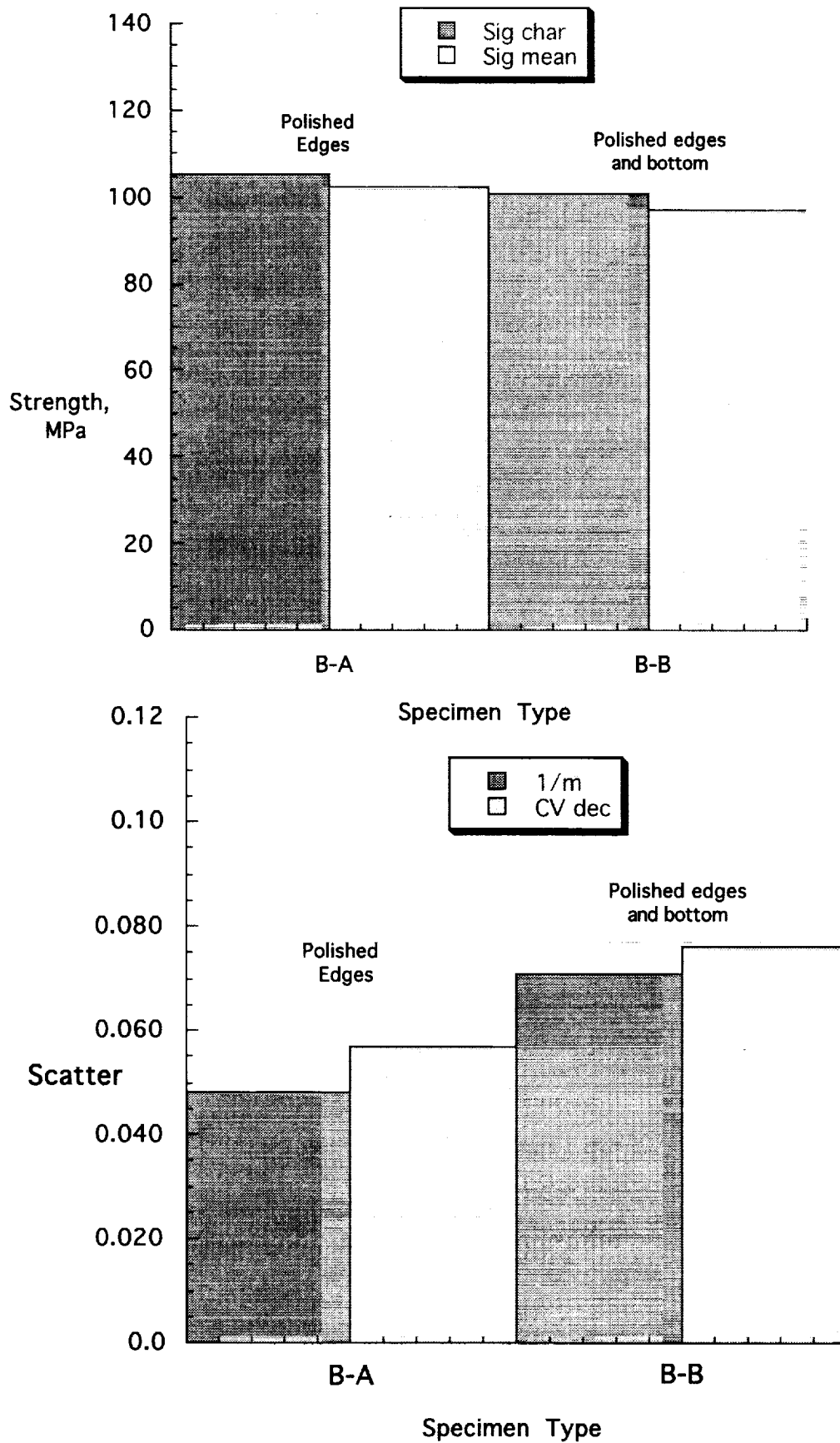
Fig. 7 – Effect of Polishing on (a) Transverse Tension Strength and (b) Scatter
S2/F584, 3-Point bending, Panel TN2
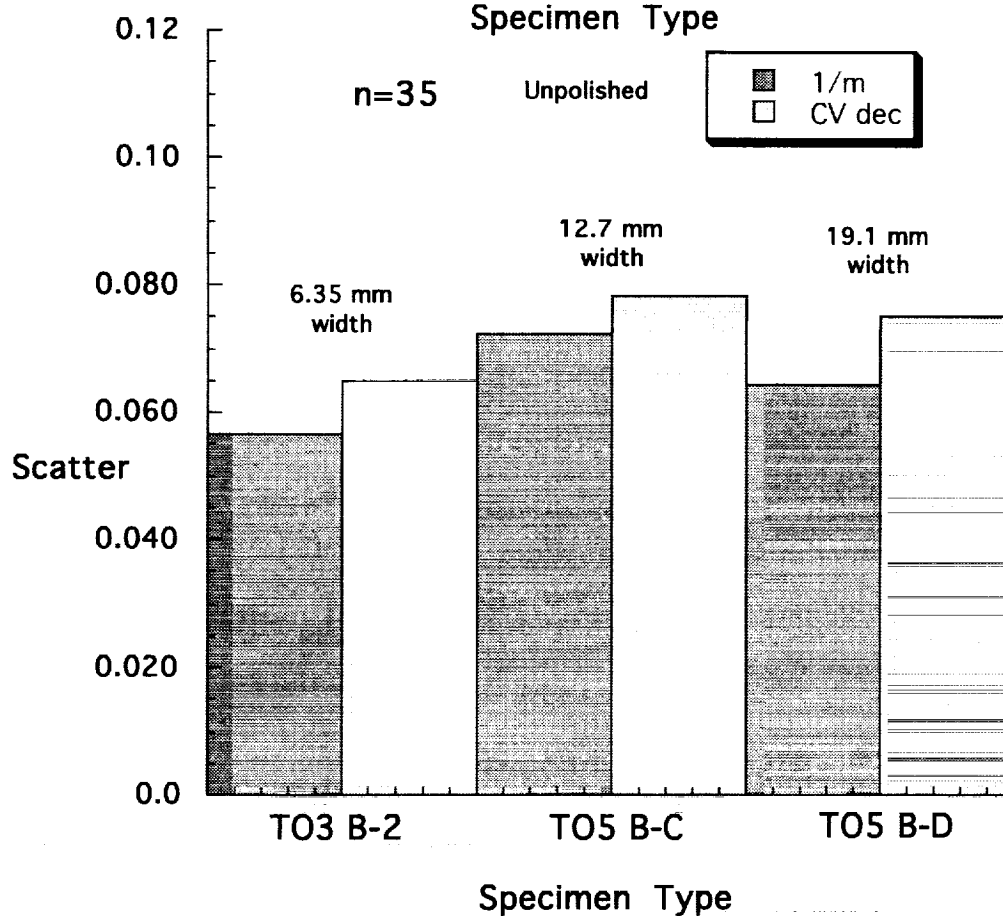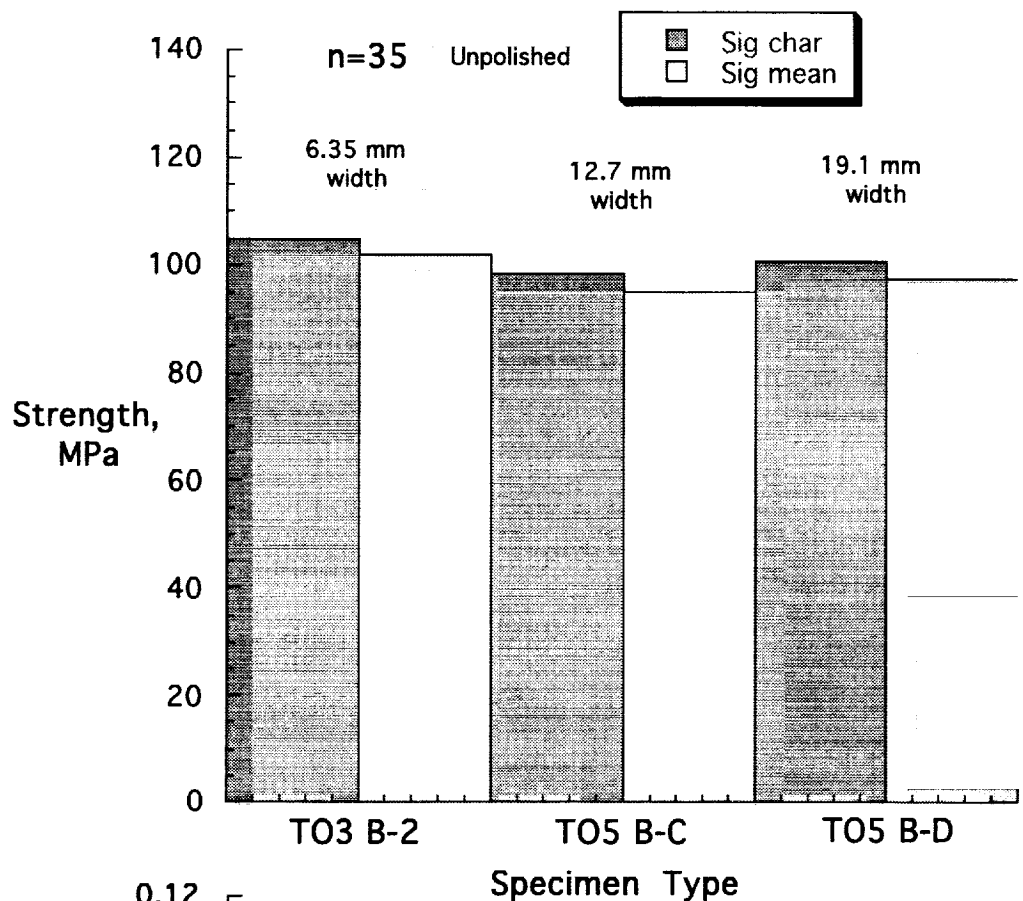
Fig. 8 – Effect of Specimen Width on (a) Transverse Tension Strength and
(b) Scatter : S2/F584, 3-Point bending, Panels TO3 and TO5, n=35
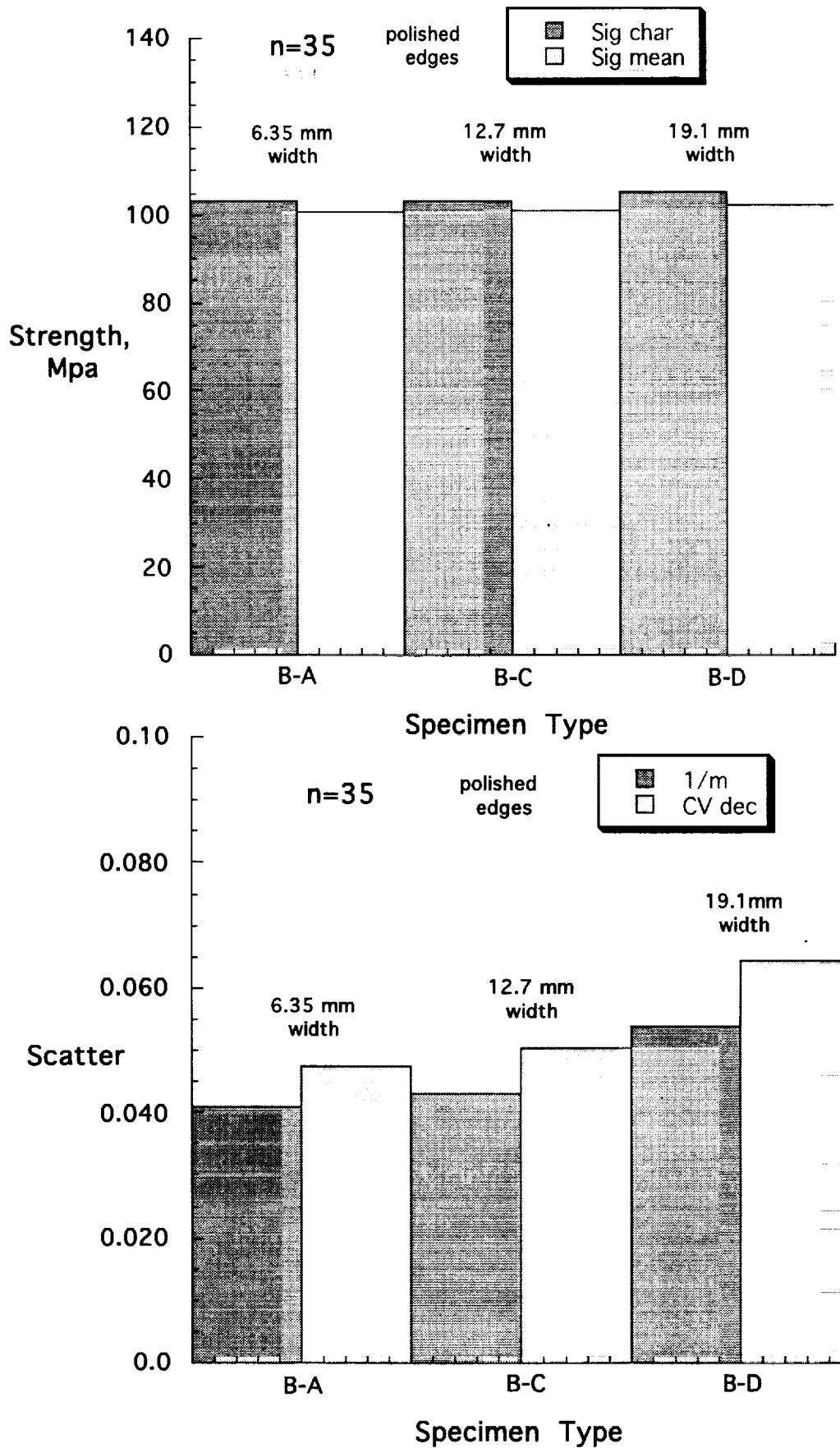
Fig. 9 – Effect of Specimen Width on (a) Transverse Tension Strength and
(b) Scatter : S2/F584, 3-Point bending, Panel TN2, n=35
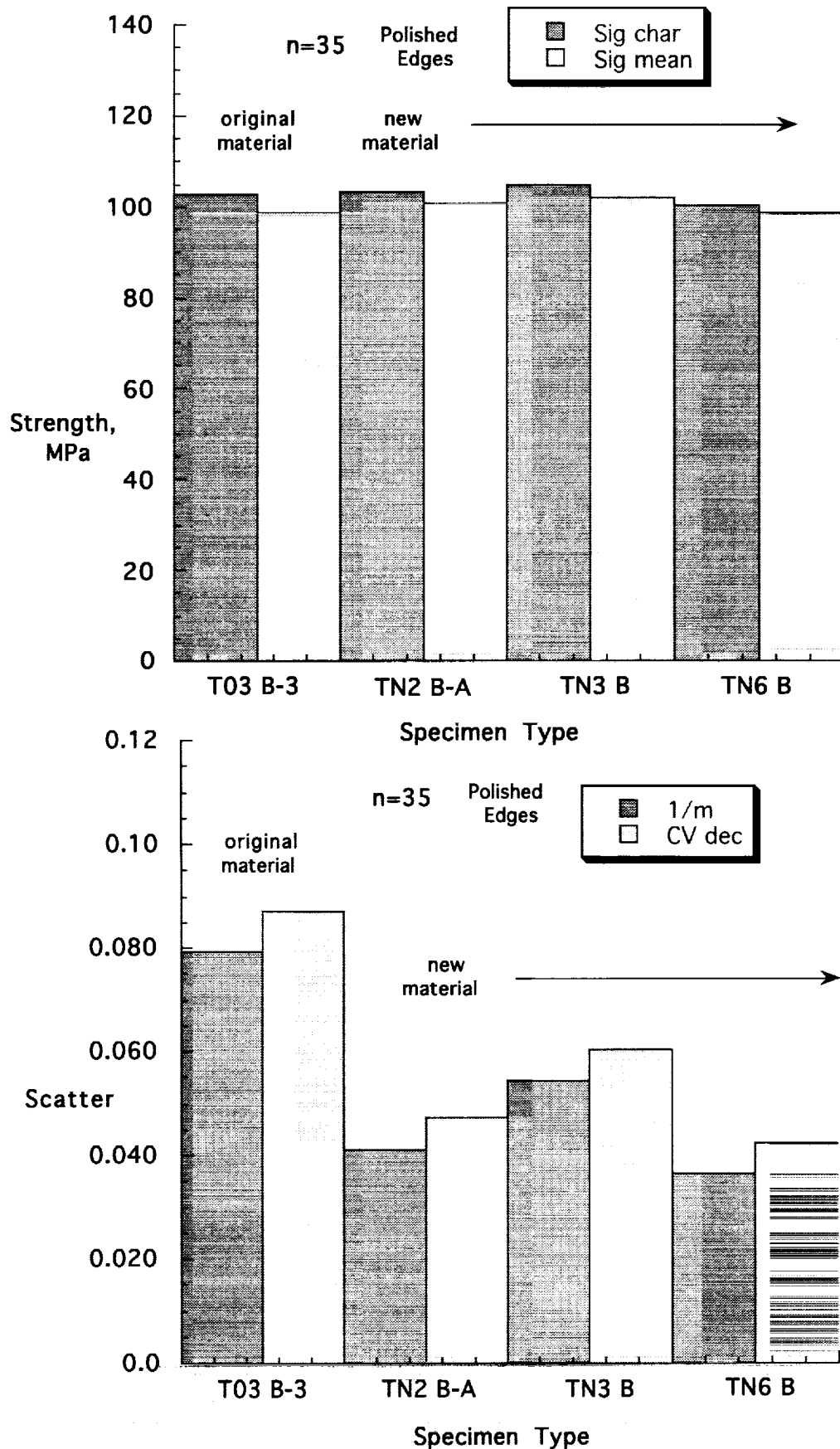
Fig. 10 – Effect of Panel Variability on (a) Transverse Tension Strength and
(b) Scatter : S2/F584, 3-Point bending, n=35
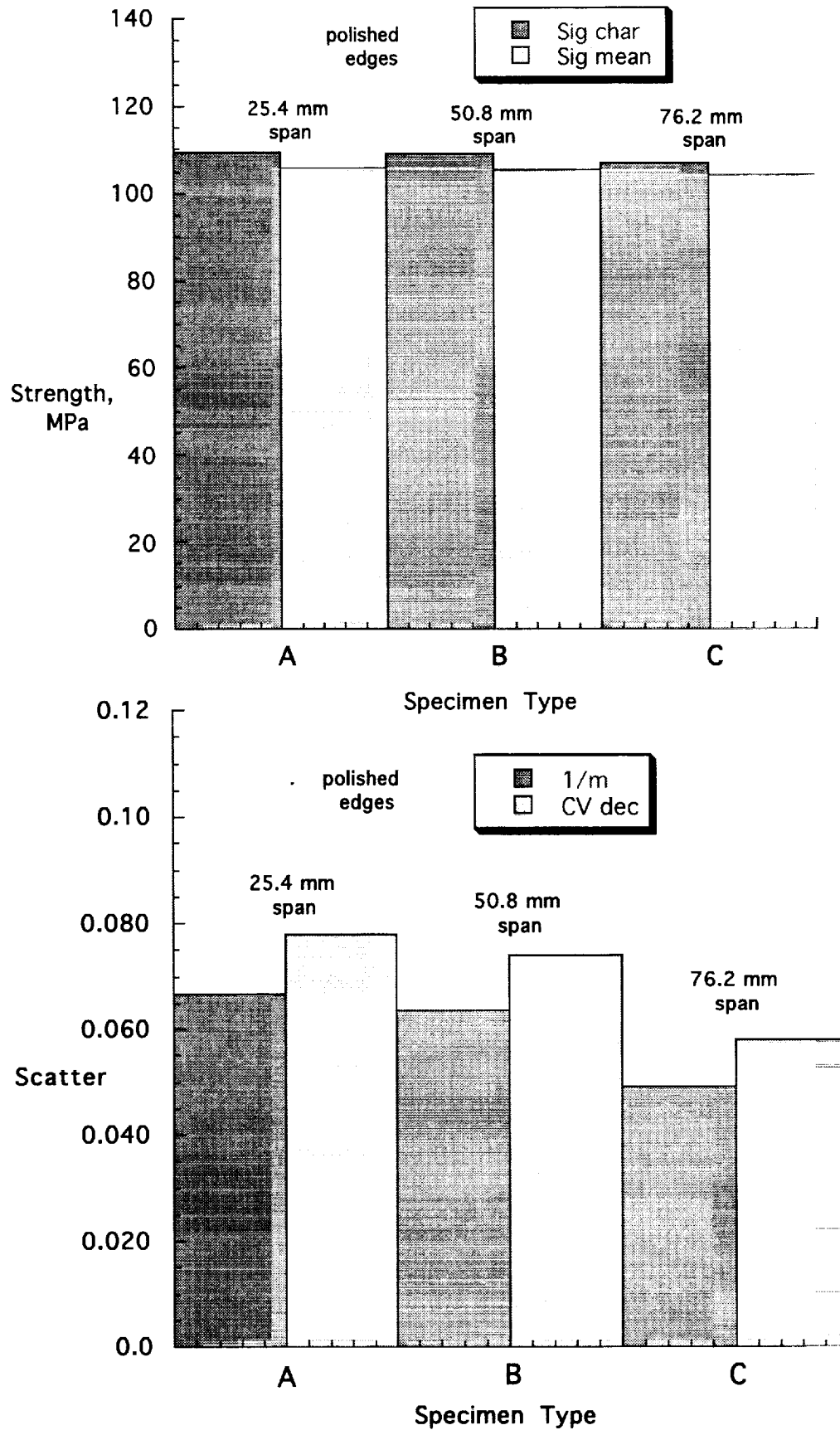
Fig. 11 – Effect of Span Length on (a) Transverse Tension Strength and
(b) Scatter : S2/F584, 3-Point bending, Panel TN3

(a)

(b)
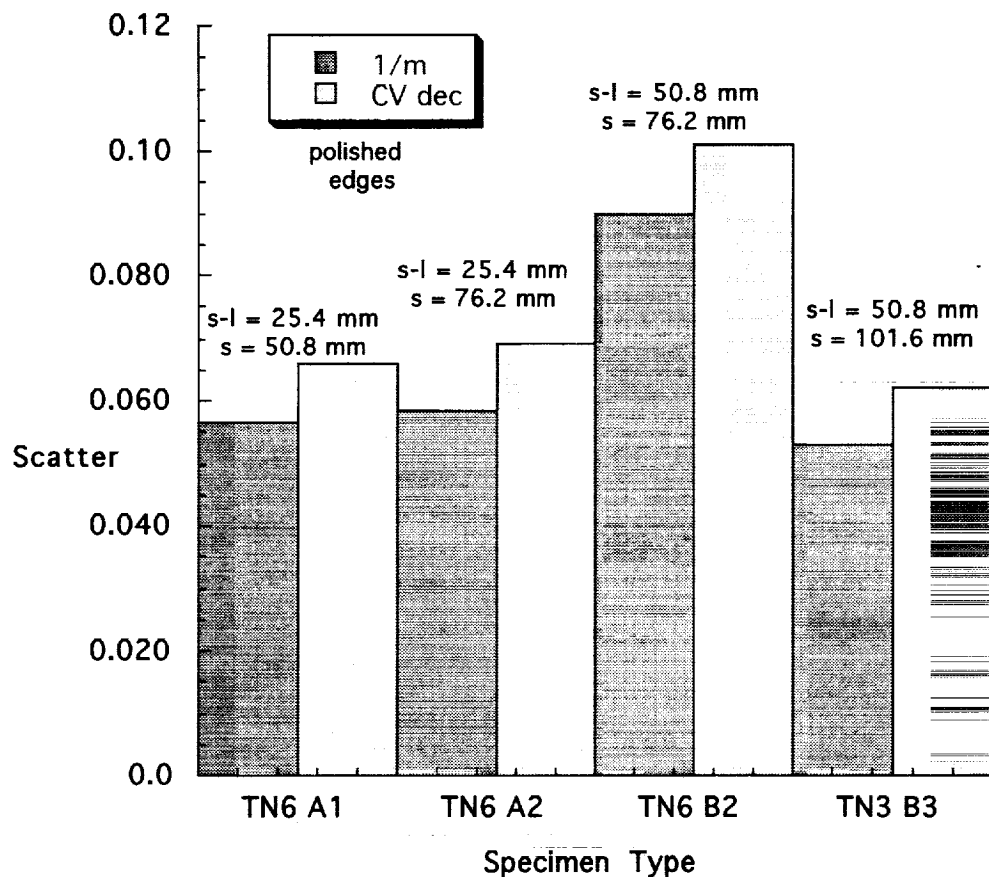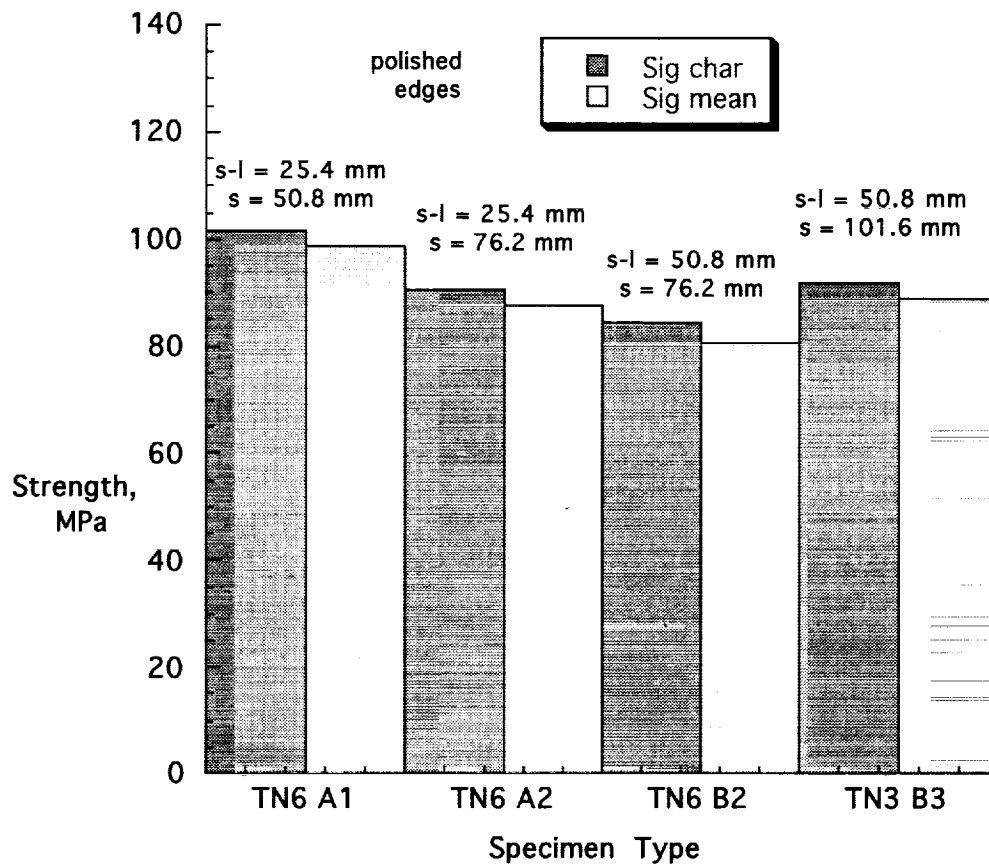
Fig. 12 – Effect of Span Length on (a) Transverse Tension Strength and (b) Scatter : S2/F584, 4-Point bending
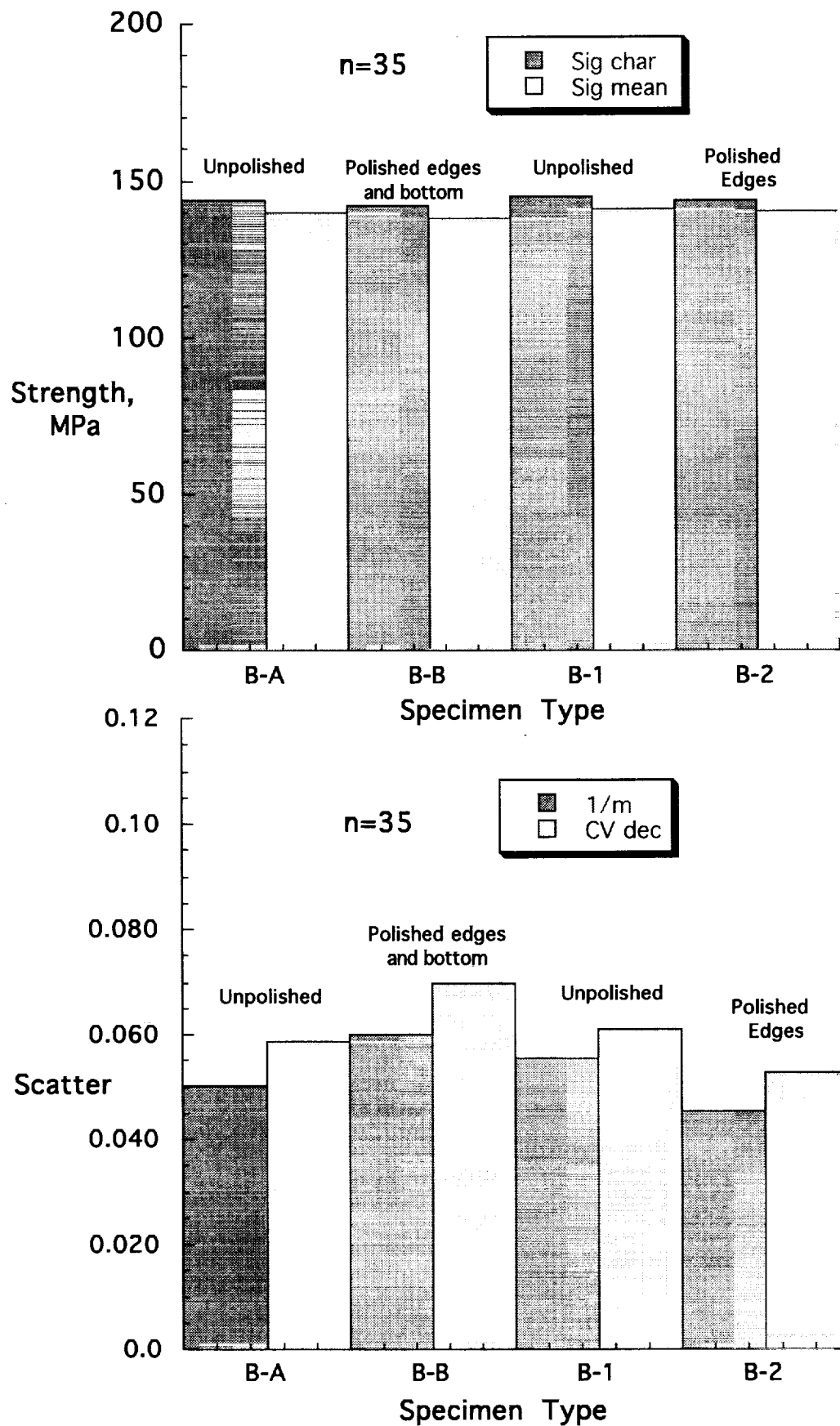
Fig. 13 – Effect of Polishing on (a) Transverse Tension Strength and (b) Scatter
S2/8552, 3-Point bending, n=35
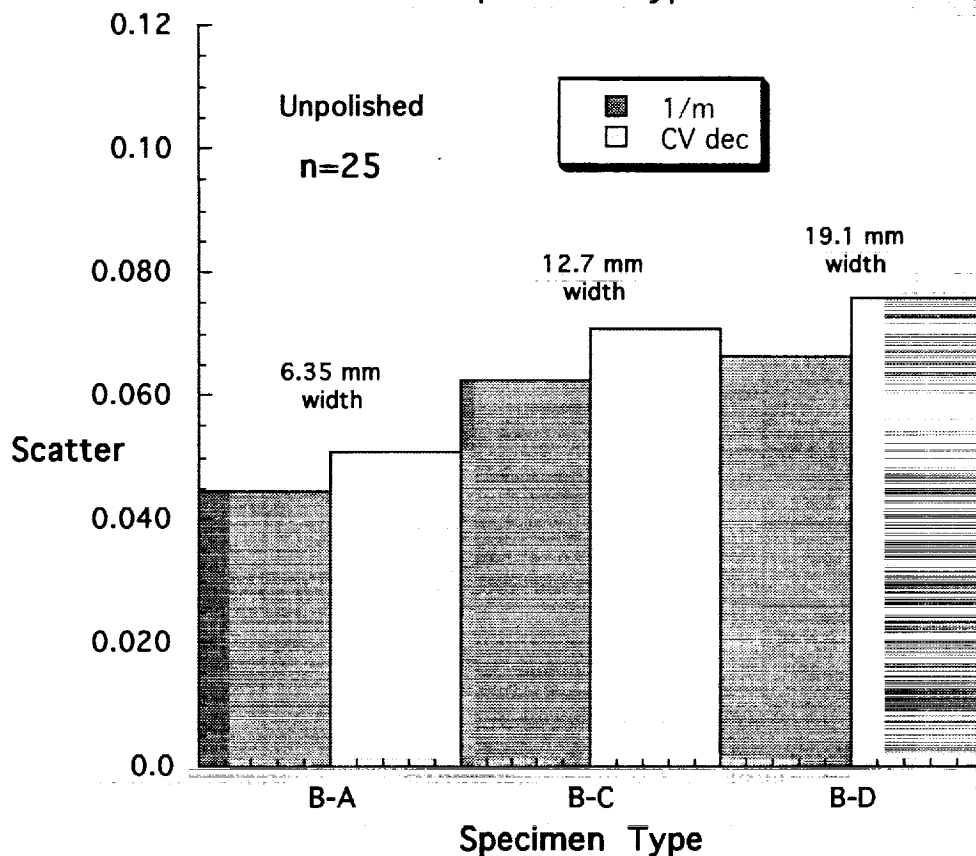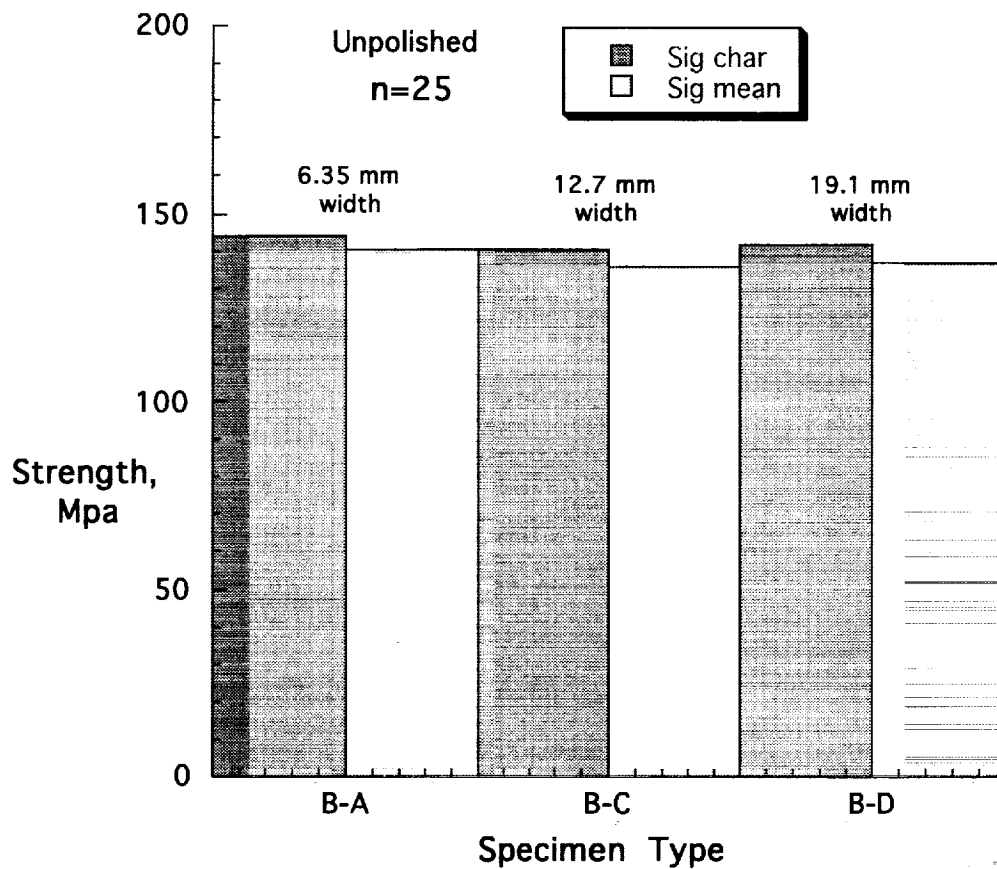
Fig. 14 – Effect of Specimen Width on (a) Transverse Tension Strength and (b) Scatter : S2/8552, 3-Point bending, n=25
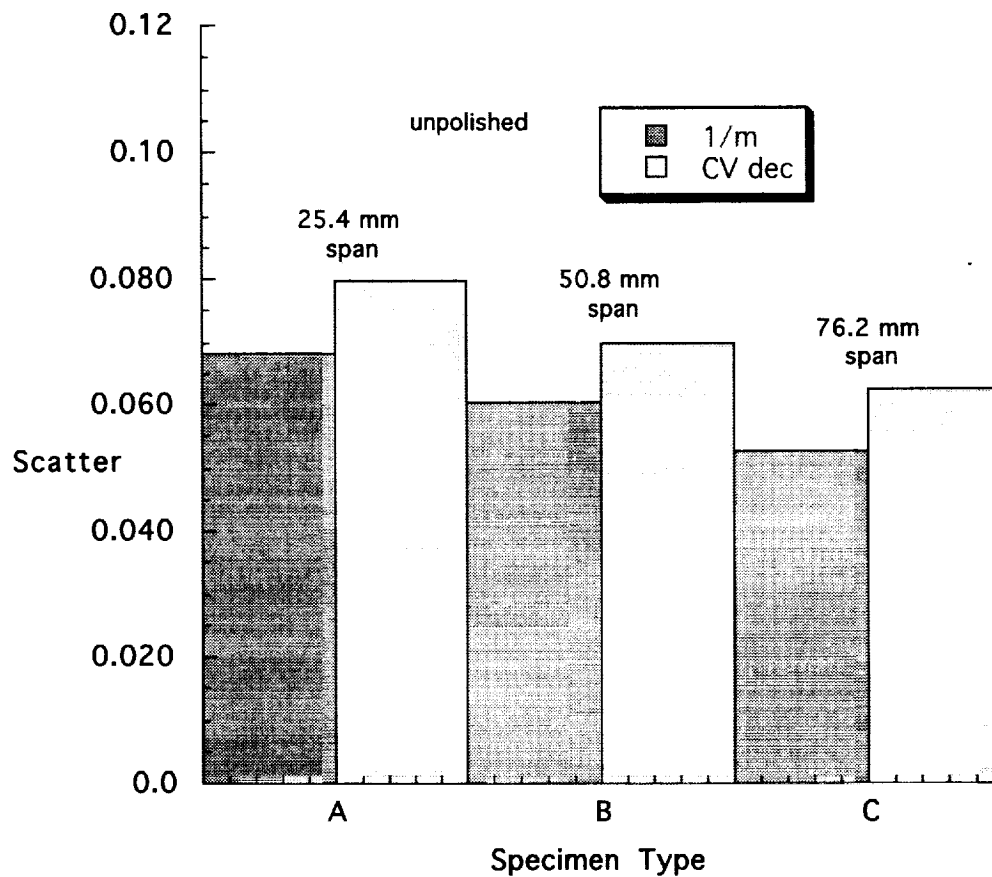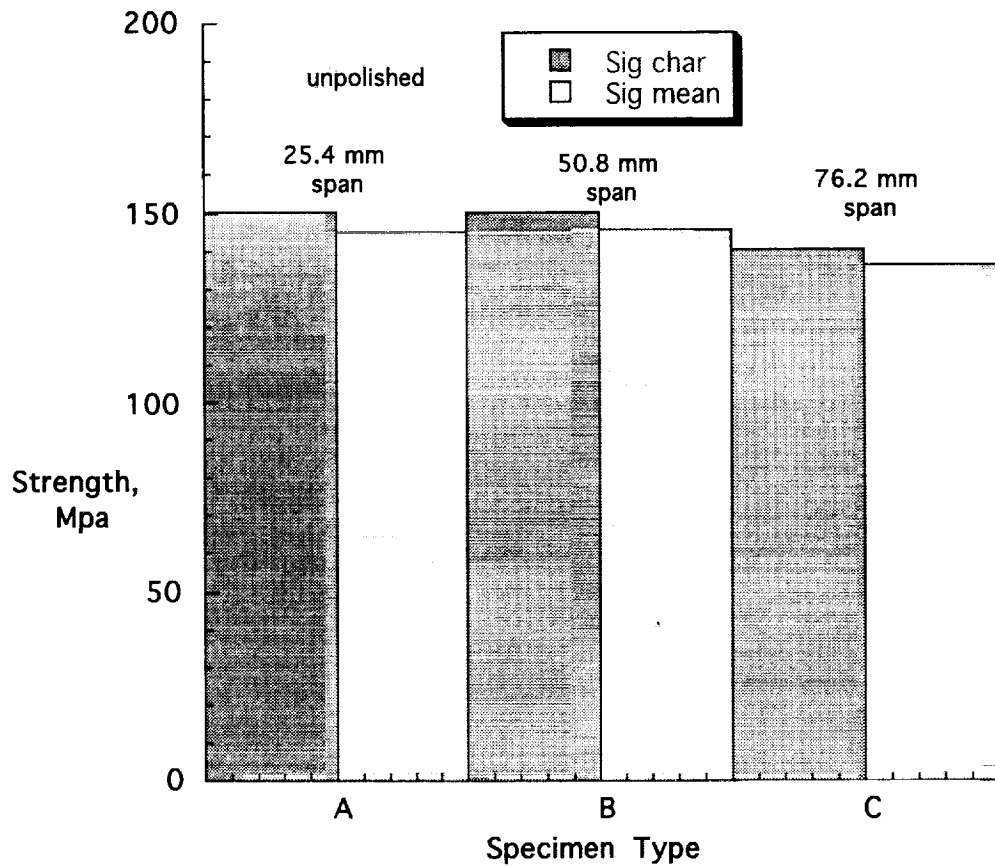
Fig. 15 – Effect of Span Length on (a) Transverse Tension Strength and (b) Scatter : S2/8552, 3-Point bending
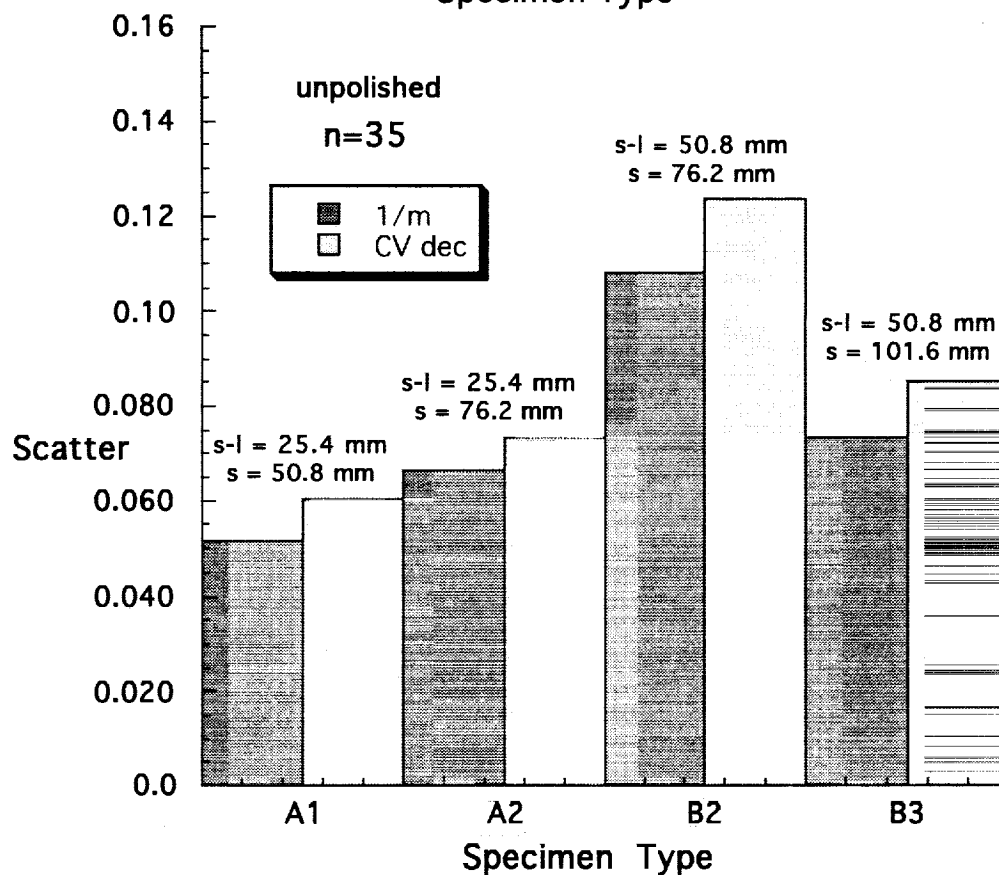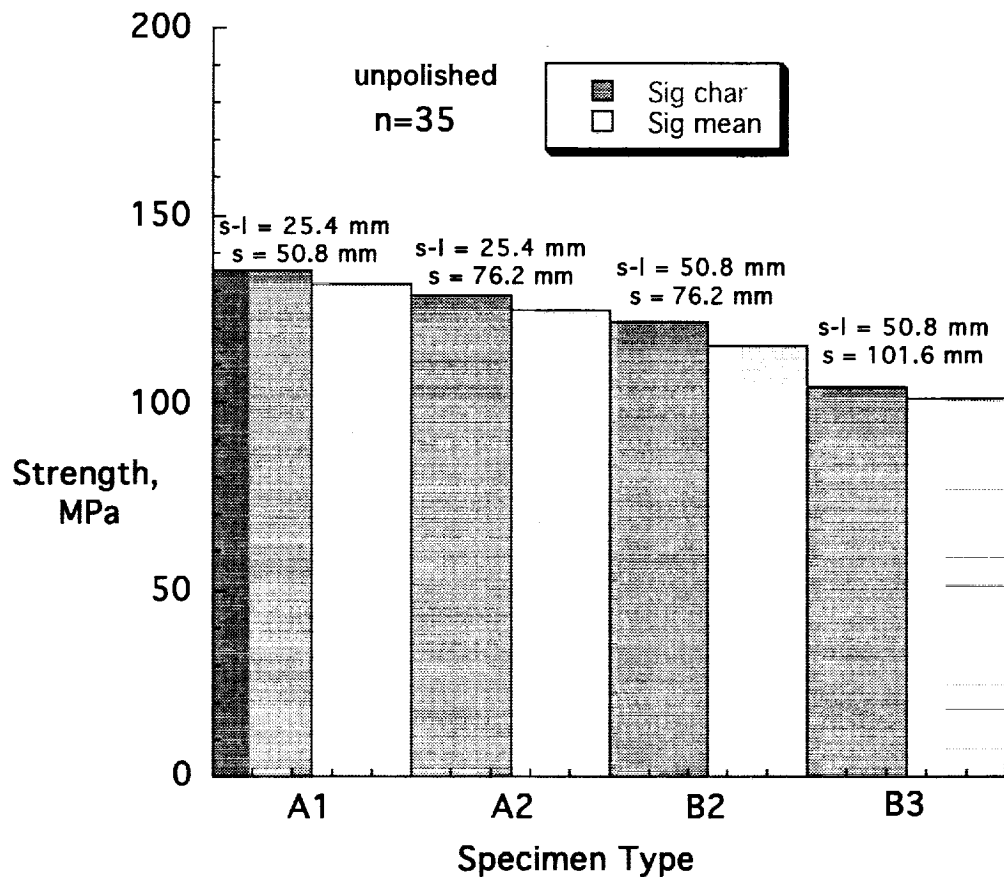
Fig. 16 – Effect of Span Length on (a) Transverse Tension Strength and
(b) Scatter : S2/8552, 4-Point bending, n=35
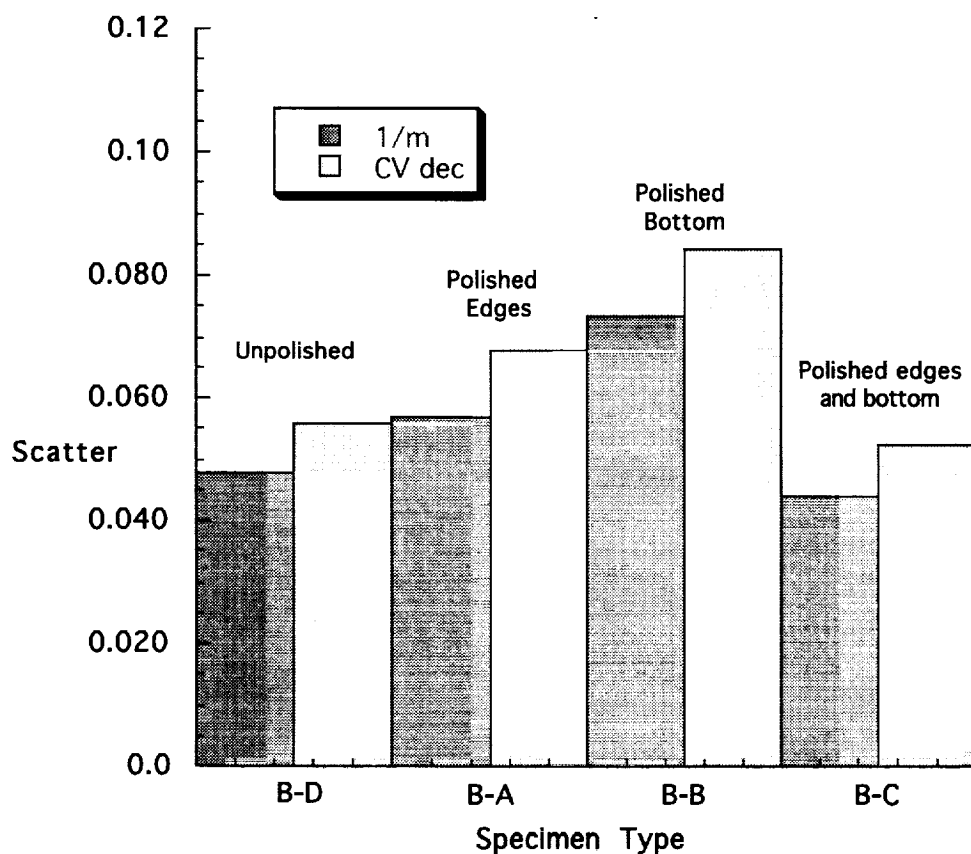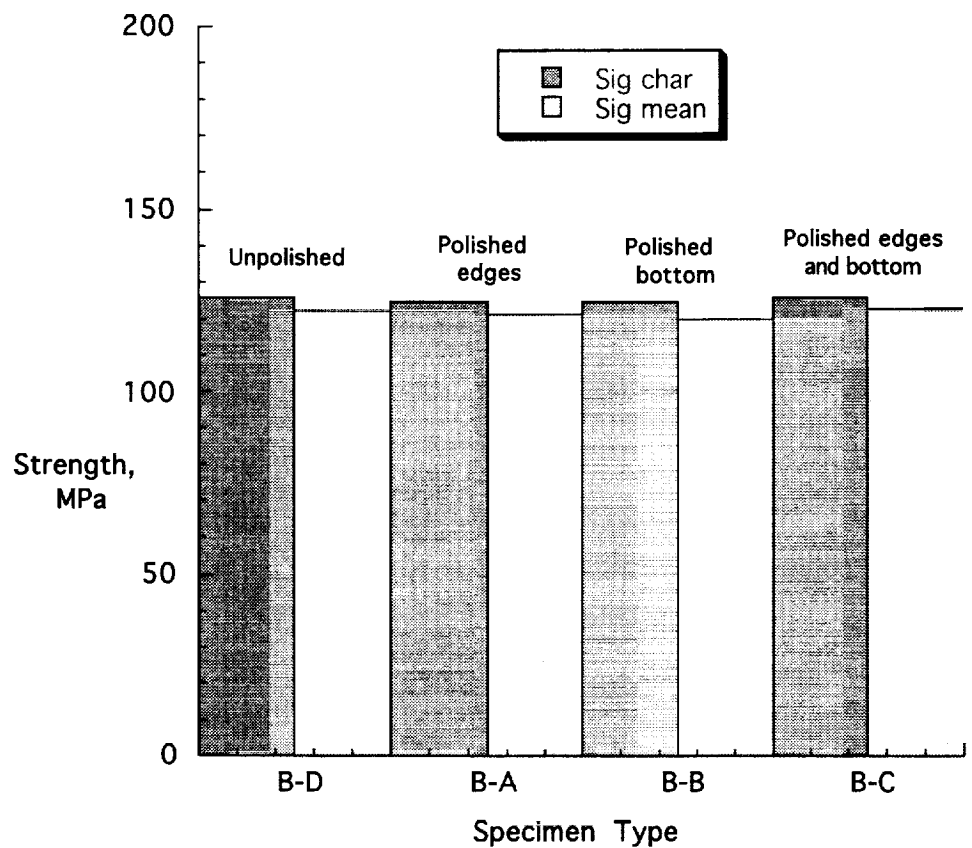
Fig. 17 – Effect of Polishing on (a) Transverse Tension Strength and (b) Scatter
24-ply, IM7/8552, 3-Point bending
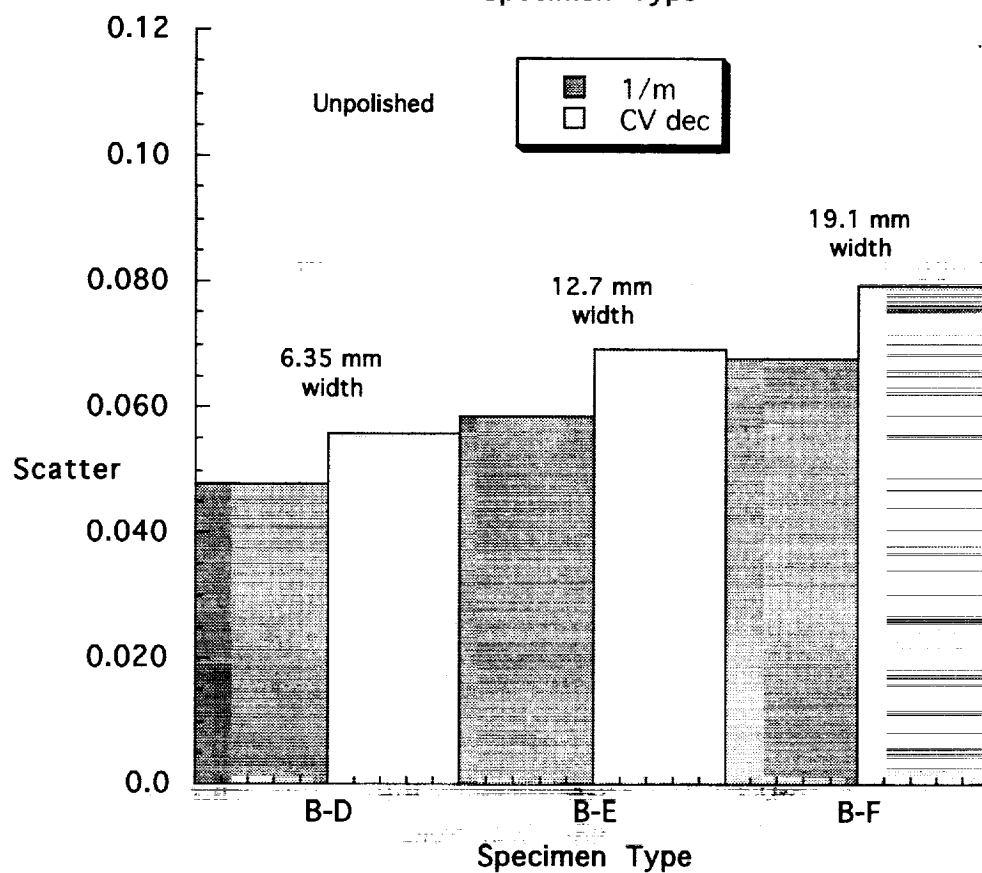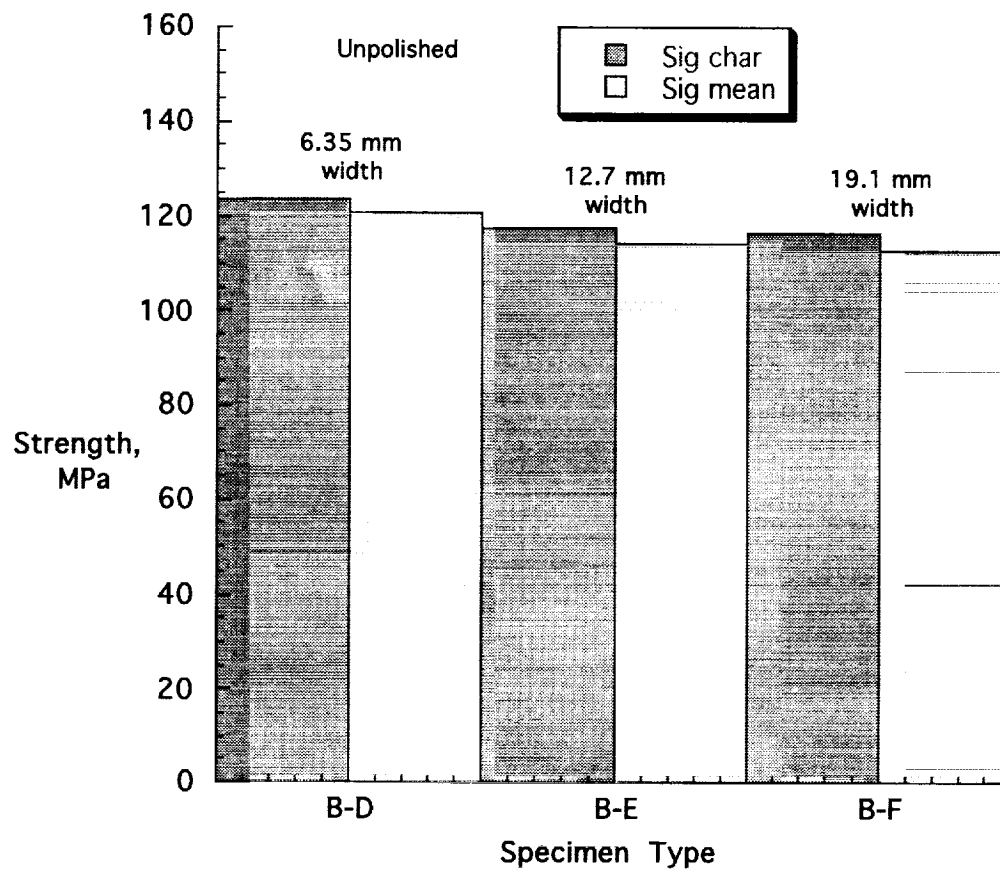
Fig. 18 – Effect of Specimen Width on (a) Transverse Tension Strength and (b) Scatter : 24-ply, IM7/8552, 3-Point bending
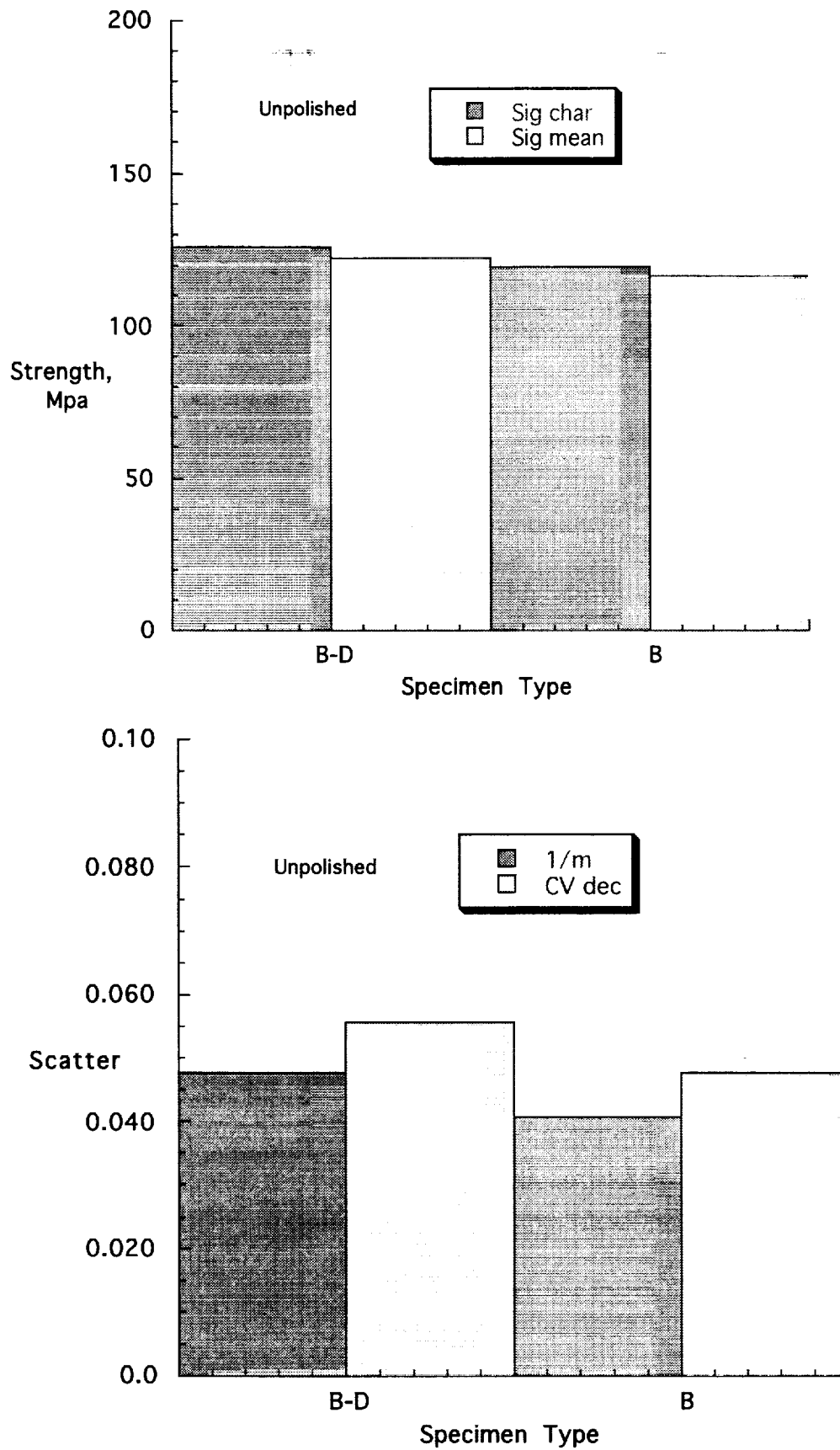
Fig. 19 – Effect of Panel Variability on (a) Transverse Tension Strength and (b) Scatter : 24-ply, IM7/8552, 3-Point bending
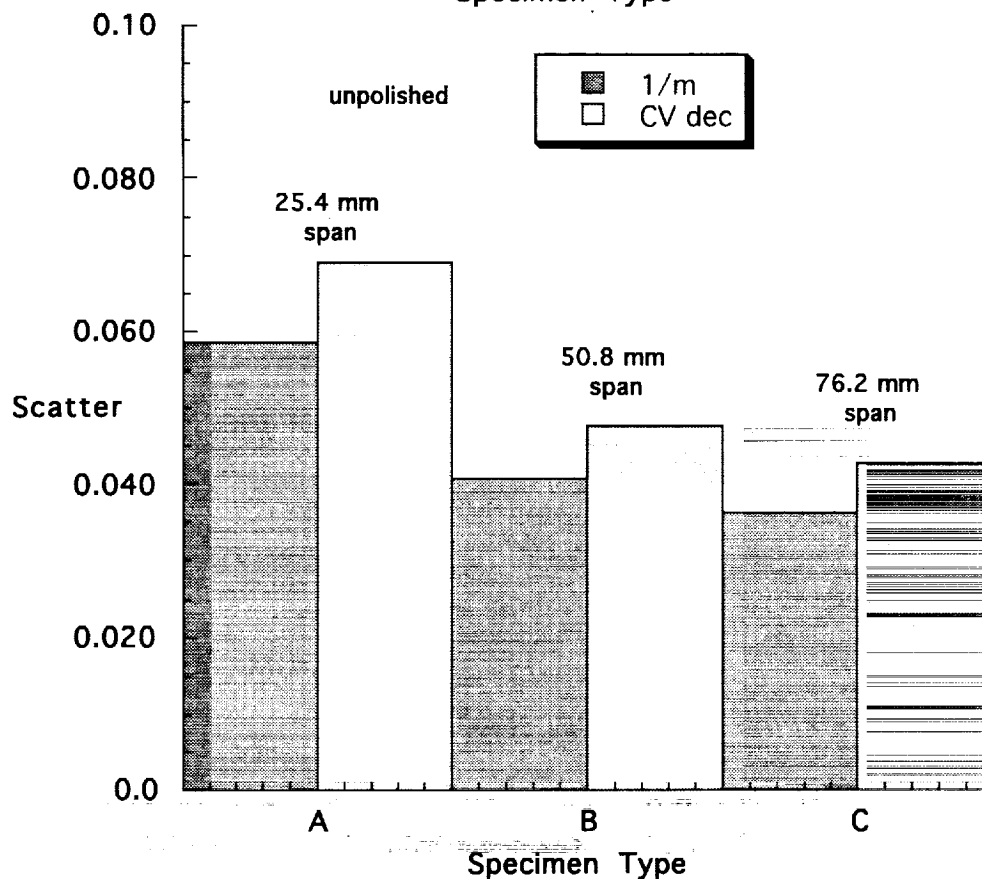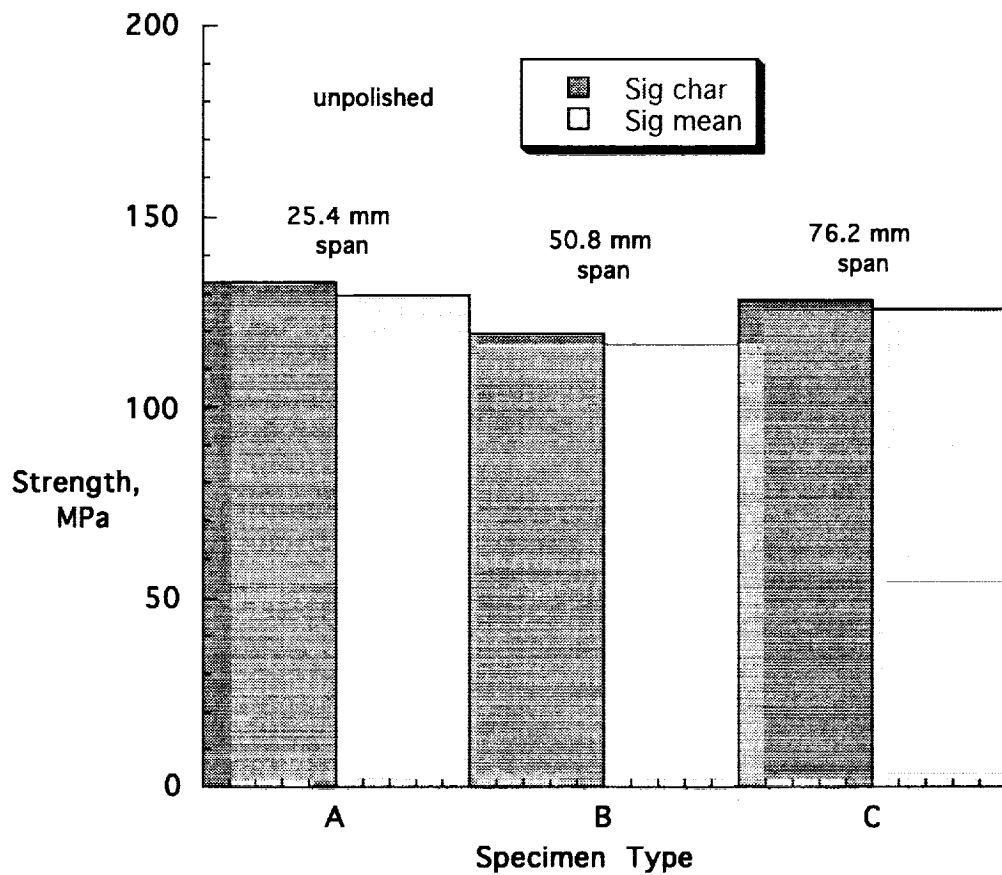
Fig. 20 – Effect of Span Length on (a) Transverse Tension Strength and
(b) Scatter : 24-ply, IM7/8552, 3-Point bending
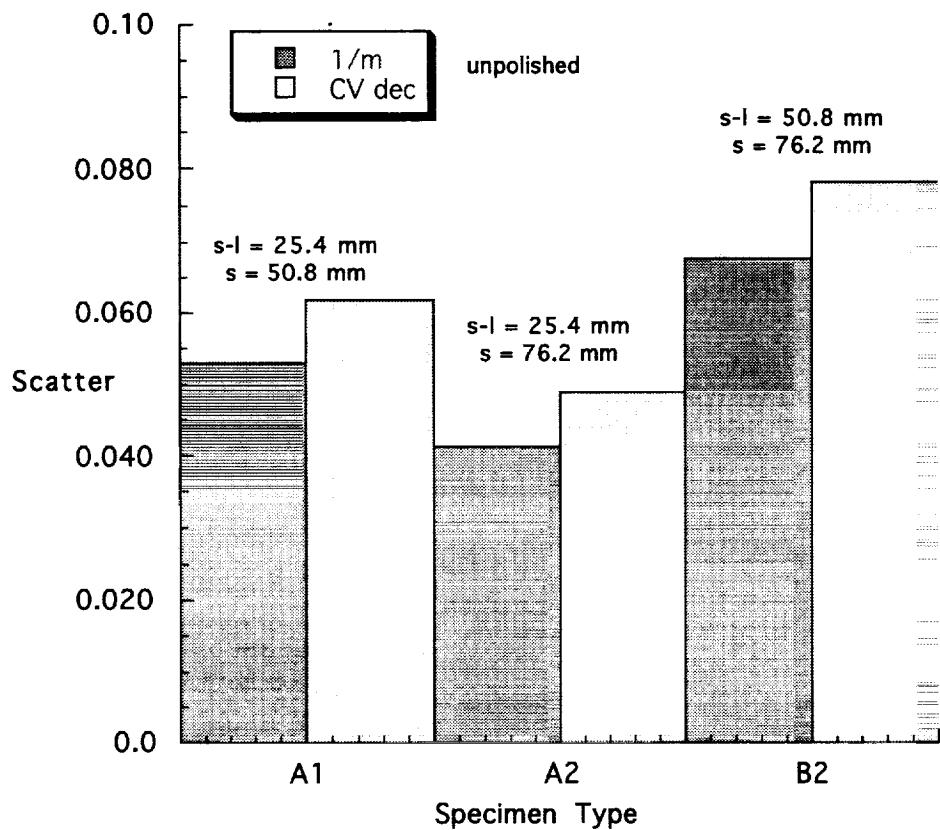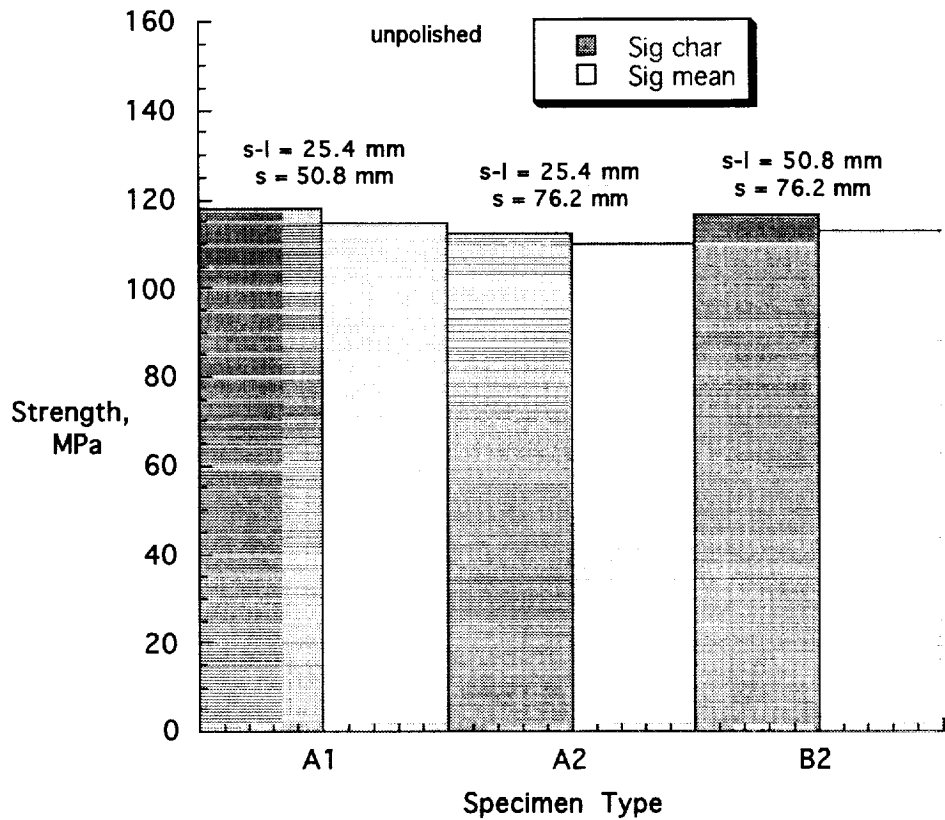
Fig. 21 – Effect of Span Length on (a) Transverse Tension Strength and (b) Scatter : 24-ply, IM7/8552, 4-Point bending
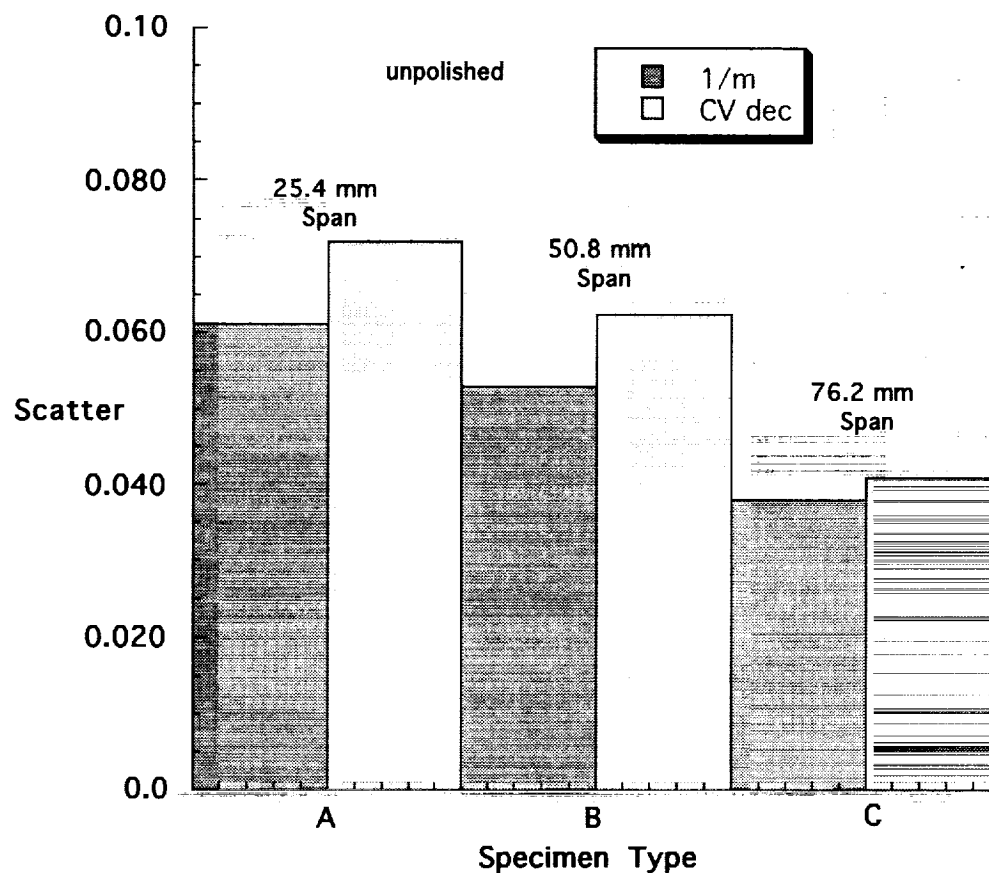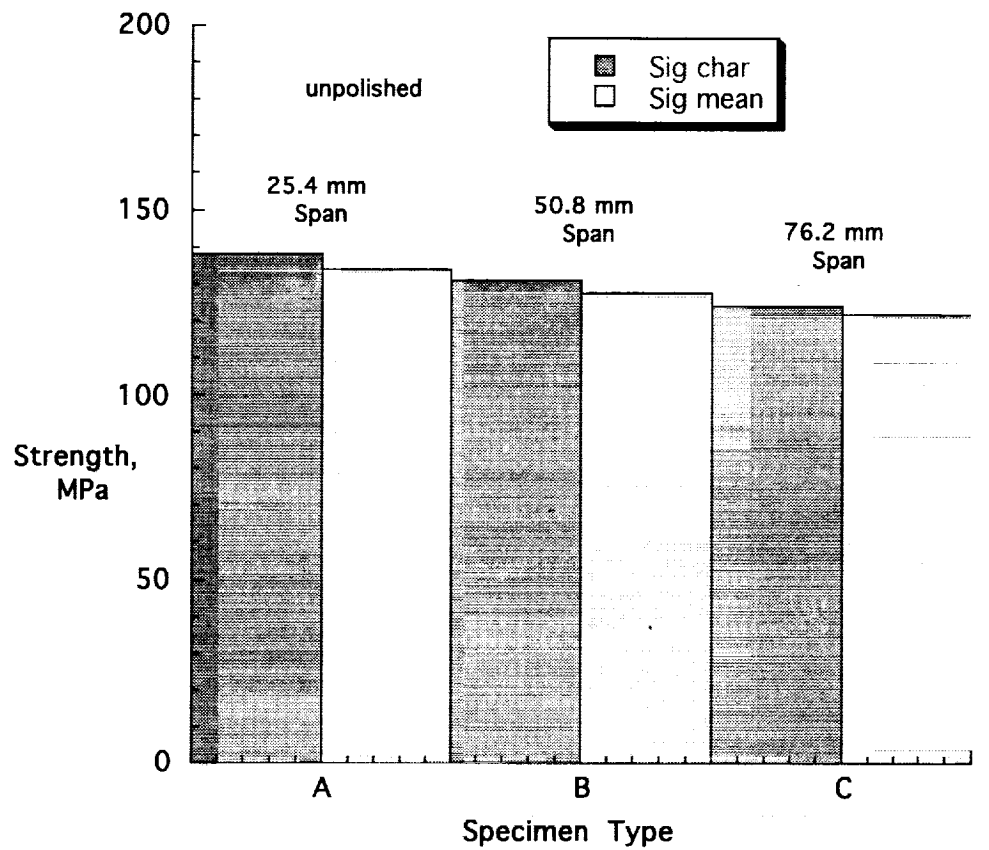
Fig. 22 – Effect of Span Length on (a) Transverse Tension Strength and
(b) Scatter : 36-ply, IM7/8552, 3-Point bending
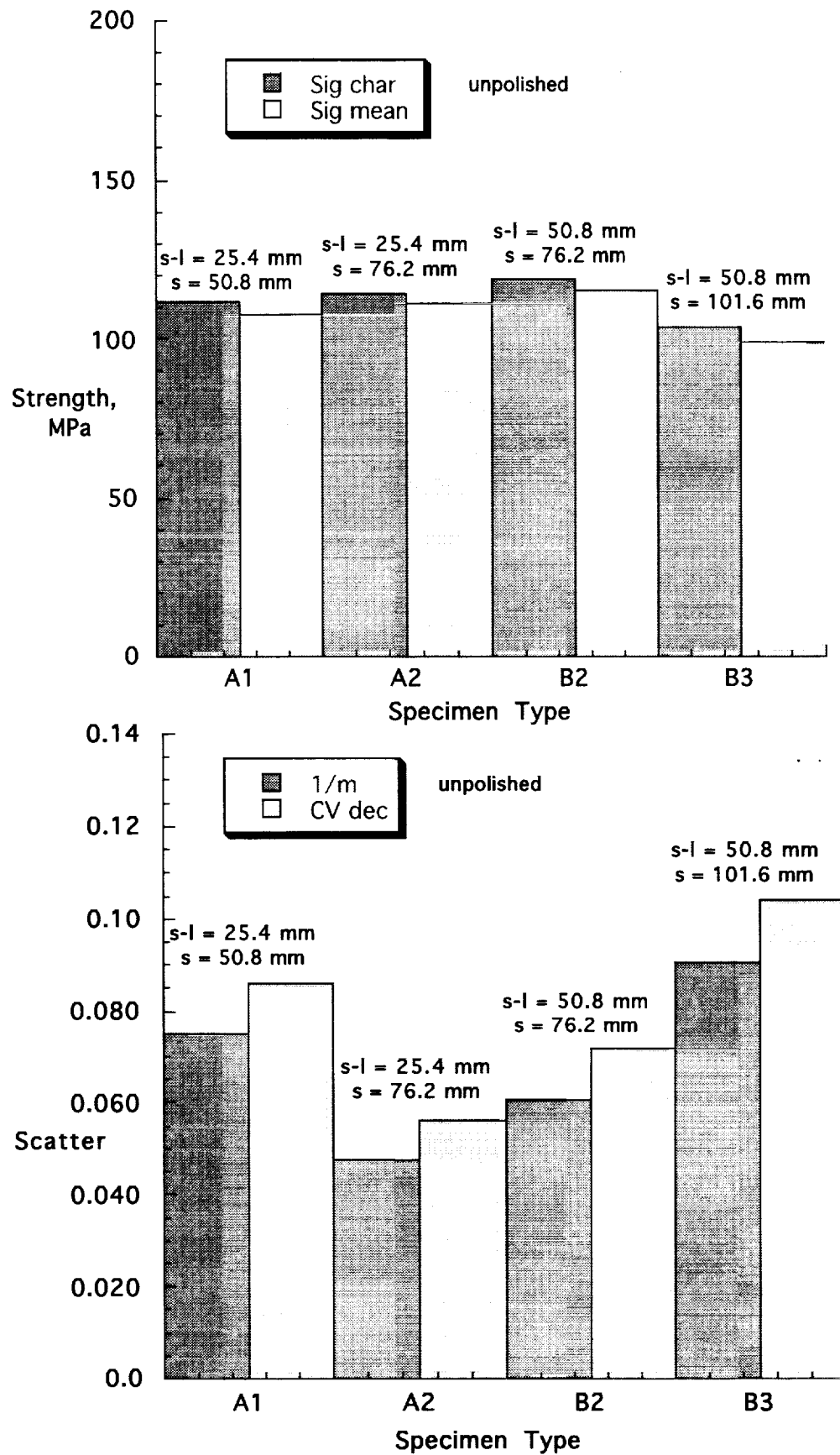
Fig. 23 – Effect of Span Length on (a) Transverse Tension Strength and
(b) Scatter : 36-ply, IM7/8552, 4-Point bending
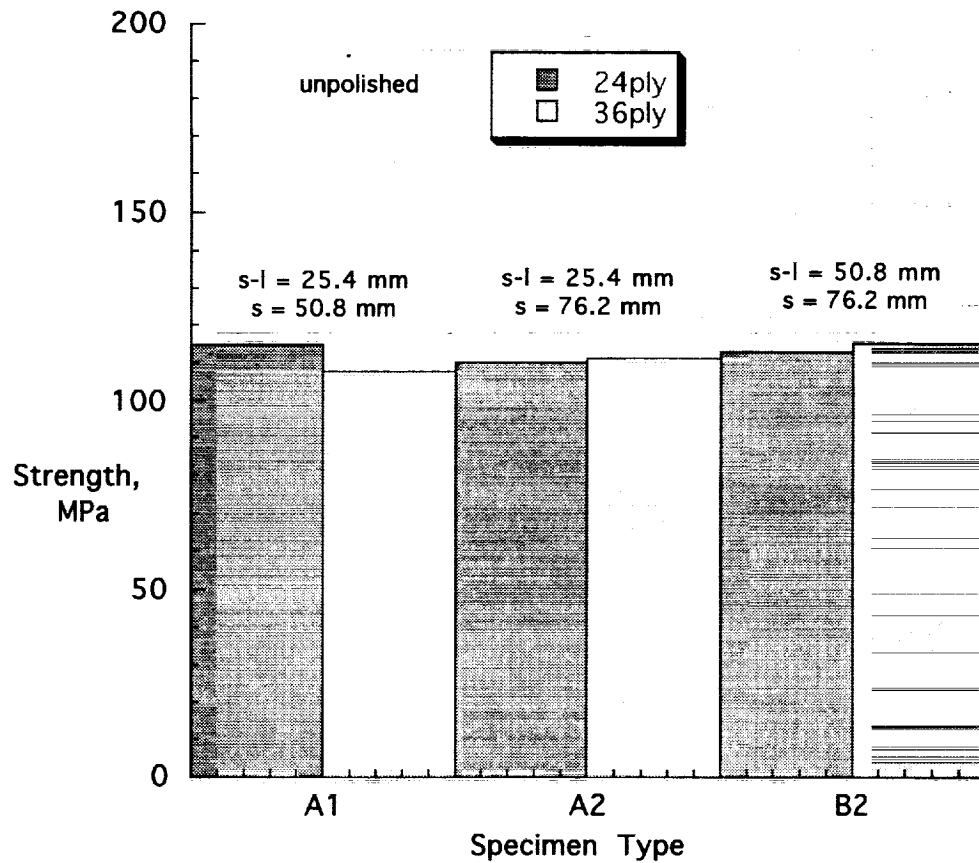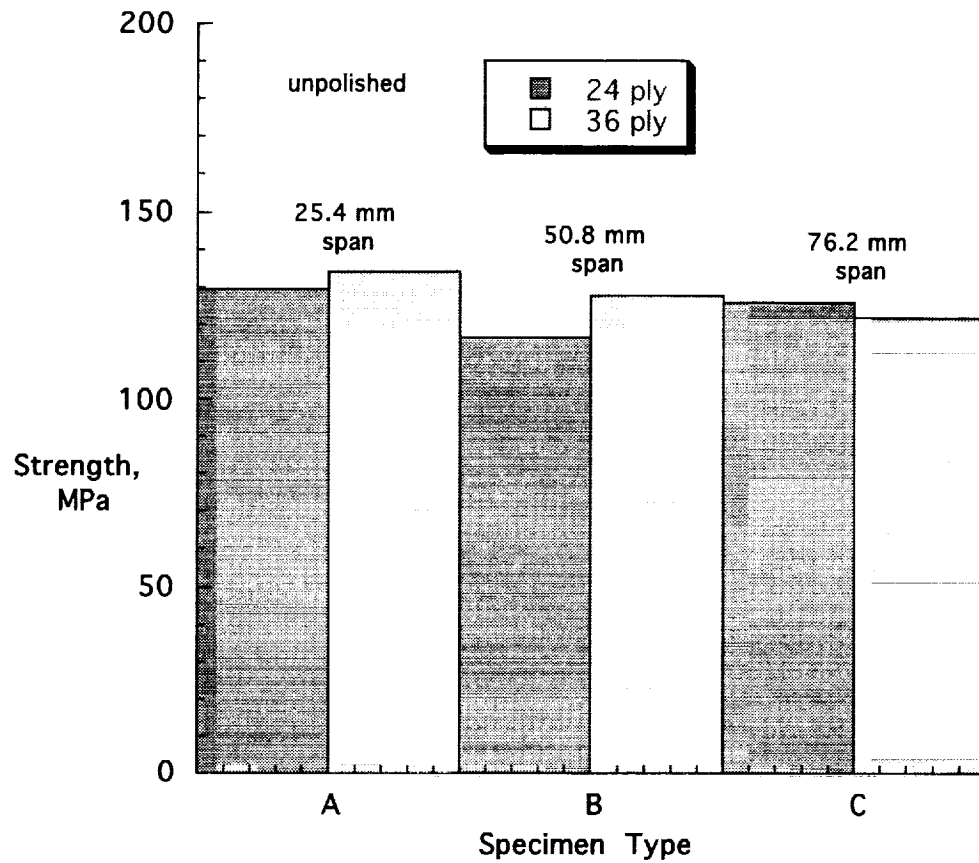
Fig. 24 – Effect of Thickness on Transverse Tension Strength of IM7/8552
(a) 3-Point bending, (b) 4-Point bending
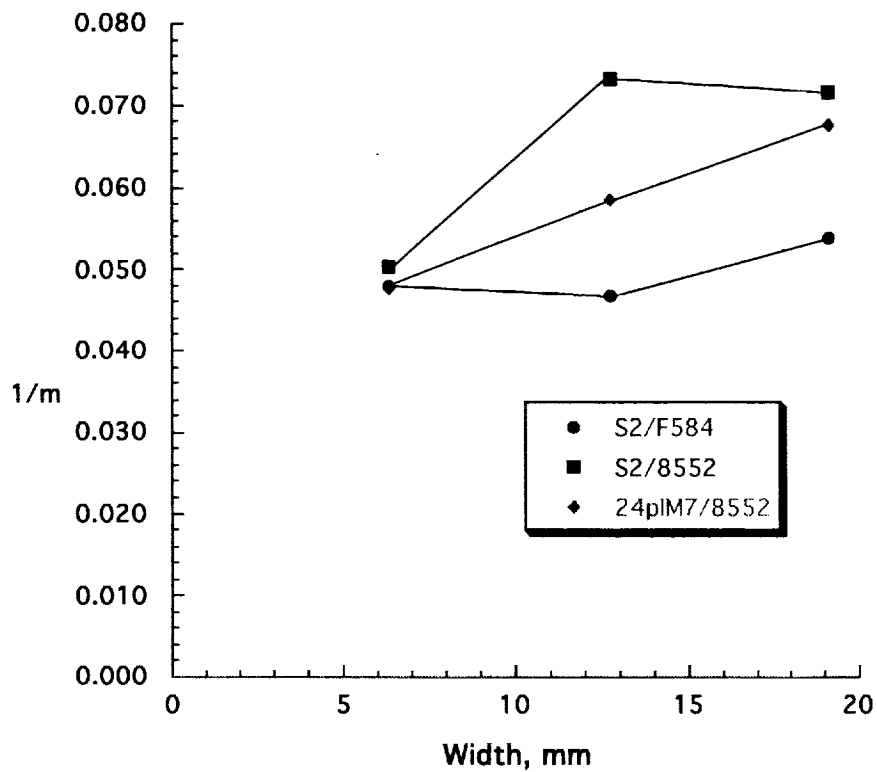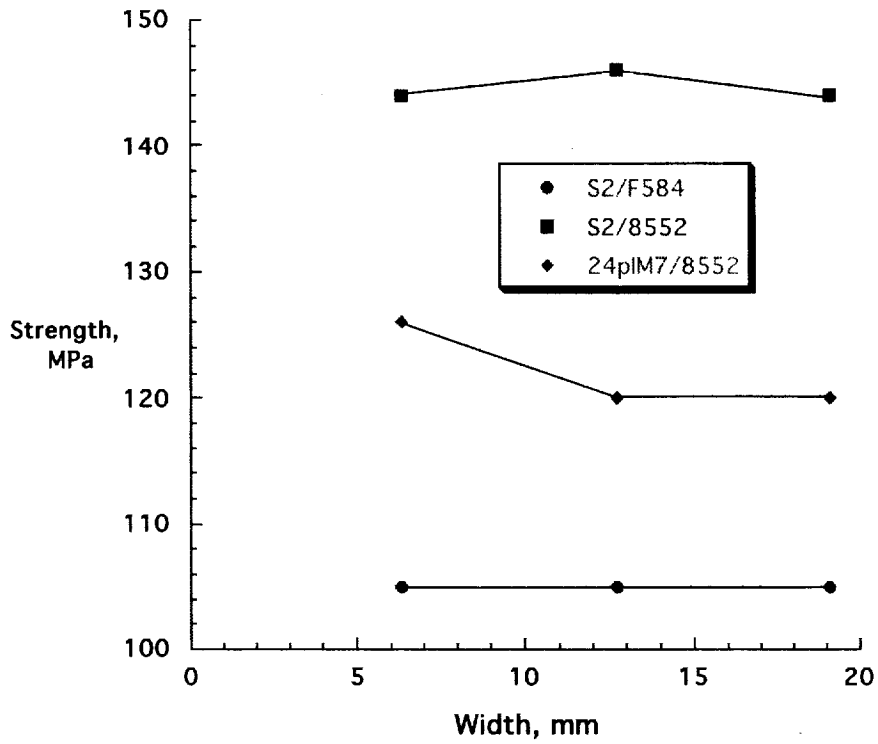
Fig.25 Influence of Specimen Width on Characteristic Strength
and Scatter for 3-point bending Configuration B
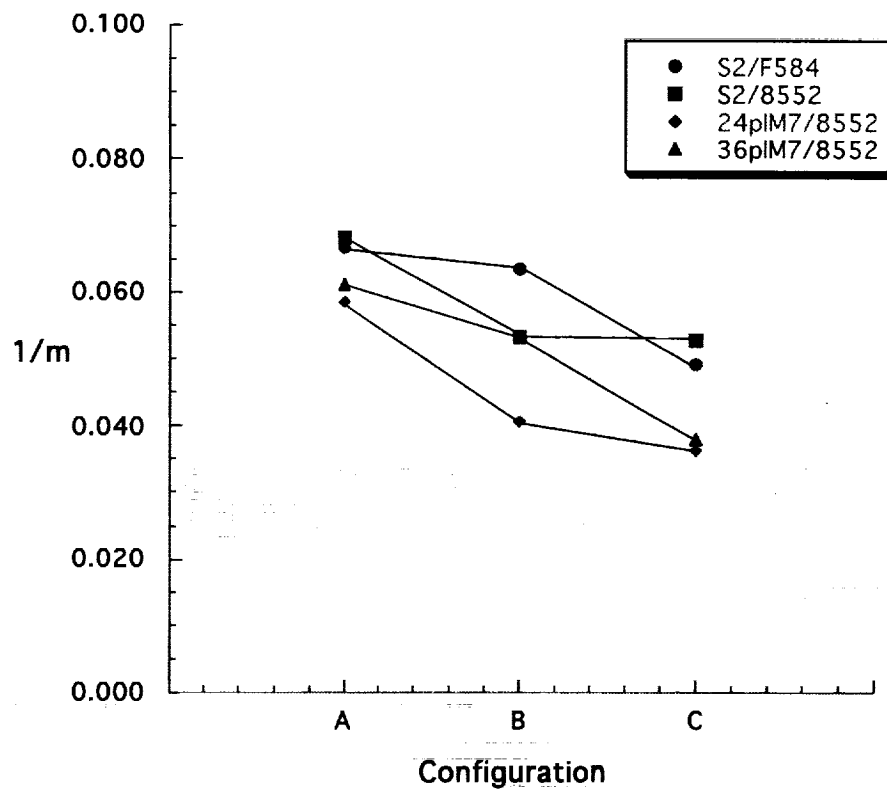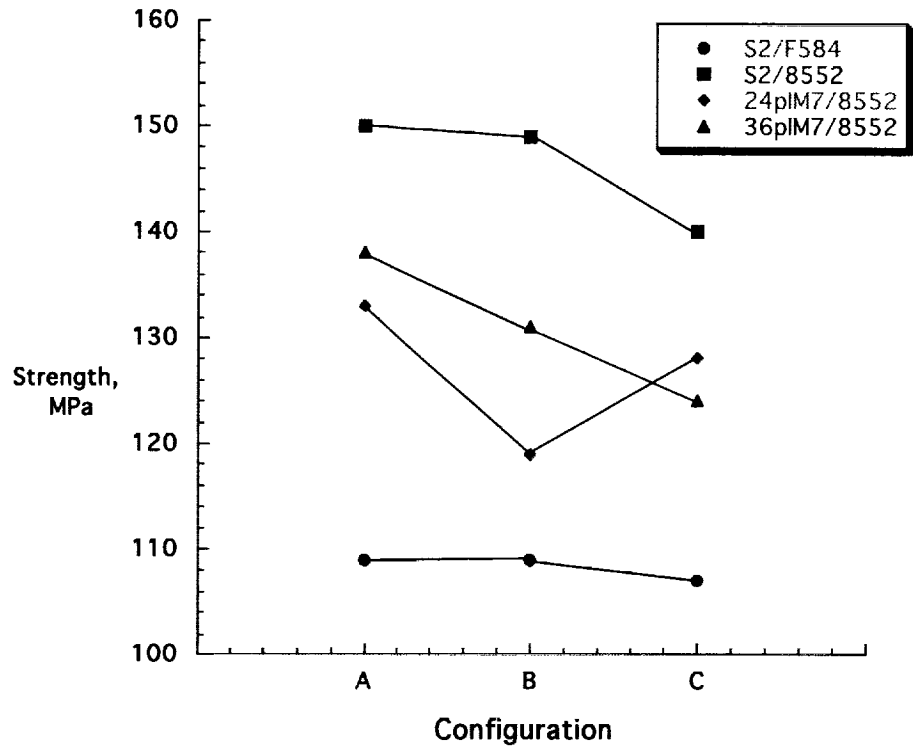
Fig.26 Influence of Span Length on Characteristic Strength
and Scatter for 3-point bending
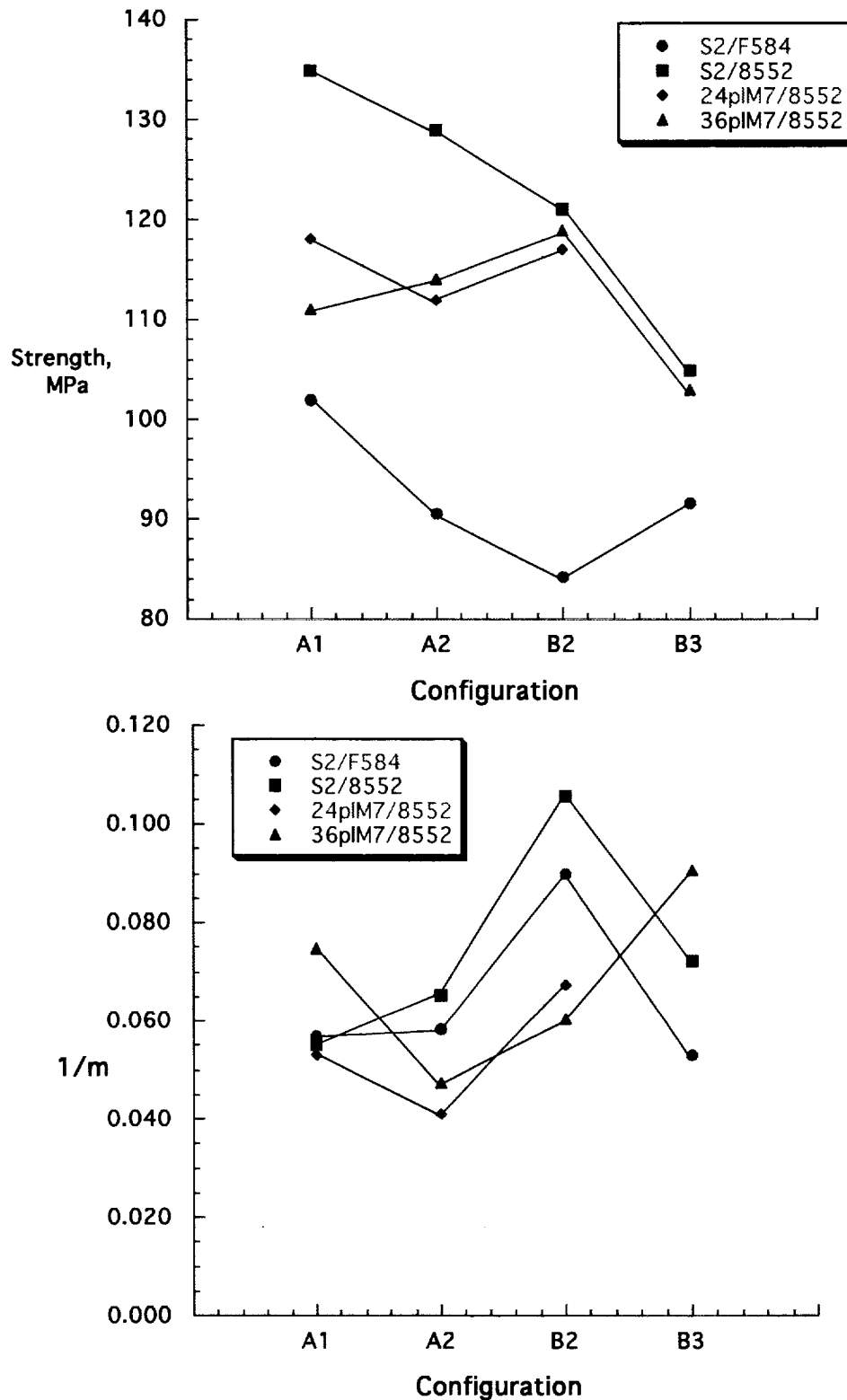
Fig.27 Influence of Span Length on Characteristic Strength
and Scatter for 4-point bending
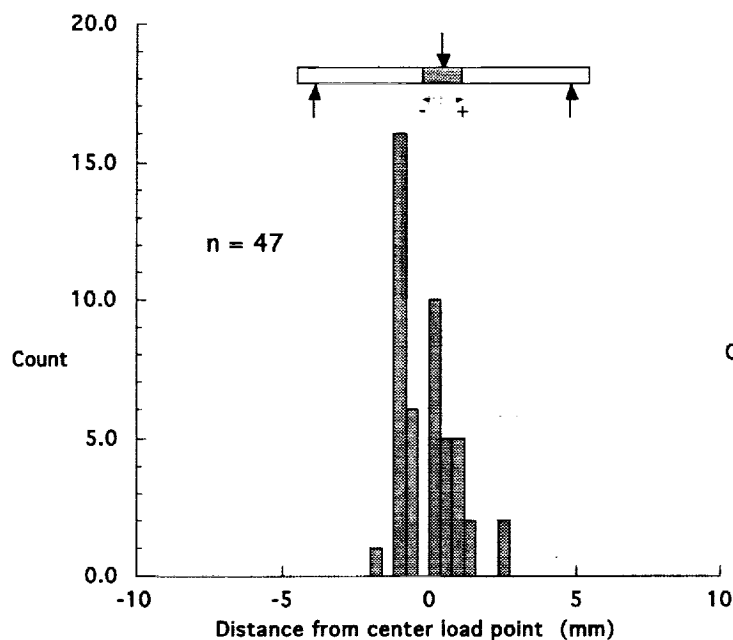
(a) Configuration A
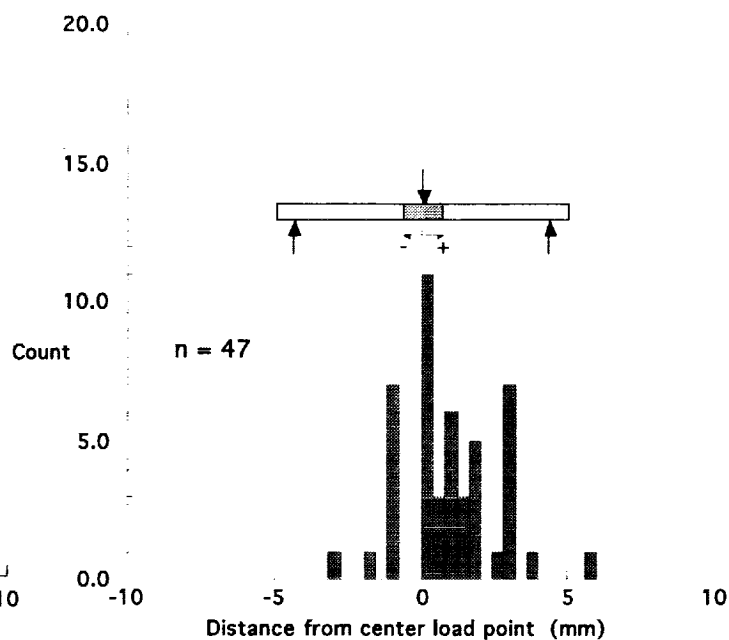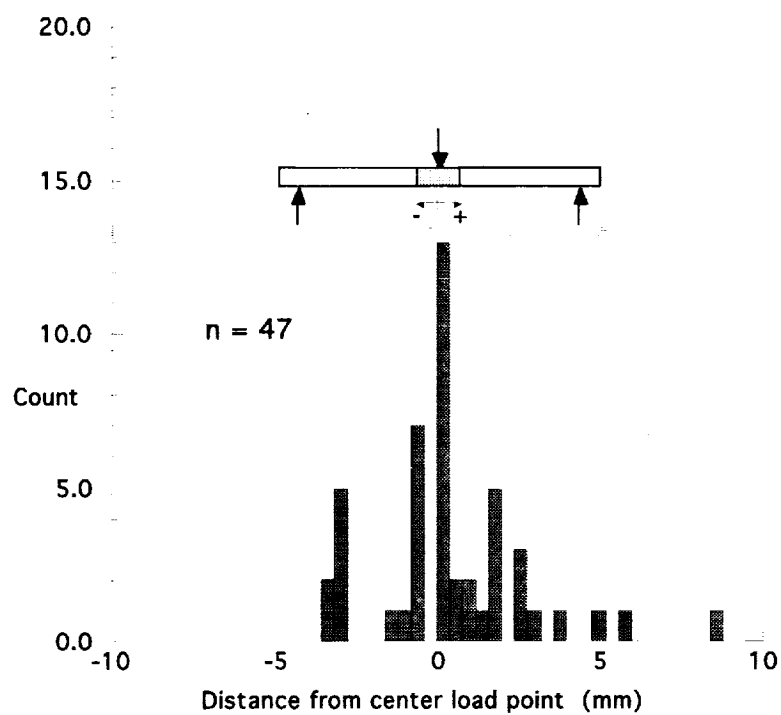
(b) Configuration B

(c) Configuration C

Fig. 28 – Histogram of Failure Locations, S2/F584, 3-point Bending, Panel TN3
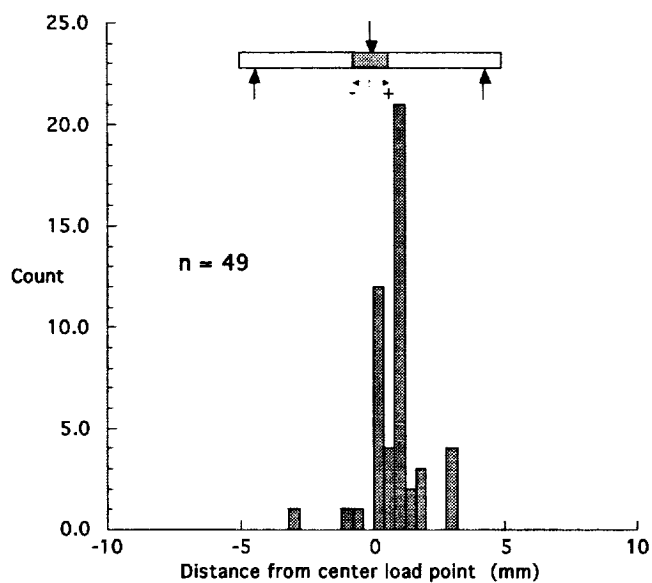
(a) Configuration A
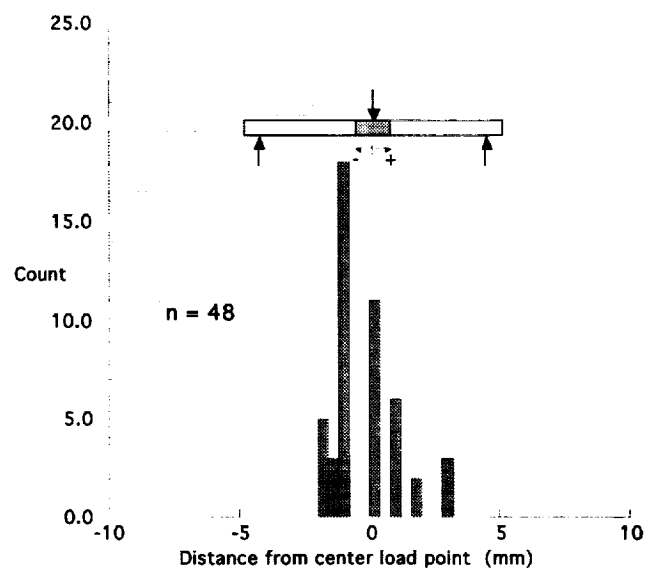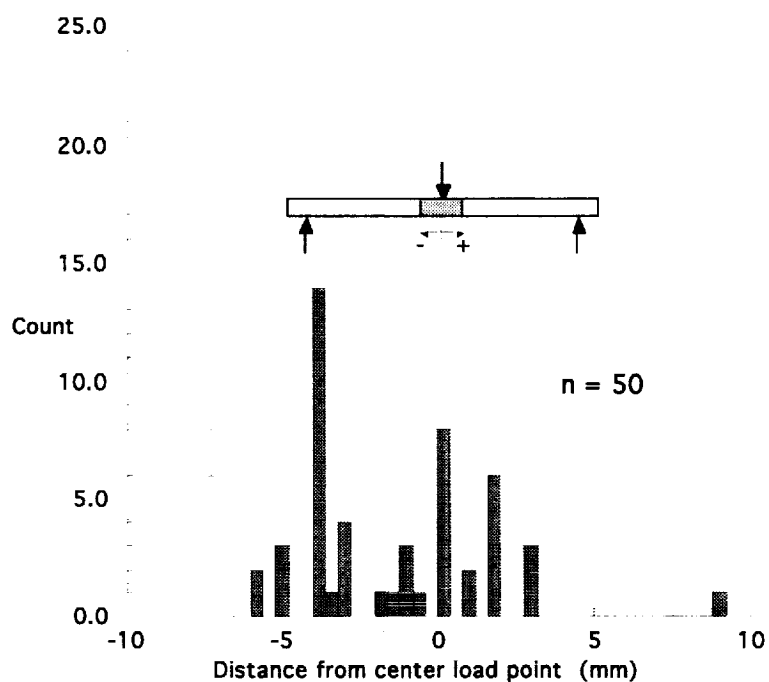
(b) Configuration B

(c) Configuration C

Fig. 29 – Histogram of Failure Locations, S2/8552, 3-point Bending
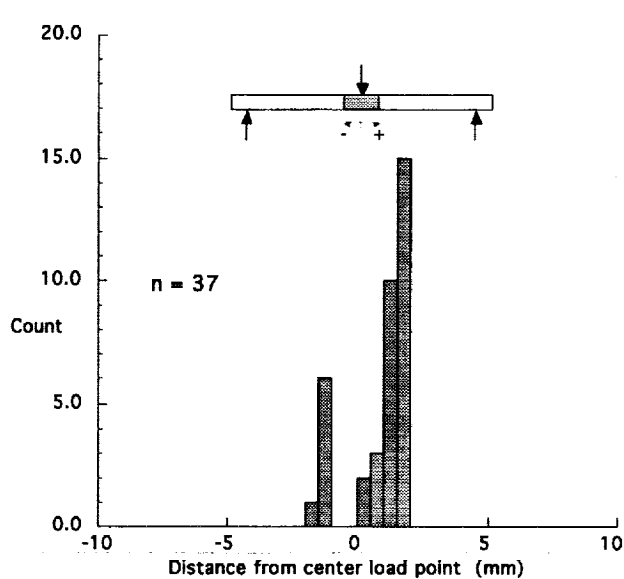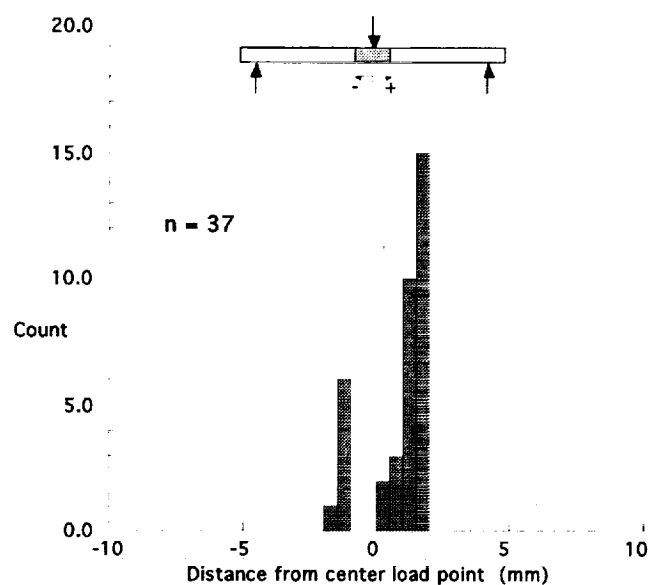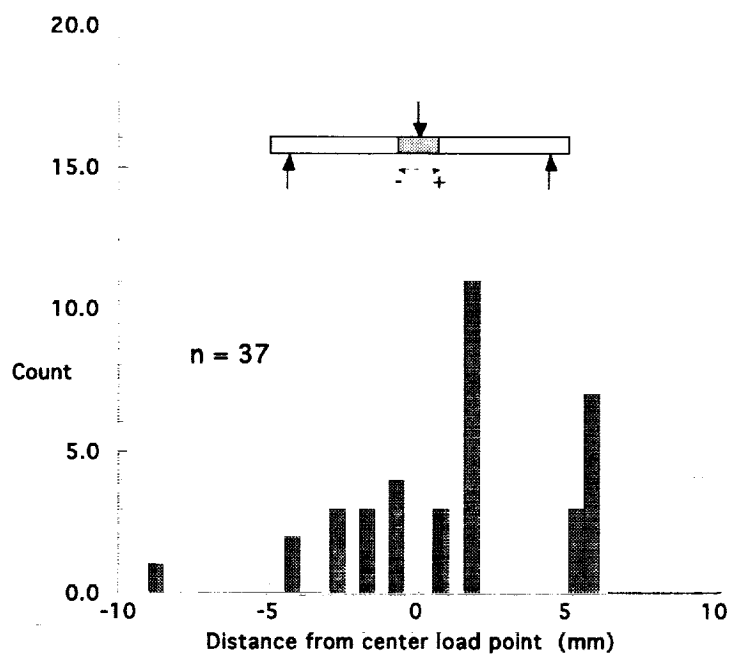
Fig. 30 – Histogram of Failure Locations, 24-ply IM7/8552, 3-point Bending
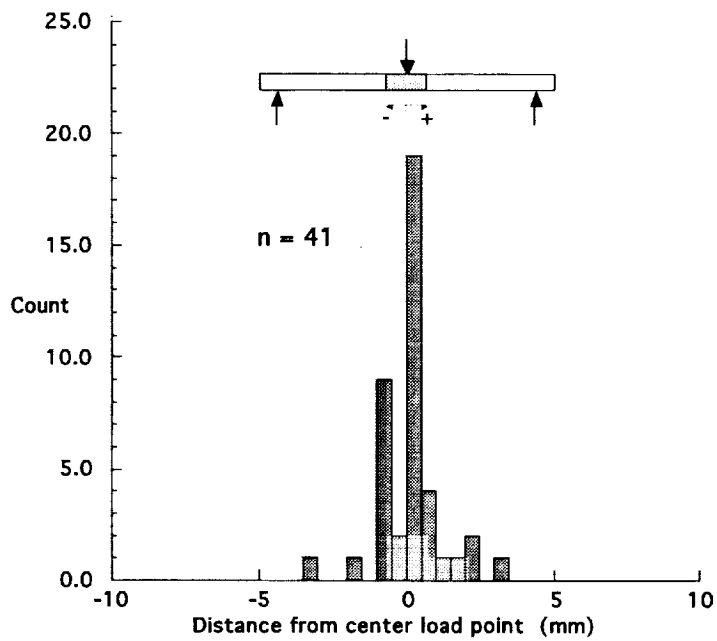
(a) Configuration A
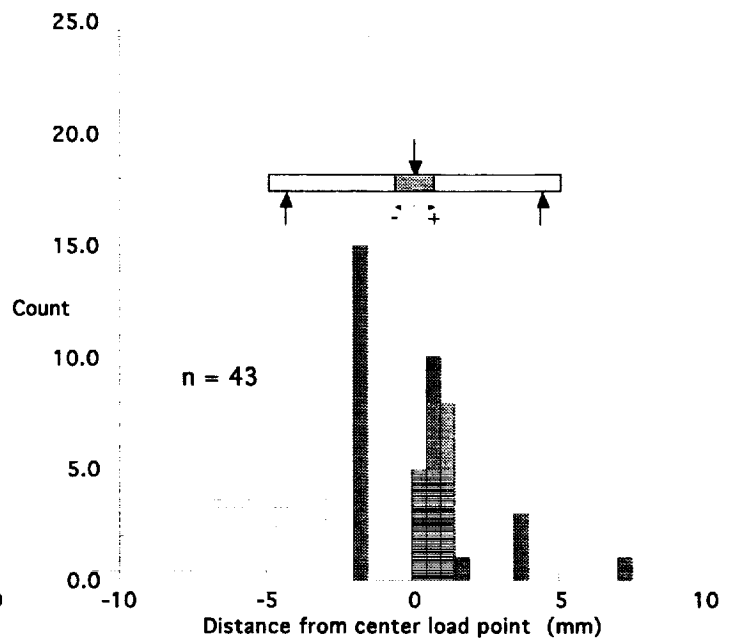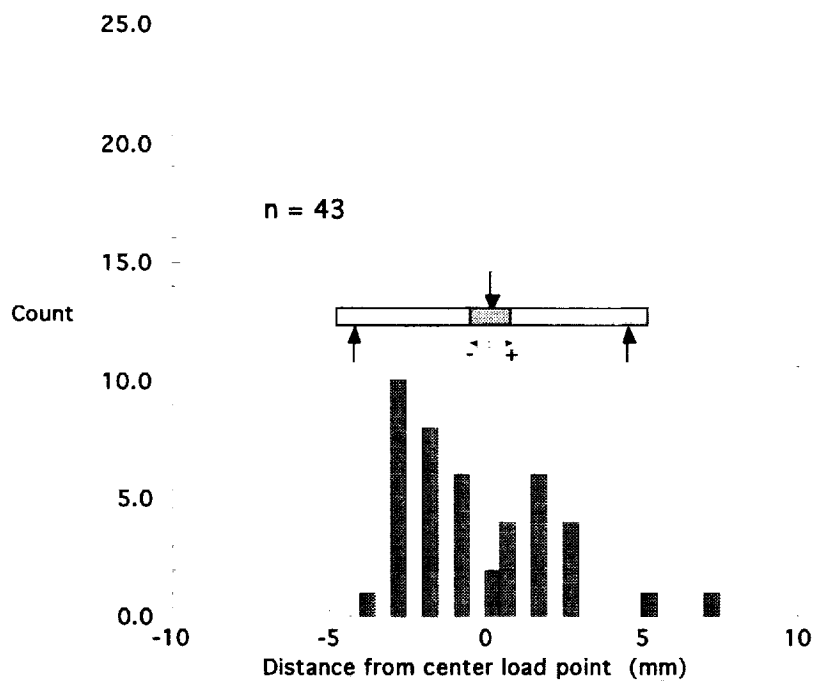
(b) Configuration B

(c) Configuration C

Fig. 31 – Histogram of Failure Locations, 36-ply IM7/8552, 3-point Bending
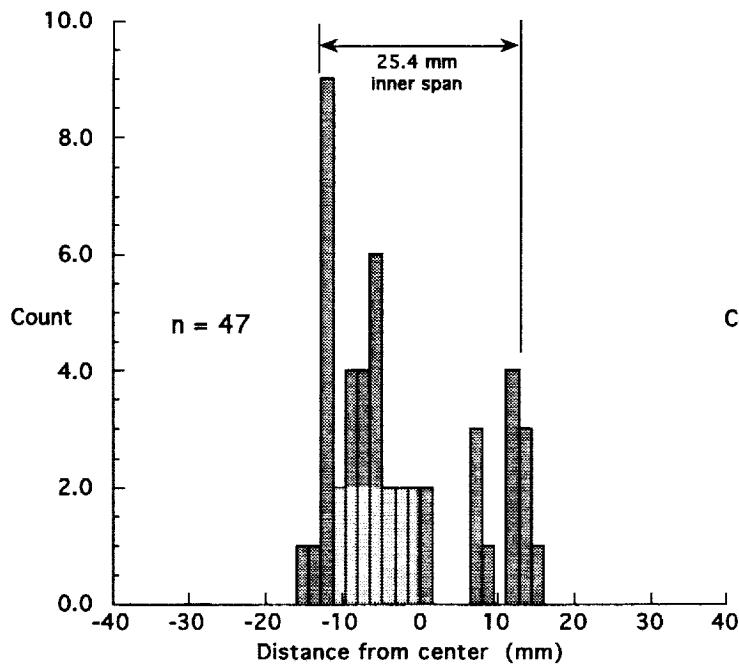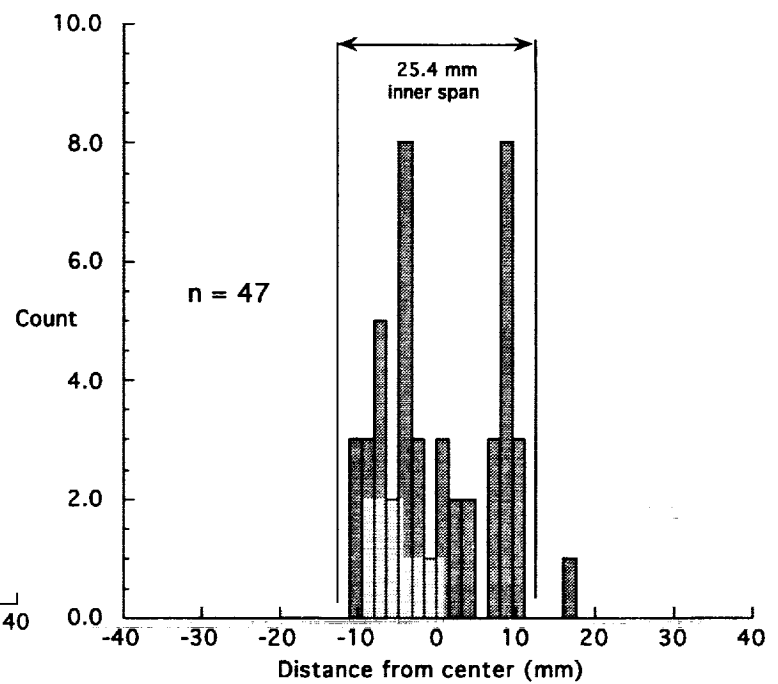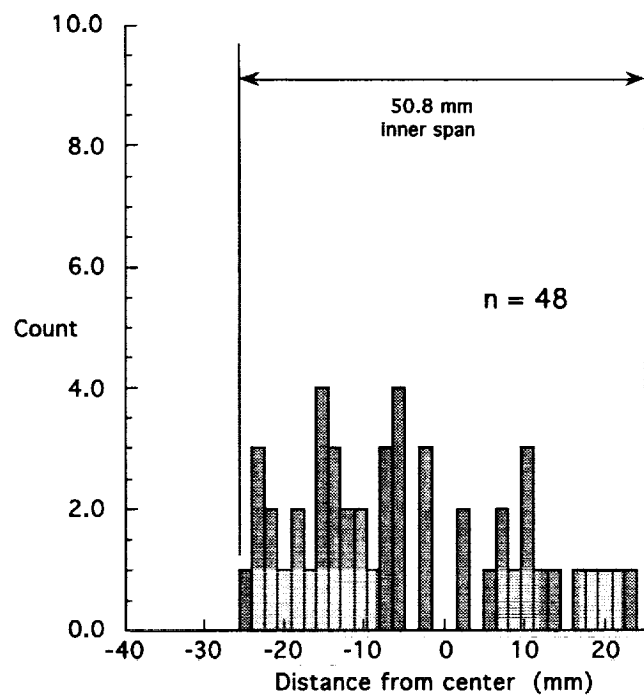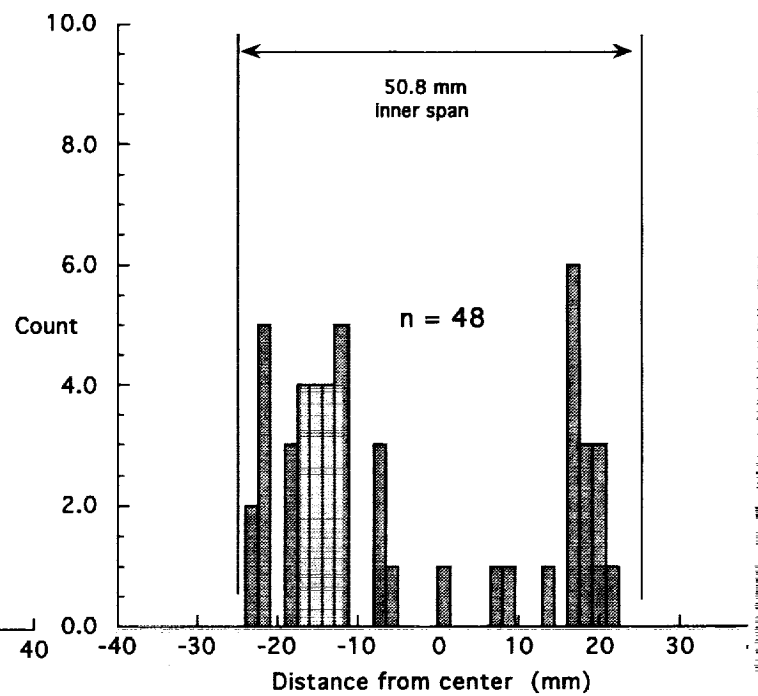
Fig. 32 – Histogram of Failure Locations, S2/F584, 4-point Bending
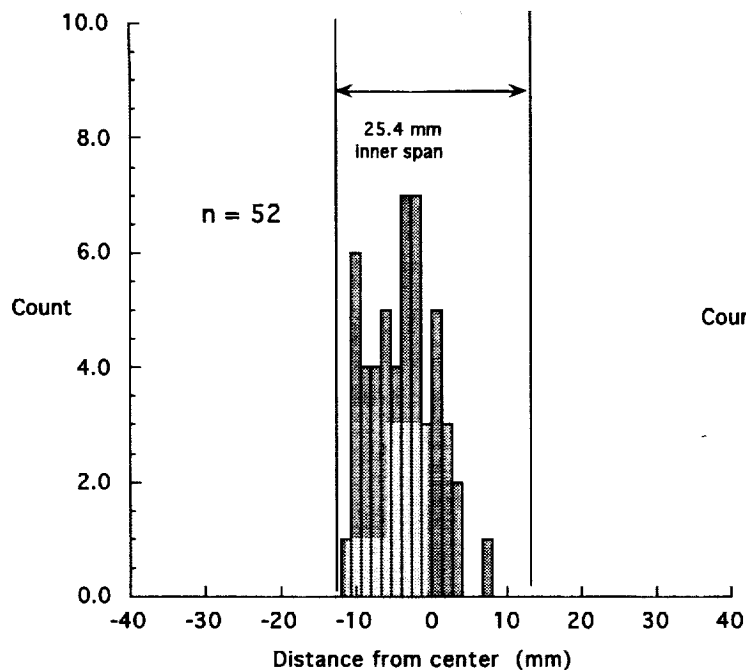
(a) Configuration A1
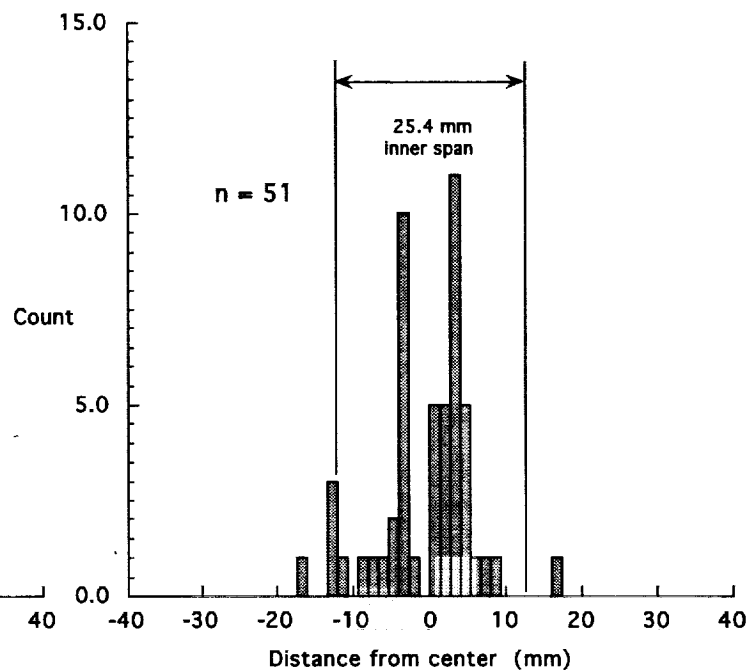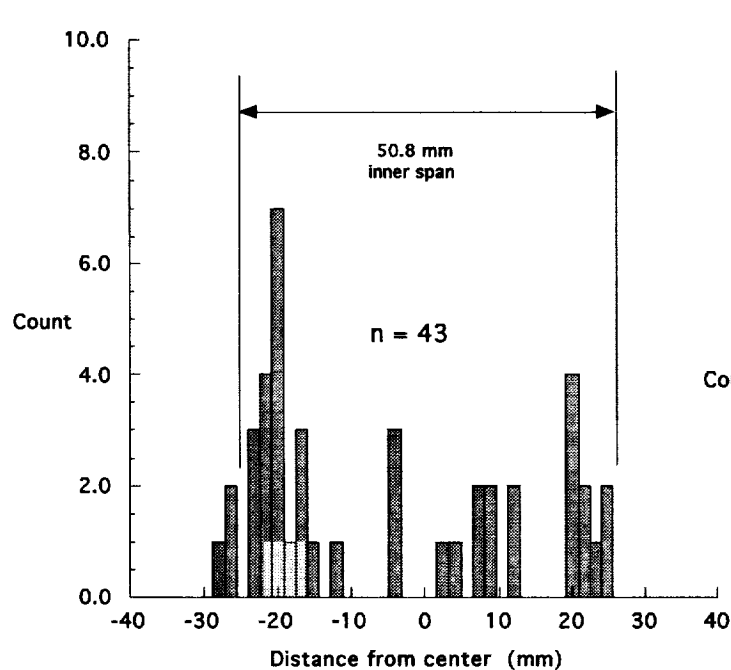
(b) Configuration A2
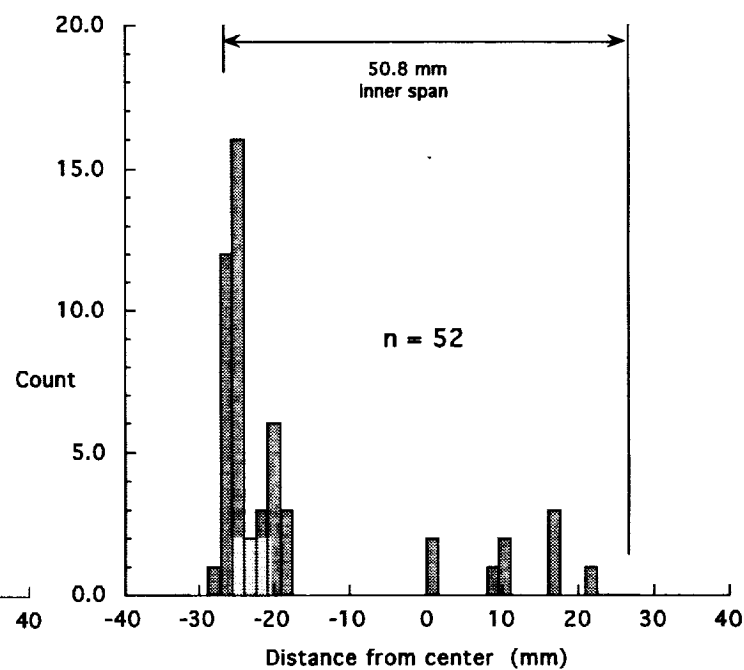
(c) Configuration B2

(d) Configuration B3

Fig. 33 – Histogram of Failure Locations, S2/8552, 4-point Bending
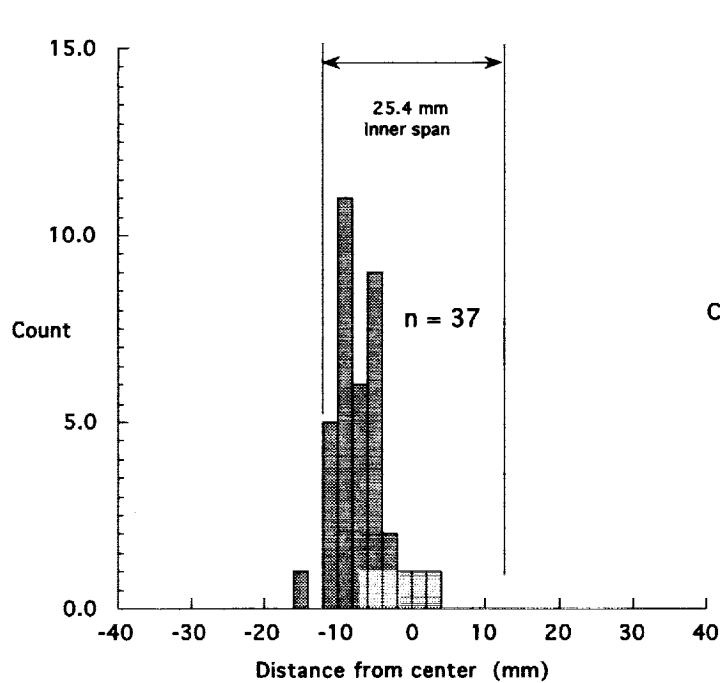
(a) Configuration A1
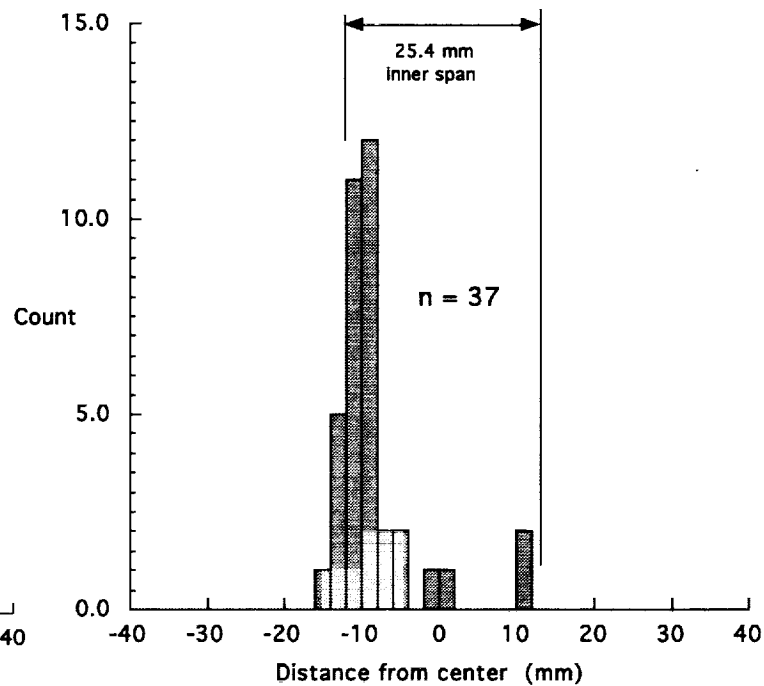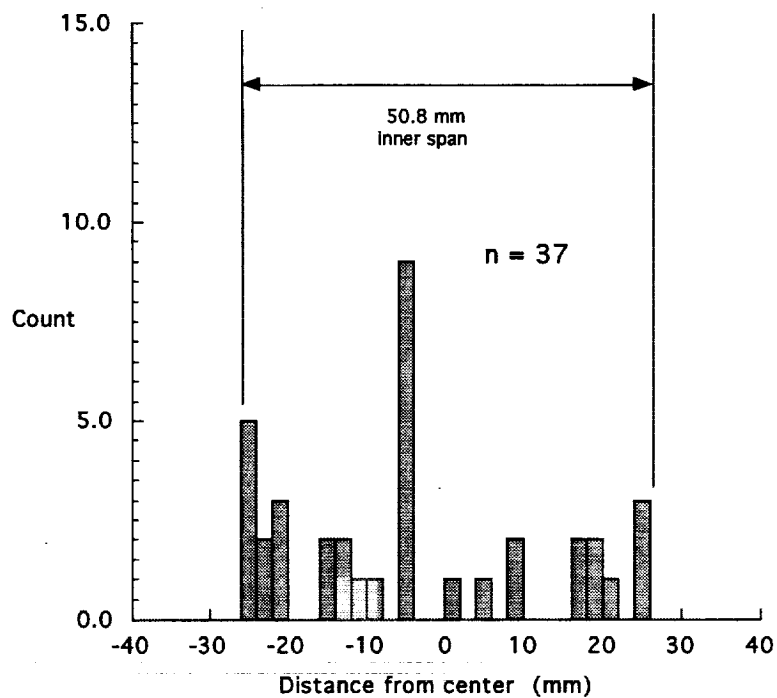
(b) Configuration A2

(c) Configuration B2

(d) Configuration B3

Fig. 34 – Histogram of Failure Locations, 24-ply IM7/8552, 4-point bending
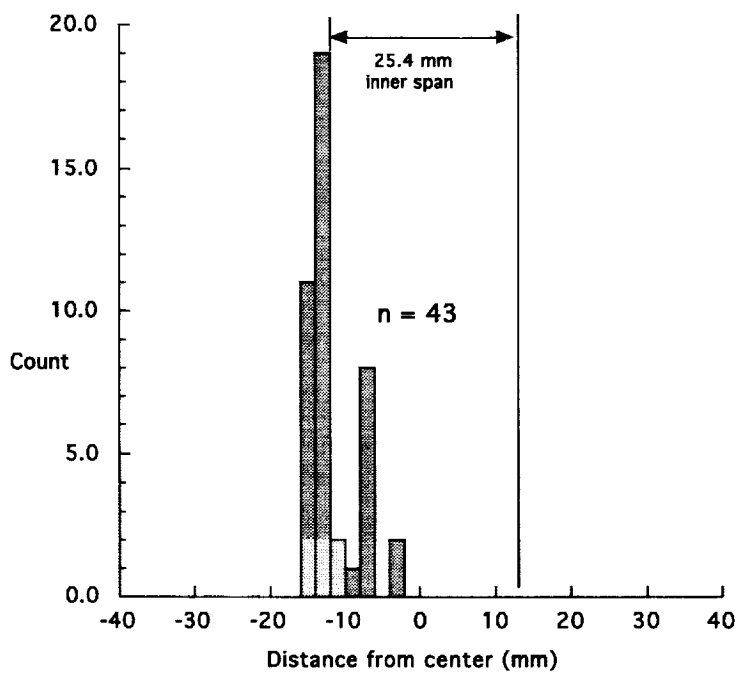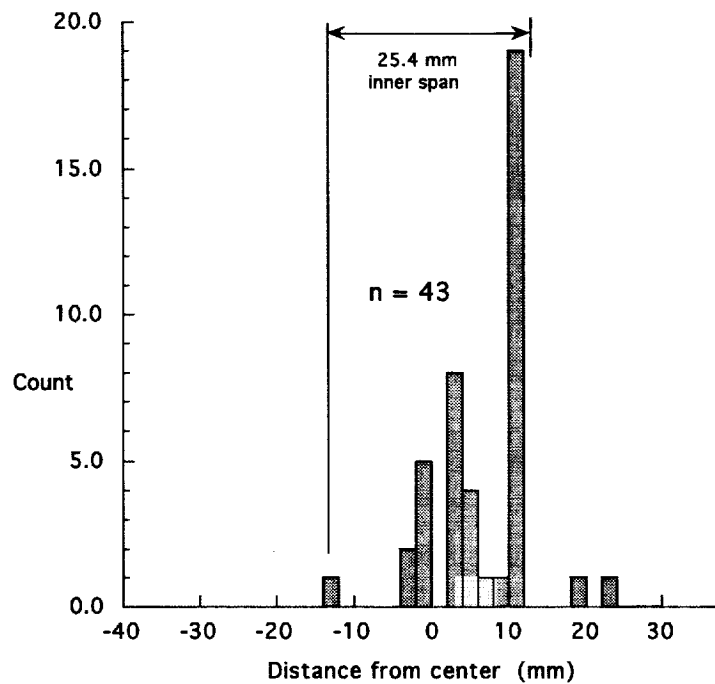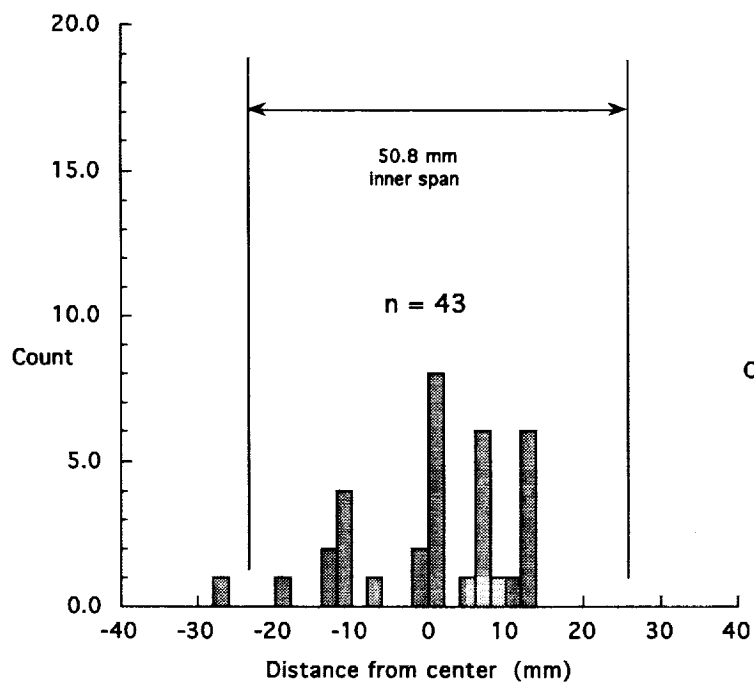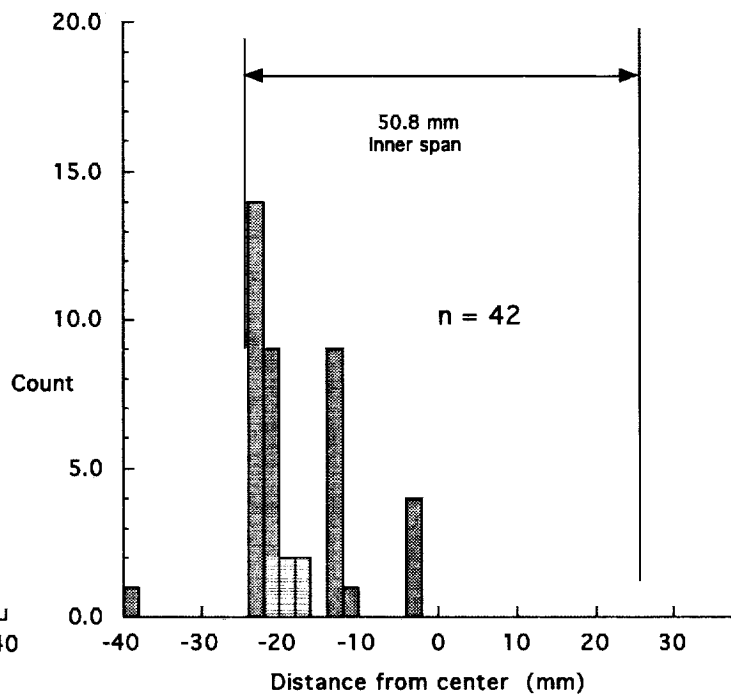
Fig. 35 – Histogram of Failure Locations, 36-ply IM7/8552, 4-point bending

3-pt, static, polished edge and bottom, high strength
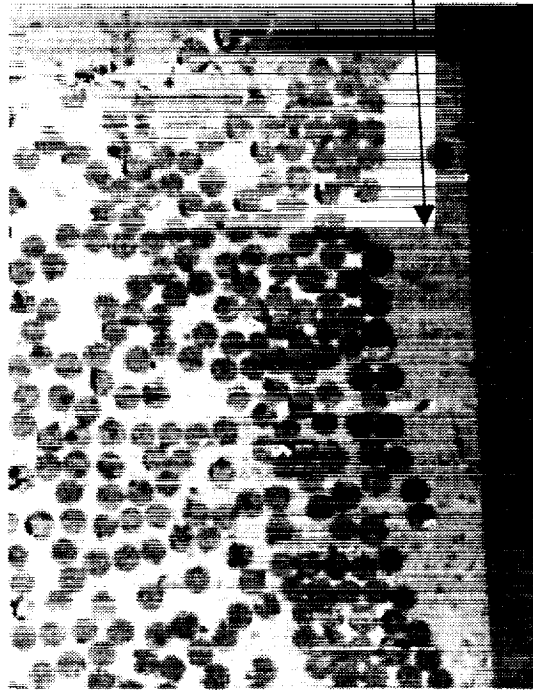
3-pt, static, polished edge and bottom, low strength

Resin pocket

Fig. 36 – Photomicrographs of specimen failure locations
S2/8552 Configuration B

74
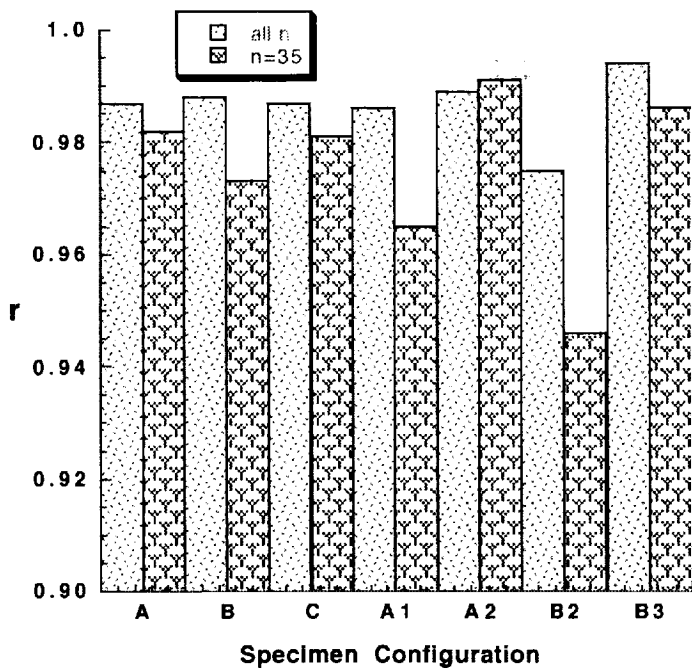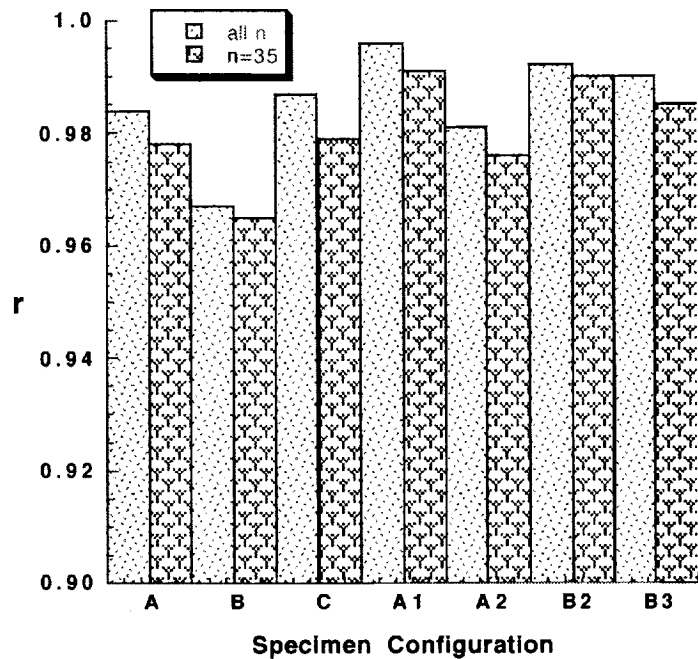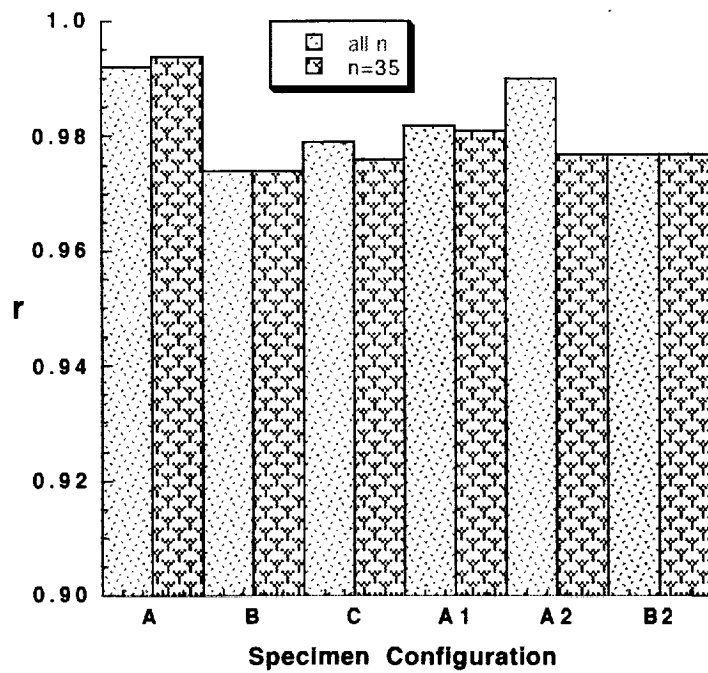
(a) S2/F584

(b) S2/8552
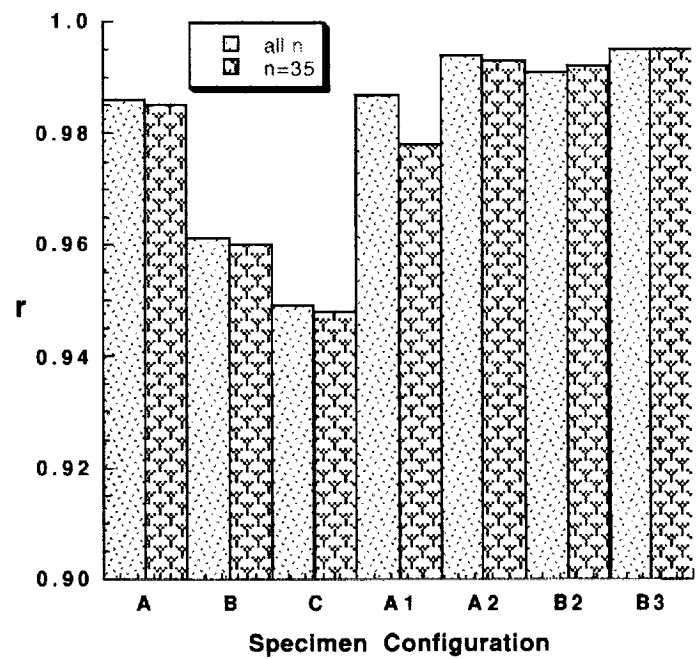
(c) 24-ply IM7/8552

(d) 36-ply IM7/8552

Fig. 37 – Weibull Distribution fit, Pearson's "r" value
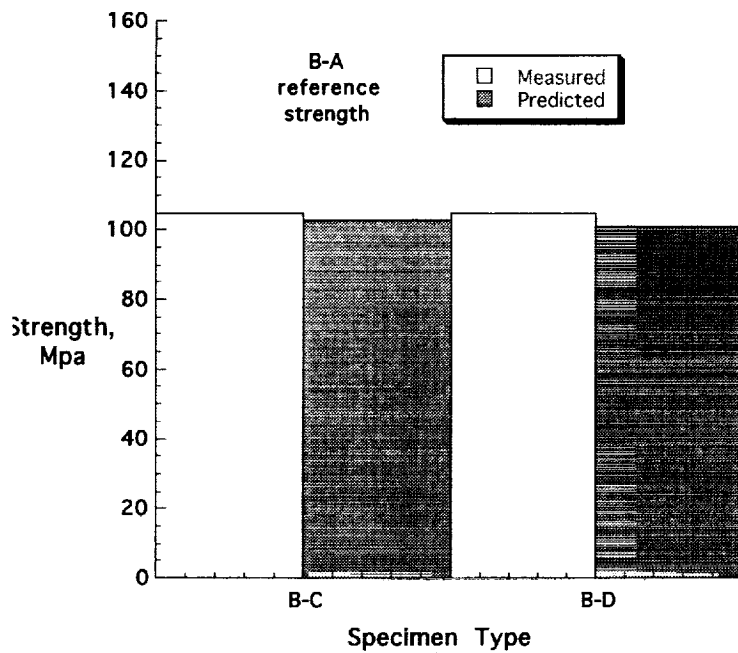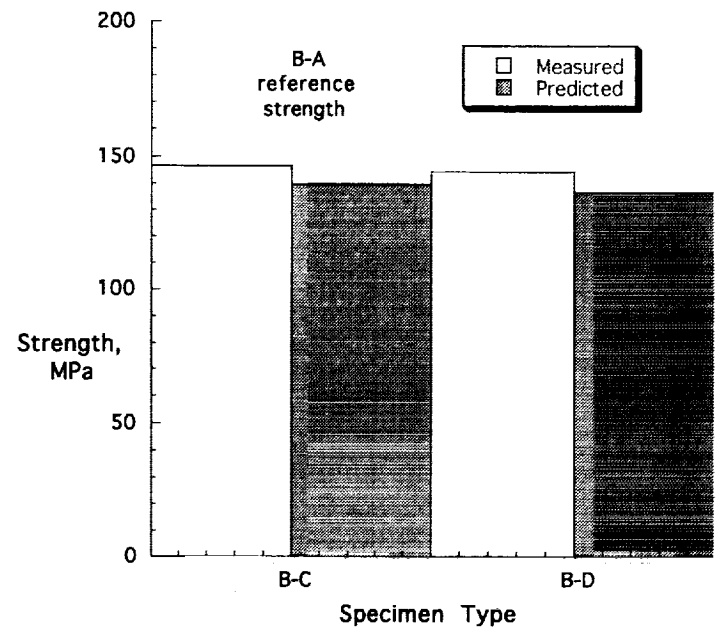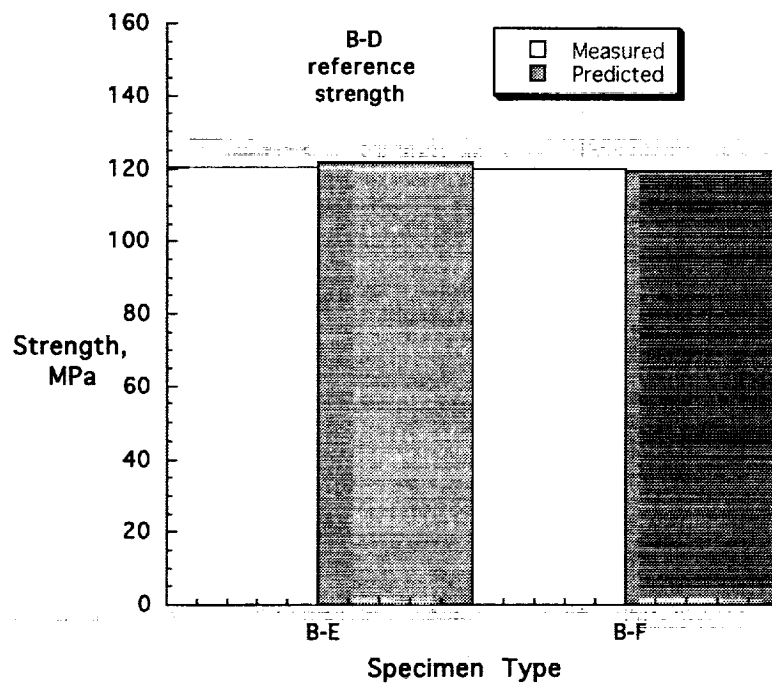
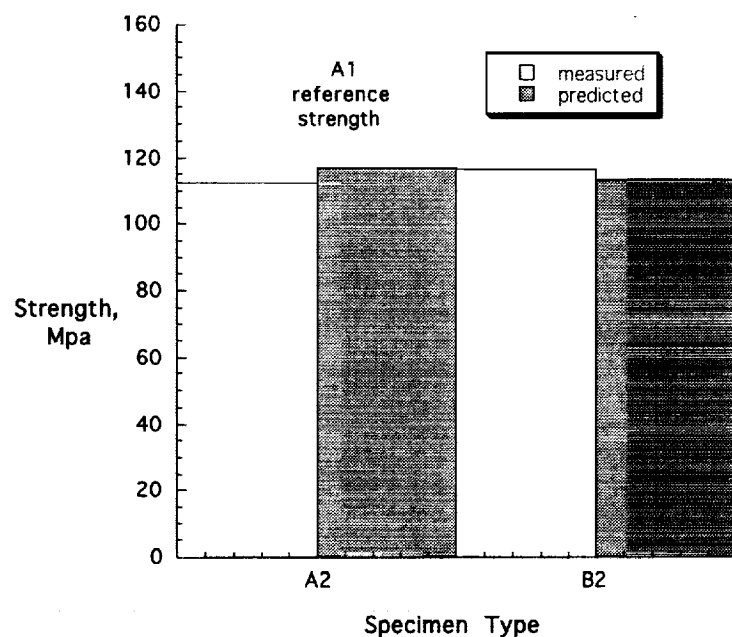Fig. 38 – Weibull Strength Prediction, Width Effect, 3-point bending
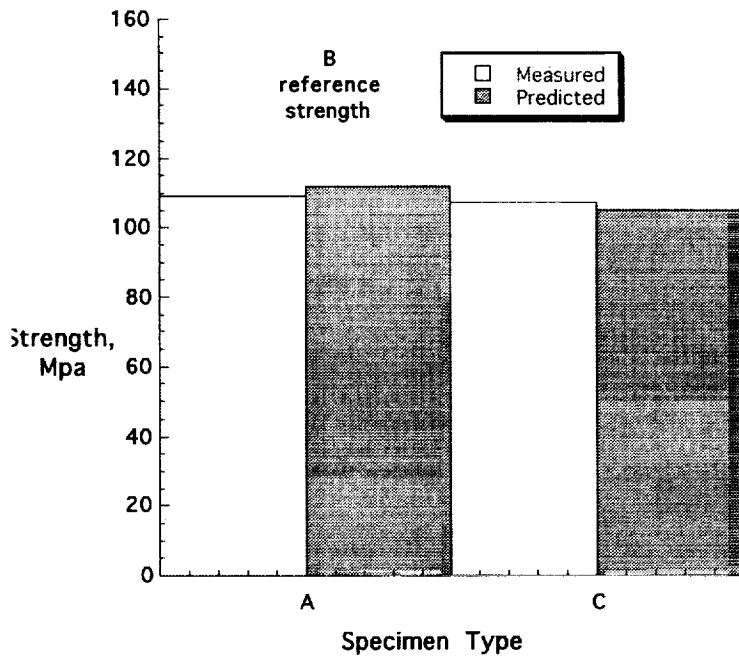
Fig. 39 – Weibull Strength Prediction, Span Effect, 3-point bending
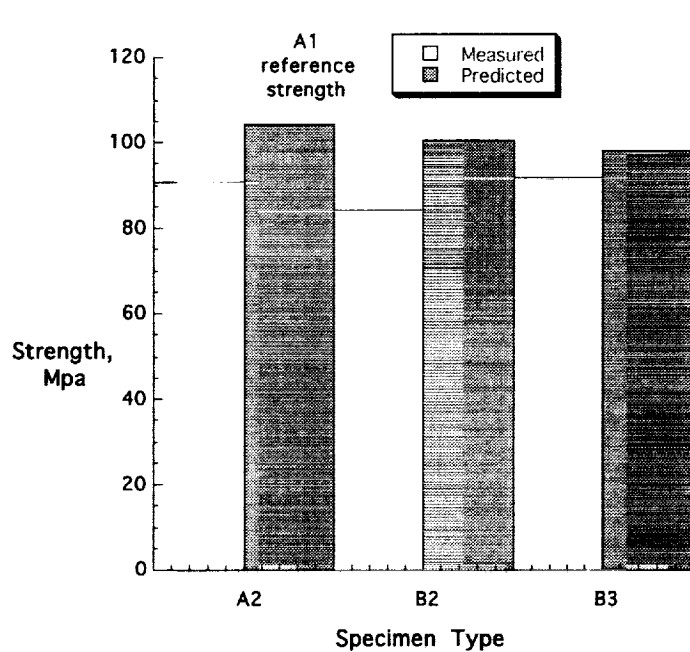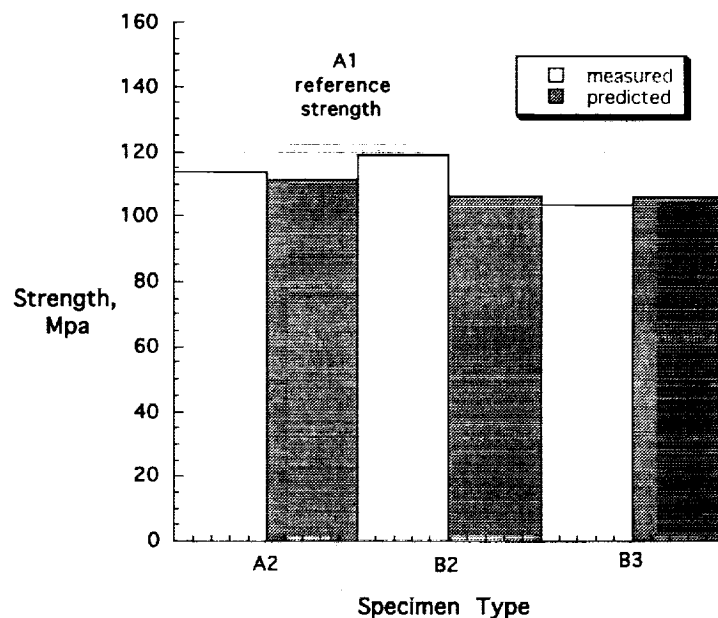
(a) S2/F584
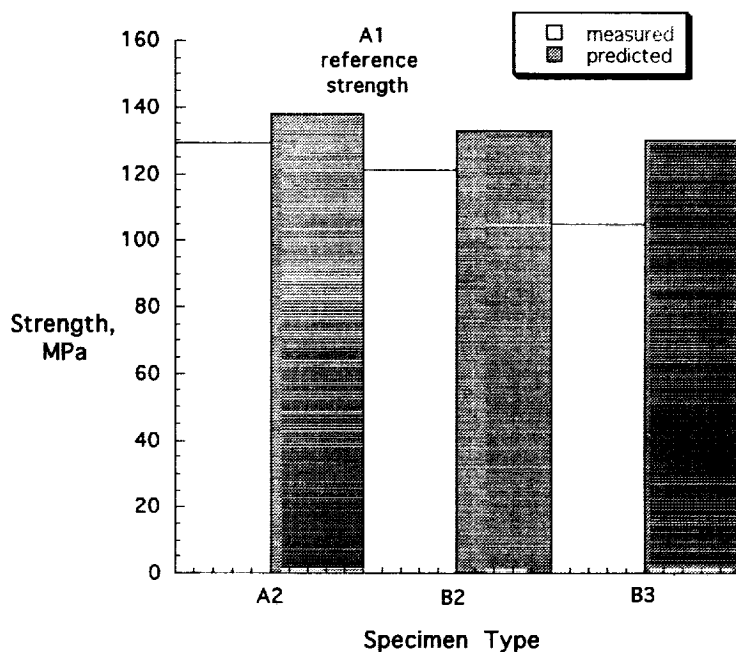
(b) S2/8552

(c) 24-ply IM7/8552

(d) 36-ply IM7/8552

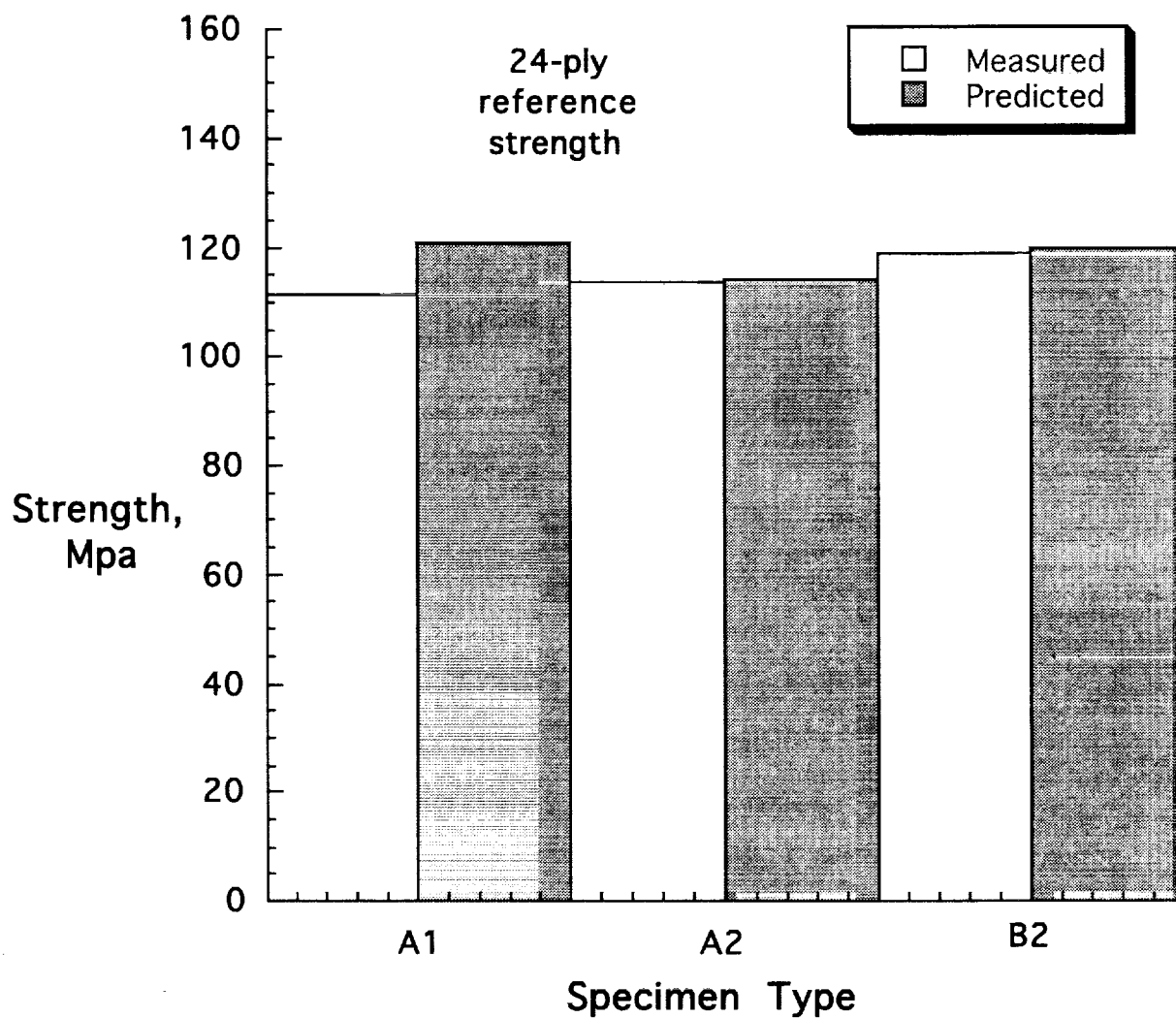Fig. 40 – Weibull Strength Prediction, Span Effect, 4-point bending
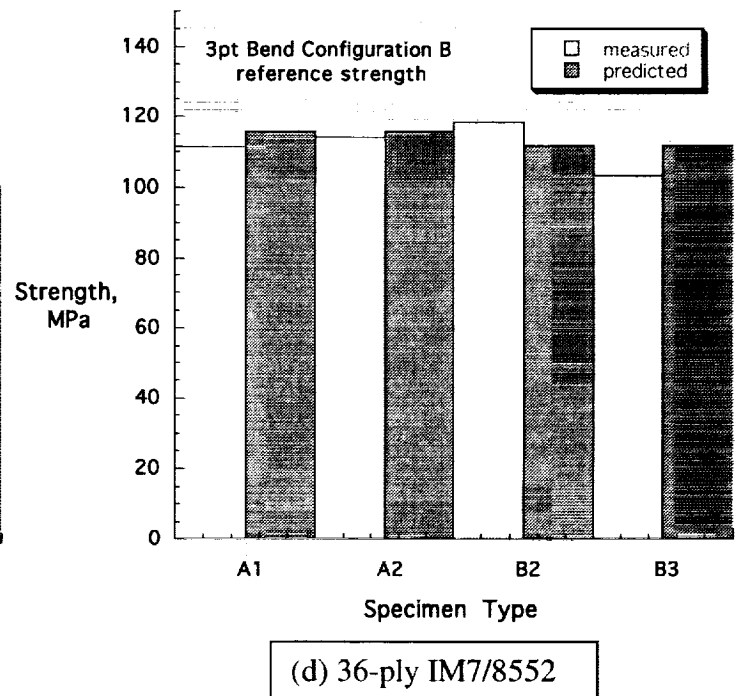
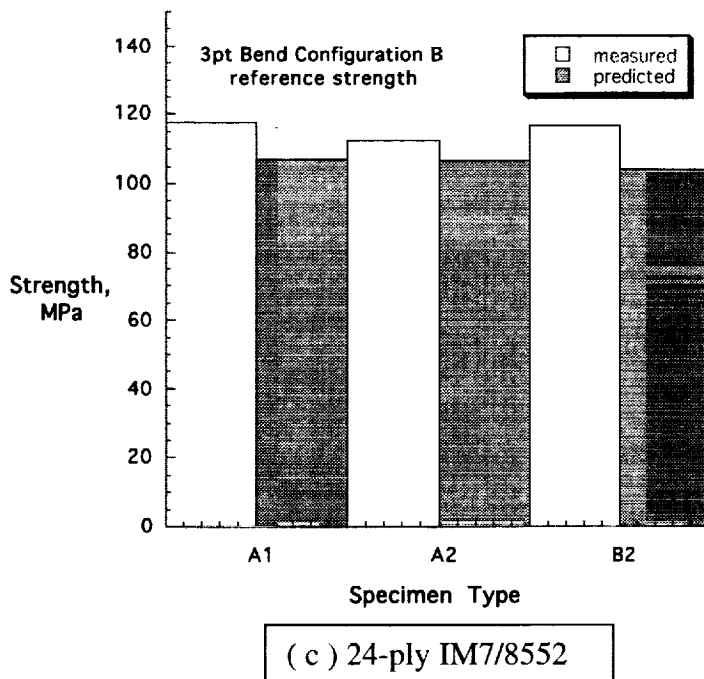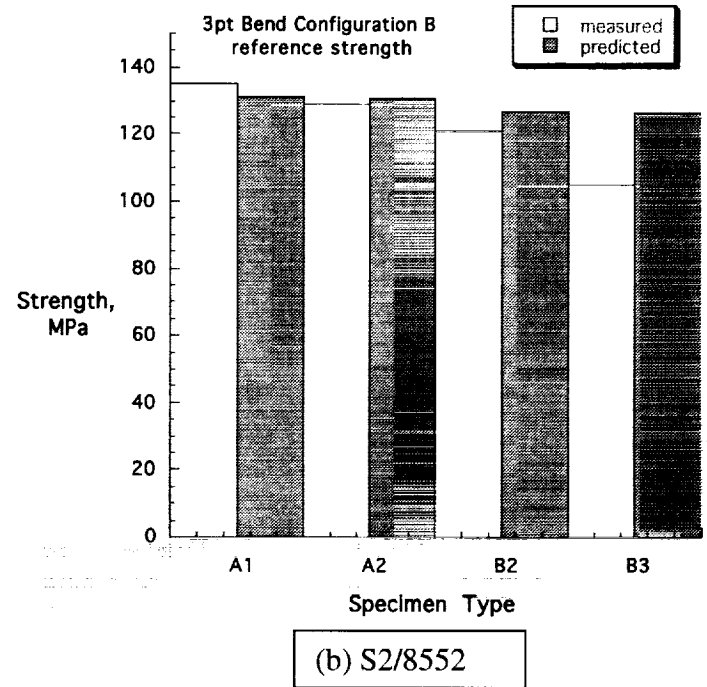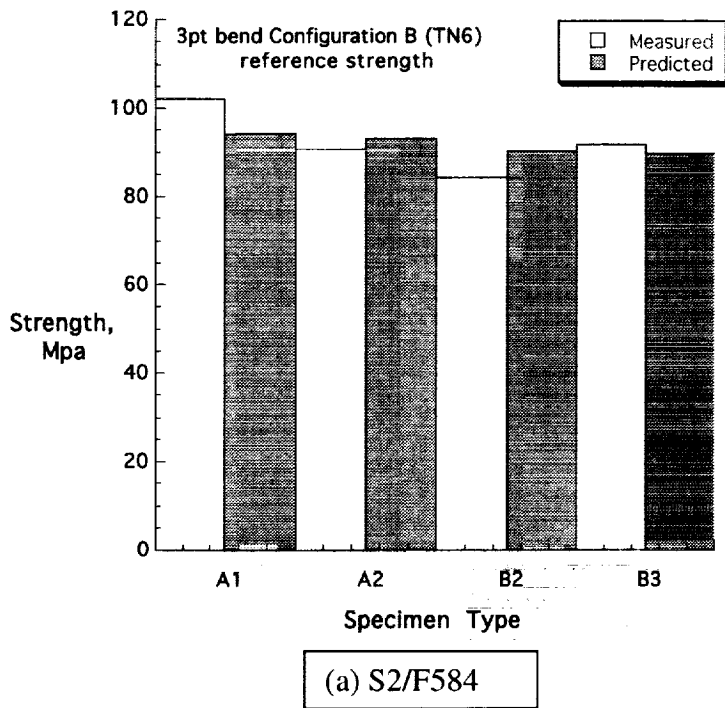Fig. 41– Weibull 4-point bending Strength Prediction for 36-ply IM7/8552
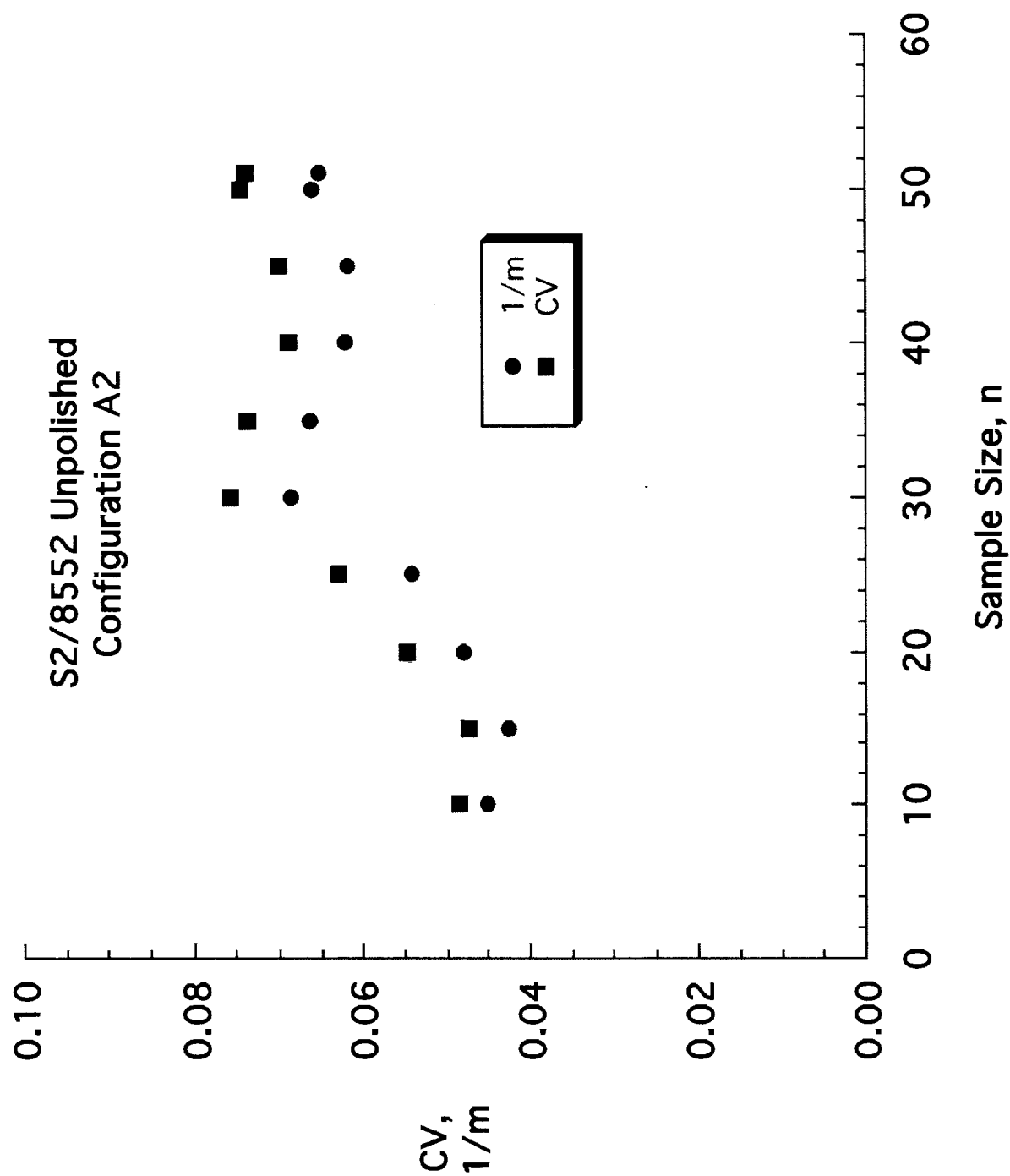
Fig. 42– Weibull 4-point bending Strength Prediction

Fig. 43 – Influence of Sample Size on Scatter

REPORT DOCUMENTATION PAGE

Public reporting burden for this collection of information is estimated to average 1 hour per response, including the time for reviewing instructions, searching existing data sources, gathering and maintaining the data needed, and completing and reviewing the collection of information. Send comments regarding this burden estimate or any other aspect of this collection of information, including suggestions for reducing this burden, to Washington Headquarters Services, Directorate for Information Operations and Reports, 1215 Jefferson Davis Highway, Suite 1204, Arlington, VA 22202-4302, and to the Office of Management and Budget, Paperwork Reduction Project (0704-0188), Washington, DC 20503.

1. AGENCY USE ONLY (Leave blank)	2. REPORT DATE July 2001	3. REPORT TYPE AND DATES COVERED Technical Memorandum

4. TITLE AND SUBTITLE
Influence of Specimen Preparation and Specimen Size on Composite Transverse Tensile Strength and Scatter

5. FUNDING NUMBERS
WU 712-10-21-01

6. AUTHOR(S)
T. Kevin O'Brien, Arun D. Chawan, Kevin DeMarco, Isabelle Paris

7. PERFORMING ORGANIZATION NAME(S) AND ADDRESS(ES)

NASA Langley Research Center
Hampton, VA 23681-2199

U.S. Army Research Laboratory
Vehicle Technology Directorate
NASA Langley Research Center
Hampton, VA 23681-2199

8. PERFORMING ORGANIZATION REPORT NUMBER
L-18092

9. SPONSORING/MONITORING AGENCY NAME(S) AND ADDRESS(ES)
National Aeronautics and Space Administration
Washington, DC 20546-0001
and
U.S. Army Research Laboratory
Adelphi, MD 20783-1145

10. SPONSORING/MONITORING AGENCY REPORT NUMBER
NASA/TM-2001-211030
ARL-TR-2540

11. SUPPLEMENTARY NOTES
Chawan: Syracuse University, Syracuse, New York
DeMarco: Virginia Polytechnic Institute & State University, Blacksburg, VA
Paris: National Research Council Associate, NASA Langley Research Center, Hampton, VA

12a. DISTRIBUTION/AVAILABILITY STATEMENT
Unclassified-Unlimited
Subject Category 24   Distribution: Standard
Availability: NASA CASI (301) 621-0390

12b. DISTRIBUTION CODE

13. ABSTRACT (Maximum 200 words)
The influence of specimen polishing, configuration, and size on the transverse tension strength of two glass-epoxy materials, and one carbon-epoxy material, loaded in three and four point bending was evaluated. Polishing machined edges, and/or tension side failure surfaces, was detrimental to specimen strength characterization instead of yielding a higher, more accurate, strength as a result of removing inherent manufacture and handling flaws. Transverse tension strength was typically lower for longer span lengths due to the classical weakest link effect. However, strength was less sensitive to volume changes achieved by increasing specimen width. The Weibull scaling law typically over-predicted changes in transverse tension strengths in three point bend tests and under-predicted changes in transverse tension strengths in four point bend tests. Furthermore, the Weibull slope varied with specimen configuration, volume, and sample size. Hence, this scaling law was not adequate for predicting transverse tension strength of heterogeneous, fiber-reinforced, polymer matrix composites.

14. SUBJECT TERMS
Composite Materials, Transverse Tensile Strength, matrix cracking, Weibull distribution

15. NUMBER OF PAGES
86

16. PRICE CODE
A05

17. SECURITY CLASSIFICATION OF REPORT	18. SECURITY CLASSIFICATION OF THIS PAGE	19. SECURITY CLASSIFICATION OF ABSTRACT	20. LIMITATION OF ABSTRACT
Unclassified	Unclassified	Unclassified	UL